AD_____

Award Number: W81XWH-04-1-0025

TITLE: An imaging system to monitor efficacy of adenovirus-based virotherapy agents

PRINCIPAL INVESTIGATOR: David. T. Curiel, M.D., Ph.D.

CONTRACTING ORGANIZATION: The University of Alabama at Birmingham
                                                  Birmingham, AL 35294-0109

REPORT DATE: February 2006

TYPE OF REPORT: Final

PREPARED FOR: U.S. Army Medical Research and Materiel Command
                          Fort Detrick, Maryland 21702-5012

DISTRIBUTION STATEMENT: Approved for Public Release;
                                        Distribution Unlimited

REPORT DOCUMENTATION PAGE			*Form Approved* OMB No. 0704-0188

1. REPORT DATE *(DD-MM-YYYY)* February 2006	2. REPORT TYPE Final		3. DATES COVERED *(From - To)* 1 Feb 04 – 31 Jan 06
4. TITLE AND SUBTITLE An imaging system to monitor efficacy of adenovirus-based virotherapy agents			5a. CONTRACT NUMBER
			5b. GRANT NUMBER W81XWH-04-1-0025
			5c. PROGRAM ELEMENT NUMBER
6. AUTHOR(S) David. T. Curiel, M.D., Ph.D.			5d. PROJECT NUMBER
			5e. TASK NUMBER
E-mail: curiel@uab.edu			5f. WORK UNIT NUMBER
7. PERFORMING ORGANIZATION NAME(S) AND ADDRESS(ES) The University of Alabama at Birmingham Birmingham, AL 35294-0109			8. PERFORMING ORGANIZATION REPORT NUMBER
9. SPONSORING / MONITORING AGENCY NAME(S) AND ADDRESS(ES) U.S. Army Medical Research and Materiel Command Fort Detrick, Maryland 21702-5012			10. SPONSOR/MONITOR'S ACRONYM(S)
			11. SPONSOR/MONITOR'S REPORT NUMBER(S)
12. DISTRIBUTION / AVAILABILITY STATEMENT Approved for Public Release; Distribution Unlimited			
13. SUPPLEMENTARY NOTES			

14. ABSTRACT
Our preliminary data establish a number of important key points. Foremost, these results show that adenovirus can be genetically labeled with a fluorescent structural fusion protein through a complete replacement with IX-EGFP in a chimeric context. At least for our pIX-EGFP strategy, the label was incorporated into virions conferring a fluorescent property that allowed detection of individual particles. Ad-IX-EGFP binding and infection could both be detected via the fluorescent label. This capsid-labeling system is applicable to CRAds because it slightly decreased progeny yield but did not affect the cytopathic effect and spread of the virus. Notably, the level of pIX-EGFP fluorescence directly correlated with the amount of progeny production due to its dependence on E1 activity for expression. The data with pIX-EGFP fulfills all the requirements of the ideal monitoring system for CRAds except noninvasive detection which we propose to accomplish. Both our proposed capsid-labeling approaches demonstrate great promise for detection of viral replication and spread and hence monitoring of CRAds.

15. SUBJECT TERMS
Prostate, cancer, CRAd, Adenovirus

16. SECURITY CLASSIFICATION OF:			17. LIMITATION OF ABSTRACT	18. NUMBER OF PAGES	19a. NAME OF RESPONSIBLE PERSON USAMRMC
a. REPORT U	b. ABSTRACT U	c. THIS PAGE U	UU	70	19b. TELEPHONE NUMBER *(include area code)*

Standard Form 298 (Rev. 8-98)
Prescribed by ANSI Std. Z39.18

Table of Contents

Introduction

The emergence of targeted therapeutics has revealed a novel paradigm for prostate cancer therapy which offers the potential to eradicate tumor while sparing normal tissue. One such targeted therapy is represented by virotherapy, i.e. replicating viral agents which accomplish selective replication in and lysis of tumor cells. In this regard, virotherapy agents have been derived from a variety of parent virus types including herpes virus, measles virus, adenovirus, and others. Adenoviruses have shown particular promise as conditionally replicative adenoviral agents (CRAds) and have been rapidly translated into the context of human clinical trials where suggestions of efficacy have been noted, at least in selected cases. Specifically for prostate cancer, CRAd agents have been proposed which exploit the characterized pathobiology of this disease. A limitation of the clinical use of CRAd agents, however, is the difficulty in obtaining critical efficacy data in the context of endeavored human trials. Basic issues such as vector localization and tumor selective replicative capacity have not been rigorously determined in a human use context. The lack of this critical interval endpoint information has hindered the full understanding of the requirements for CRAd efficacy and thus hampered steps directed towards additional development. Further impacting this scenario is the recognition that available imaging systems which are operative in gene transfer vector applications are not functional in a replicating vector context. On this basis it is clear that the development of an imaging system for CRAds would allow the acquisition of key interval endpoint data in human clinical trials and therefore provide a useful data base for advancement of these promising agents for carcinoma of the prostate.

To this end, we have conceptualized an approach to achieve direct biological labeling of adenoviruses for CRAd imaging. Specifically, we have identified a capsid protein of adenovirus, pIX, which allows genetic incorporation of heterologous peptides which are thereby presented on the surface of the virion. We have recently demonstrated that we can incorporate into this locale an enhanced green fluorescent protein (EGFP) marker. Of note, the EGFP-labeled CRAd retain replication and packaging capacities comparable to native adenovirus. Moreover, the capsid-incorporated EGFP allows detection of particles by a range of fluorometric modalities. We hypothesized that the pIX-GFP label would on this basis, provide a means to achieve dynamic/real time imaging of CRAd replication and localization and that this capacity will allow an improved understanding of CRAd efficacy parameters.

Our Specific Aims were thus:
(1) To develop prostate cancer CRAds which incorporate the pIX-EGFP label and to validate their imaging capacity in prostate cancer cells *in vitro*.
(2) To employ the labeled CRAd *in vivo* in murine models of human prostate cancer to validate their imaging utility.

Body

We have pursued a genetic labeling system for adenovirus by applying one of our proposed strategies, namely capsid labeling through a fusion of EGFP with pIX. Most of the following section illustrates key data we have obtained which demonstrates proof of principle and feasibility for this concept. Also included at the end are preliminary results we have acquired for the core labeling approach.

1. Expression and localization of pIX-EGFP fusion label

Conservation of cellular localization of the fusion protein label relative to the native structural protein is imperative because of consequences associated with function and likelihood of being packaged into virions. This issue is especially important when a transgene is expressed in an adenoviral context where viral factors or perturbations of the cellular environment due to infection may affect the localization and function of the protein. To verify the localization of our fusion capsid label, an E1-deleted shuttle plasmid was constructed containing a IX-EGFP carboxy-terminal fusion gene in place of wildtype IX. Following transient transfection of this plasmid into 911 cells, pIX-EGFP was expressed and accumulated in intranuclear clear amorphous inclusions as previously reported[107] (data not shown). This shuttle plasmid was used to construct E1- and E3-deleted Ad-IX-EGFP (Fig. 3*a*) which was successfully rescued. **In an adenoviral context, pIX-EGFP was expressed and also accumulated in the nucleus** (Fig. 3*b*).
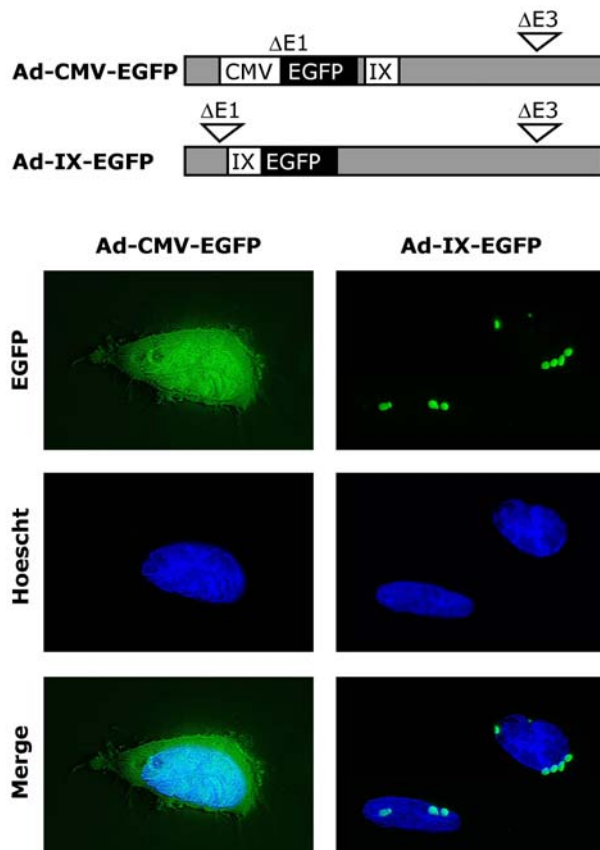

Figure 1. pIX-EGFP intracellular localization. *a*, Control Ad-CMV-EGFP construct with native pIX and Ad-IX-EGFP construct with pIX-EGFP in place of native pIX. *b*, EGFP localization from Ad-CMV-EGFP and pIX-EGFP nuclear localization from Ad-IX-EGFP.

5

2. Incorporation of pIX-EGFP into Ad-IX-EGFP particles

Ad-IX-EGFP was examined further with regards to effectiveness of pIX-EGFP labeling of the virus. Propagated viruses were purified by double cesium chloride (CsCl) ultracentrifugation where the top and bottom bands were preserved through both cycles. The resulting gradients of virus were fractionated and analyzed for fluorescence by fluorometry and D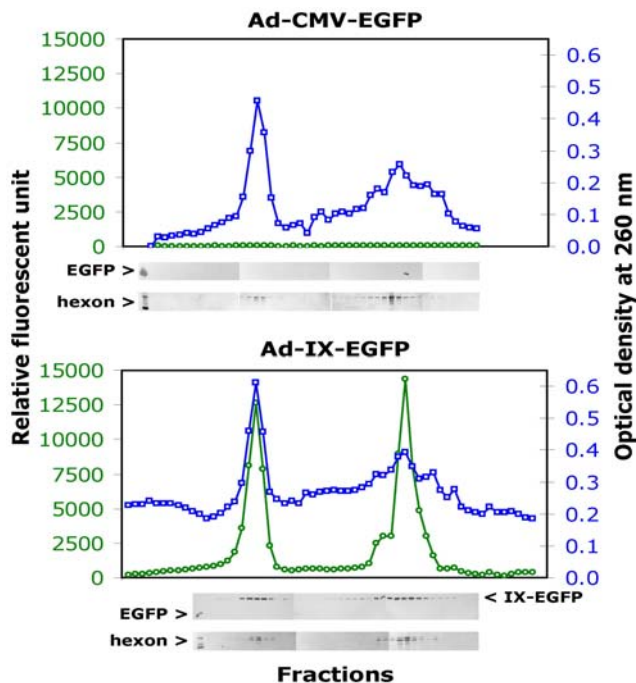NA content by optical density at 260 nm. Fluorescent peaks were observed for the top and bottom band fractions of Ad-IX-EGFP which were significantly greater than those of control Ad-CMV-Luc (data not shown) and Ad-CMV-EGFP (more than 2 log factors). For all viruses, a major DNA content peak was present in the bottom band where mature virions normally migrate (Fig. 2). Infectious, mature Ad-IX-EGFP particles were present in the bottom band as indicated by an infectivity peak in a quick CPE assay[108] (data not shown). The same gradient fractions for Ad-IX-EGFP and Ad-CMV-EGFP were also analyzed with western blot using GFP and hexon antibodies. The blots show accumulations of pIX-EGFP and hexon in both the top and bottom band regions for Ad-IX-EGFP, confirming the colocalization of pIX-EGFP with the capsid and hence virions. While hexon was also detected both in the bottom and top bands for Ad-CMV-EGFP, EGFP was only present above the top band where cellular proteins migrate (Fig. 2). **These data validate the successful labeling of adenovirus with pIX-EGFP**.

Figure 2.   Characterization of Ad-IX-EGFP particles. Fluorescence (○) and DNA content (□) of Ad-CMV-EGFP and Ad-IX-EGFP CsCl gradient fractions following double ultracentrifugation. Fractions were also analyzed using anti-GFP and anti-hexon western blotting following SDS-PAGE.

3. Visualization of Ad-IX-EGFP

Functional and molecular verification of pIX-EGFP incorporation into virions was encouraging. Whether or not the extent of labeling confers actual detectability of viral particles was assessed by **fluorescence microscopy of Ad-IX-EGFP bottom and top band fractions which revealed abundant punctate green particles**. The fluorescence of bottom band mature particles was uniform whereas the fluorescence of top band empty particles had variable intensities. No fluorescent particles were detected for control Ad-CMV-Luc (data not shown) or Ad-CMV-EGFP (Fig. 3).
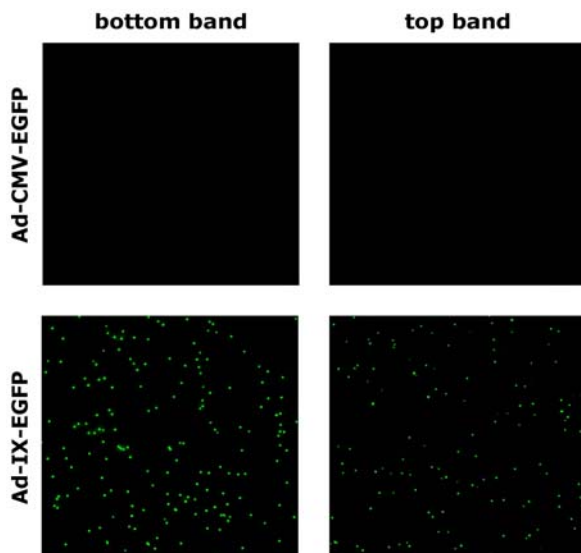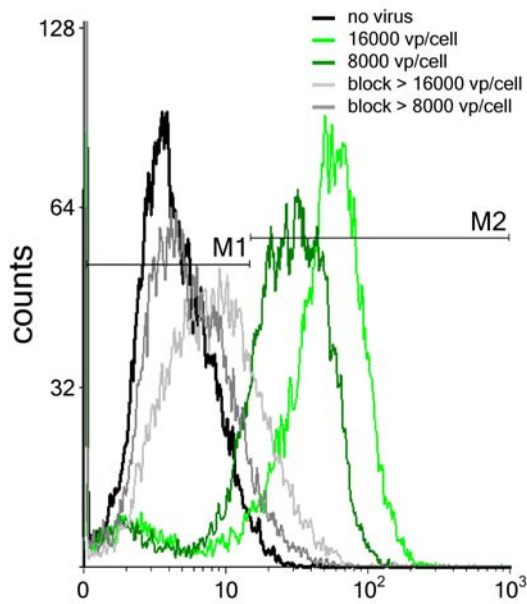

Figure 3.   Visualization of Ad-IX-EGFP particles. Dilutions (1:100) of representative top and bottom band fractions for Ad-CMV-EGFP and Ad-IX-EGFP were visualized with epifluorescence microscopy using a 100X oil immersion objective.

Figure 4.   Ad-IX-EGFP FACS binding assay.
911 cells (positive for primary adenovirus receptor)
were incubated with (gray) or without (green) Ad5
knob before addition of virus. After the virus was
allowed to bind, the cells were analayzed by FACS
to detect cells positive for bound virus. Black line
represents control cells incubated without knob
block and without virus.

4. Detection of Ad-IX-EGFP binding

Ad-IX-EGFP detection in a functional context was
demonstrated by exploiting the fluorescent property of this
virus to assay its binding to cells. 911 cells which express
the coxsackie and adenovirus receptor (CAR) were
incubated with or without a recombinant adenovirus type 5
fiber-knob protein prior to addition of Ad-IX-EGFP for 30
minutes binding at 4°C with shaking. The cells were then
washed and analyzed by FACS for any bound EGFP signal.
Without prior blocking, Ad-IX-EGFP binding to 911 cells
clearly showed positive peaks at 16000 vp/cell and 8000
vp/cell conditions compared to the uninfected control.
However, the incubation with the fiber-knob protein before
addition of virus blocked subsequent binding of Ad-IX-
EGFP to its primary receptor CAR at the same
multiplicities of infection (moi) (Fig. 4). These results
indicate the detectability of Ad-IX-EGFP for binding
activity and also that the **pIX-EGFP labeling did not have
a deleterious effect on the binding of virus**.

30 min post-infection

1-2 hours post-infection

5. Tracking of Ad-IX-EGFP infection

In addition to binding, any modification of the virus capsid
could affect its infection pathway. We used a tracking
assay to monitor the infection of Ad-IX-EGFP in 911 cells,
again exploiting the fluorescent property of the virus for its
detection. Shortly after addition of the virus to the culture
medium (30 min), numerous viral particles were observed
binding on the cell membrane periphery. After another
hour at room temperature, viruses were detected mostly in
the nucleus (Fig. 5). **Evidently, the pIX-EGFP label did
not affect the infectivity the labeled adenovirus.**

Figure 5. Tracking of Ad-IX-EGFP infection of 911 cells. Top two panels: Binding of virus on the
cell membrane at ~30 minutes after infection at room temperature. Bottom two panels: Accumulation
of virus around the nucleus ~1-2 hours after infection at room temperature. Blue represents Hoechst
stain for the nucleus.

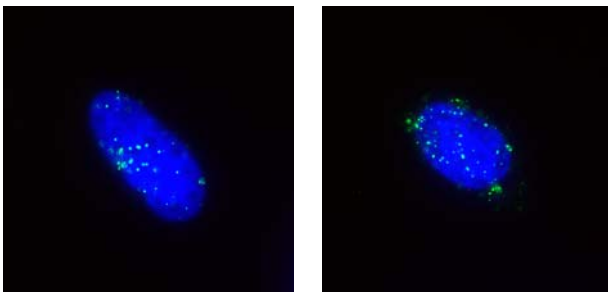## 6. DNA packaging efficiency of Ad-IX-EGFP

With successful labeling, detection, and confirmation of binding and infectivity for Ad-IX-EGFP established, we next evaluated the adaptability of this labeling strategy for a replicative system. Ideally for application in CRAds, pIX-EGFP labeling of adenovirus should minimally disrupt the efficiency of replication and virus production. Protein IX has been shown to play a number of roles in adenovirus infection, including capsid stabilization, transcriptional activity, and nuclear reorganization[107]. Although dispensable in packaging[86], adenovirus pIX is important in packaging full-length genomes and stabilizing the capsid structure[109,110]. To characterize the effect of fusing EGFP to pIX on DNA packaging and hence progeny production, viral DNA from various fractions was quantitated using Taqman quantitative PCR on days 1, 2, 3, and 4 following infection at 10 fcu/cell (fluorescent cell units/cell). These fractions included intracellular total, intracellular encapsidated, and supernatant encapsidated viral DNA. The results indicate that total viral DNA replication was the same for both Ad-IX-EGFP and control Ad-CMV-EGFP. However, both packaged DNA in the cell and packaged DNA released into the supernatant was approximately half a log factor lower for Ad-IX-EGFP compared to the control (Fig.6), indicating lower progeny yield. This effect was significant, yet the **yield of Ad-IX-EGFP was on the same order of magnitude as the control Ad-CMV-EGFP**.
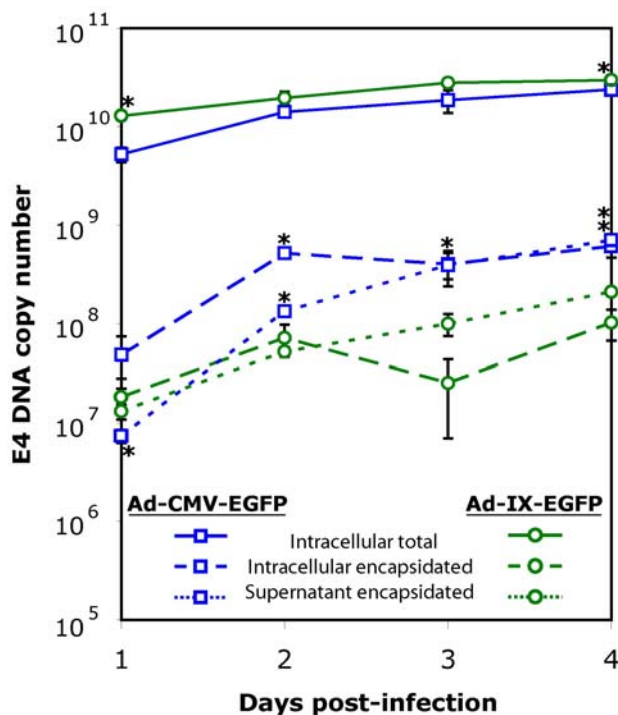
Figure 6. DNA packaging efficiency and progeny production of Ad-IX-EGFP. Post-infection copy numbers of viral DNA from various pools for Ad-CMV-EGFP [intracellular total (—□—), intracellular encapsidated (- -□- -), supernatant encapsidated (····□····)] and Ad-IX-EGFP [intracellular total (—○—), intracellular encapsidated (- -○- -), supernatant encapsidated (····○····)] ($n = 3$). * DNA copy numbers were statistically different (t-test $P < 0.05$) between the two viruses in the following cases: total intracellular DNA on days 1 and 4; intracellular encapsidated DNA on days 2, 3, and 4; and superanatant encapsidated DNA on days 1, 2, and 4.

7. Cytopathic effect of Ad-IX-EGFP

In addition to efficiency of progeny production, CRAd efficacy also depends on how well the virus can lyse infected tumor cells and spread leading to an overall cytopathic effect. To evaluate this virus quantitatively for cytopathic effect, infection of 911 and 293 cells with Ad-IX-EGFP and control virus at 10, 1, and 0.1 fcu/cell multiplicities of infection (moi) were monitored over 10 days. On days 0, 2, 4, 6, 8, and 10, the cytopathic effect of the virus was quantitated using a non-radioactive cell proliferation assay (MTS assay) (Fig. 7). Both 293 and 911 packaging cell lines for E1-deleted adenoviruses have been shown to express very low levels of wildtype pIX[109,111] (also J. Vellinga, personal communication; and data not shown). In both 293 and 911 cells, Ad-IX-EGFP cytopathic effect was the same as that of Ad-CMV-EGFP. These findings suggest that although Ad-IX-EGFP has a slightly lower yield than control virus, **pIX-EGFP did not affect the cytopathic capacity and lateralization of the virus**, critical functions of replicative adenoviral agents.
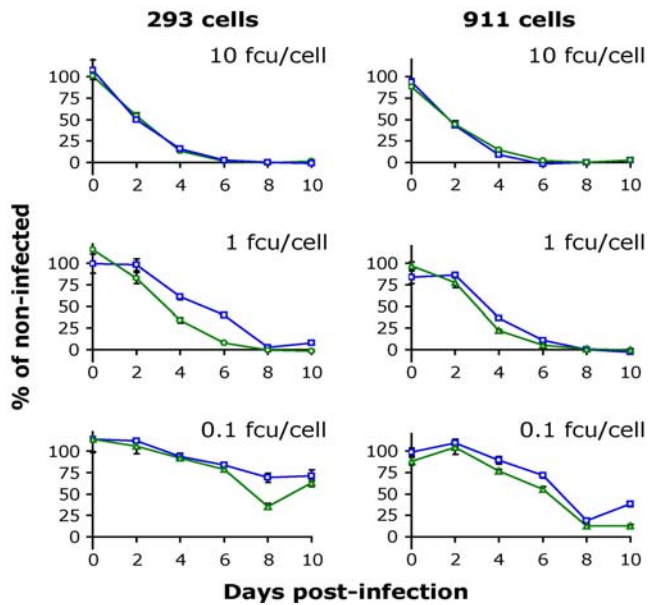
Figure 7. Cytopathic effect and spread of Ad-IX-EGFP. Cytopathic effect of Ad-CMV-EGFP (—□—) and Ad-IX-EGFP (—○—) in 293 cells (complementary pIX expression) and 911 cells (no pIX expression) at various multiplicities of infection. Cytotoxicity measured by a non-radioactive proliferation assay and expressed as percentage of non-infected cells ($n = 6$).

8. Correlation of pIX-EGFP fluorescent label with replication and progeny production

In addition to localizing the spread of progeny virions, the power of a monitoring system for replicative agents also depends on its ability to accurately represent the level of viral replication and progeny production. We determined whether our pIX-EGFP labeling approach would satisfy this criterion. 911 packaging cells were infected with Ad-IX-EGFP and control Ad-CMV-EGFP (both E1- and E3-deleted) at 1 and 0.1 fcu/cell. On days 0, 2, 4, 6, 8, and 9 post-infection, the fluorescence of pIX-EGFP and EGFP in the cells were quantitated. Cells and culture medium were collected on these days and lysed with three free/thaw cycles. The crude viral lysates from these samples were titered in terms of fluorescent cell units. The time-course fluorescence and progeny production based on fluorescent cell unit titer were plotted together to show the degree of correlation between the two measurements (Fig. 8). Correlation p values were calculated in Excel by taking the covariance between the fluorescence and fluorescent cell unit titer data sets (means only) and dividing it by the product of the variances of the two data sets (means only). At the lower moi, the correlation of pIX-EGFP fluorescence with fluorescent cell unit titer for Ad-IX-EGFP was much stronger than that of Ad-CMV-EGFP (*p = 0.99 vs. p = 0.86*, respectively) (Fig. 8). At the higher moi, both systems appear to be saturated with progeny virus by day 4 leading to a drop in titer on the following days. **The fluorescence of the pIX-EGFP label can be used to represent the level of replication and progeny production.**

9
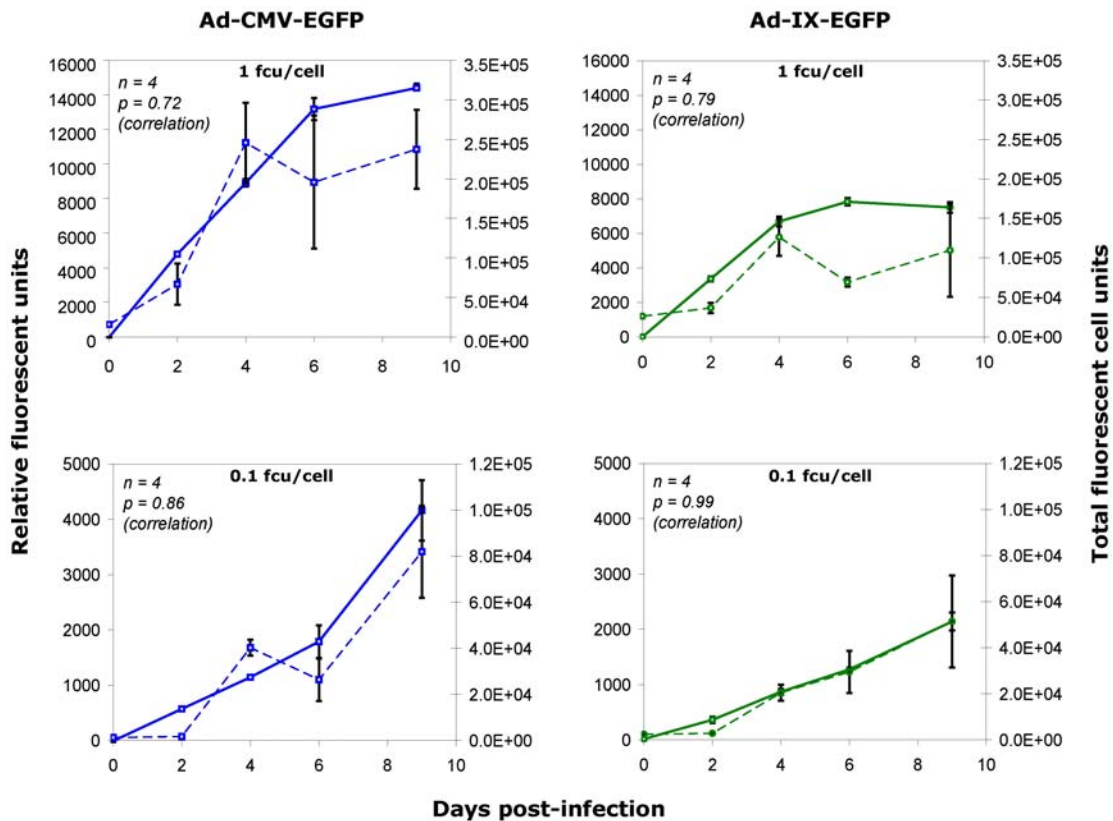
Figure 8. Correlation of fluorescent protein label with progeny production. 911 cells were infected with control Ad-CMV-EGFP and Ad-IX-EGFP at 1 and 0.1 fcu/cell. On days 0, 2, 4, 6, 8, and 9 post-infection, the fluorescence of the cells was measured and correlated with the titer of crude viral lysate prepared from the same samples. Correlation was performed in Excel. Ad-CMV-EGFP [EGFP fluorescence (—□—), fluorescent cell unit titer (- -□- -)], and Ad-IX-EGFP [pIX-EGFP fluorescence (—○—), fluorescent cell unit titer (- -○- -)].

9. Dependence of pIX-EGFP expression on viral replication

To more stringently show the utility of pIX-EGFP as an accurate indicator of viral replication, we constructed a wildtype adenovirus with the IX-EGFP gene (Ad-wt-IX-EGFP) and tested the virus in A549 human lung cancer cell line. As a negative control for replication, we used the E1- and E3-deleted replication-incompetent Ad-IX-EGFP virus which we have characterized and used up to now. Three days post-infection at 0.1 and 0.01 fcu/cell, no pIX-EGFP expression in A549 cells was detected for the replication-deficient virus. However in our previous experiments, expression was observed for this virus in 911 cells expressing E1 genes for complementation. Unlike the replication-deficient virus, pIX-EGFP expression was notable in A549 for the wildtype virus containing the IX-EGFP gene (Fig. 9). These results indicate that expression of pIX-EGFP relies on the presence of the E1 proteins, specifically the 21 kDa E1B protein[112] and also for regulation the E1a 12S and 13S proteins as well as E4 products[113]. The implications of this finding is highly relevant for CRAds considering the fact that most of the advanced generation CRAds have been designed with tumor specific promoters driving the expression of E1a gene as the checkpoint of replication[1,3]. **pIX-EGFP would serve as an accurate signal of replication** for these E1a-controlled replicative agents.

Ad-ΔE1-IX-EGFP-ΔE3

0.1 fcu/cell

Ad-wt-IX-EGFP
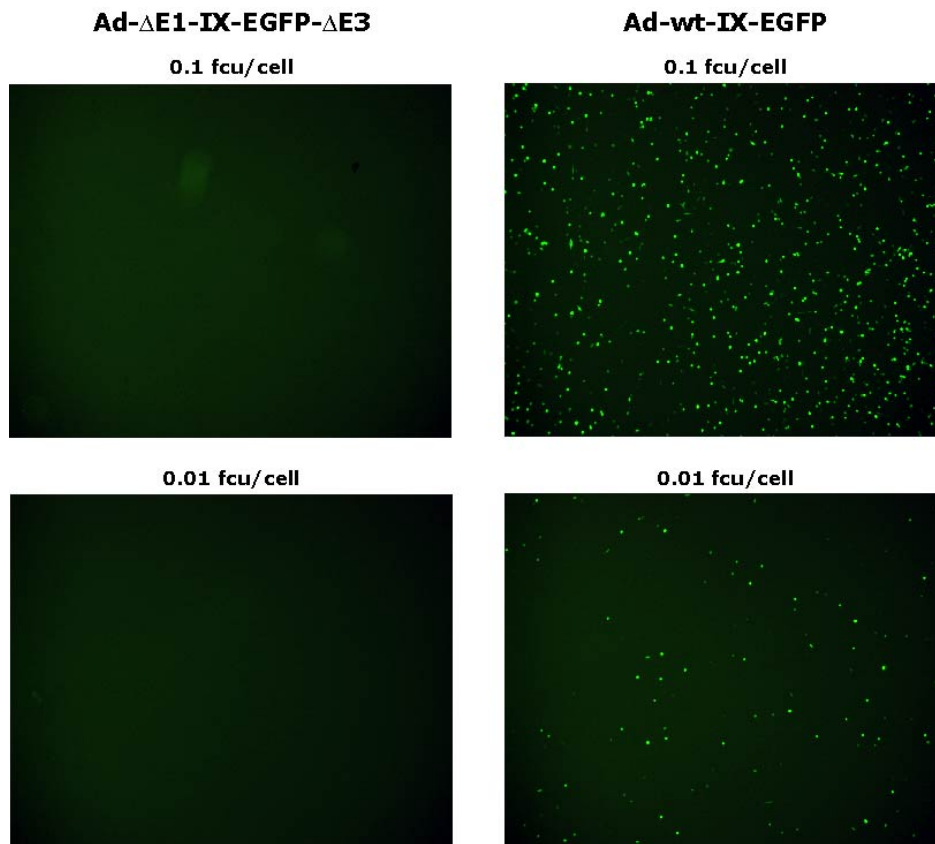
0.1 fcu/cell

Figure 9. E1-dependent expression of pIX-EGFP in A549 cells. A549 human lung cancer cells were infected with a replication-deficient E1- and E3-deleted control Ad-IX-EGFP and a replication competent Ad-wt-IX-EGFP at 0.1 and 0.01 fcu/cell. Three days post-infection, the cells were imaged for expression of pIX-EGFP.

0.01 fcu/cell

0.01 fcu/cell

10. Adenovirus capsid labeling with red fluorescent proteins.
Anticipating the difficulty of EGFP detection deep in the peritoneum, we constructed red fluorescent pIX-labeled adenoviruses with monomeric (mRFP1) and tandem dimer (tdimer2(12) red fluorescent proteins[80]. Fluorescence in the red to infrared range of the light spectrum are not as readily absorbed by tissues and therefore could be detected deeper in tissues[72]. Similar to the data gathered for Ad-IX-EGFP, both Ad-IX-mRFP1 and Ad-IX-tdimer2(12) could be rescued and detailed analysis of their CsCl gradient fractions revealed successful incorporation of the respective red fluorescent pIX fusion proteins into virions (Fig. 10). **The ability to generate red fluorescent adenoviruses expands the versatility of detecting pIX-labeled adenoviruses.**
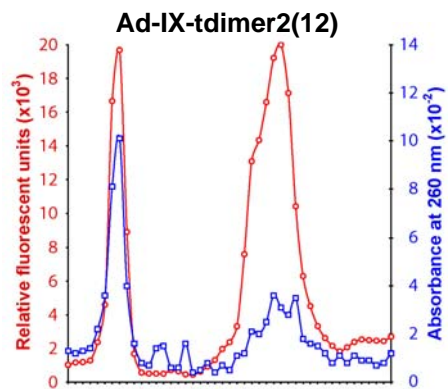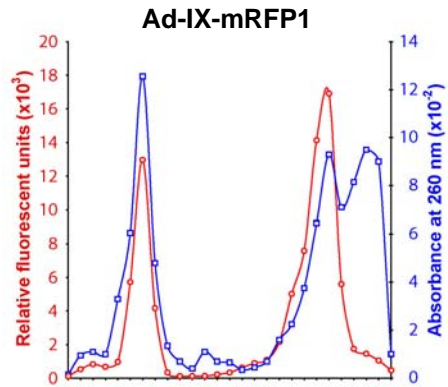
Ad-IX-mRFP1
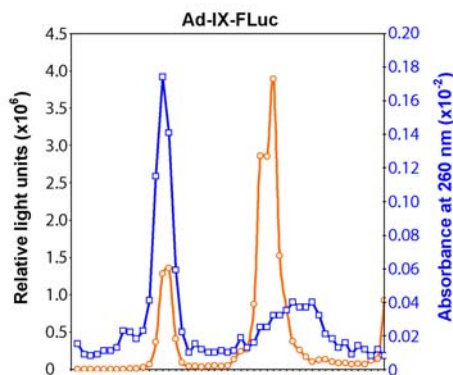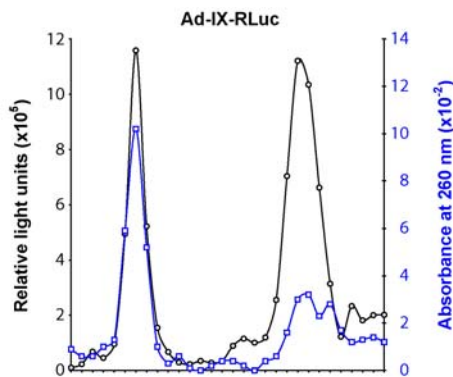
Ad-IX-tdimer2(12)

Fractions (bottom → top)

Figure 10.   Analysis of Ad-IX-mRFP1 and Ad-IX-tdimer2(12).   Cesium chloride purified Ad-IX-mRFP1 and Ad-IX-tdimer2(12) gradients were fractionated from bottom to top. Each fraction was analyzed for viral DNA content (optical density at 260 nm, blue lines) and red fluorescence (605 nm for mRFP1 and 590 nm for tdimer2(12), red lines).

11. Adenovirus capsid labeling with functional luciferases.

Recently, the ability to image bioluminescence from Firefly and *Renilla* luciferases (FLuc and RLuc, respectively) has afforded the possibility to observed molecular events *in vivo* with high sensitivity and virtually no background noise. We capitalized on this imaging modality to extend the detection mode of our adenovirus labeling strategy even further by fusing both Firefly and *Renilla* luciferases onto pIX. Rescue and analysis of CsCl gradient fractions for viral DNA and luciferase activity (from pure intact virus) show that we were able to generate bioluminescent viruses (Fig. 11). **This approach represents a novel concept in that luciferase enzymes may be incorporated onto the adenoviral capsid while retaining their function, allowing us to exploit the sensitivity, low background, and observation depth of bioluminescence imaging as a means to detect adenovirus replication.**

Fractions (bottom → top)

Figure 11. Analysis of bioluminescent Ad-IX-RLuc and Ad-IX-FLuc. Cesium chloride purified Ad-IX-RLuc and Ad-IX-FLuc gradients were fractionated from bottom to top. Each fraction was analyzed for viral DNA content (absorbance at 260 nm, blue lines) and luciferase activities (coelenterazine for RLuc – black line and D-luciferin for FLuc – orange line).

12. In vivo detection of Firefly luciferase expression in the peritoneum. We also wanted to demonstrate the feasibility of bioluminescence imaging for intraperitoneal tumors which would allow us to use our pIX-luciferase labeled vectors for adenovirus imaging with high sensitivity. In this experiment, a mouse bearing SKOV3.ip1 intraperitoneal tumors was injected i.p. with a luciferase expression vector. Two days day later we could detect bioluminescence signal emanating from the abdominal region using our custom built optical imaging system (Fig. 12). Because the applied expression vector contains the ubiquitous CMV promoter, there is likely expression along the lining of the cavity; however, the strong signals observed are localized to the tumor nodules. In contrast to the widely active CMV expression vector used here, the use of tumor-specific replicative adenovirus in our proposal would provide high signal to noise tumor detection versus background in the peritoneum. **These data demonstrate the function of our custom optical imaging system and establish the key feasibility of applying bioluminescence imaging for intraperitoneal tumors and therefore makes available another imaging modality for disease detection.**
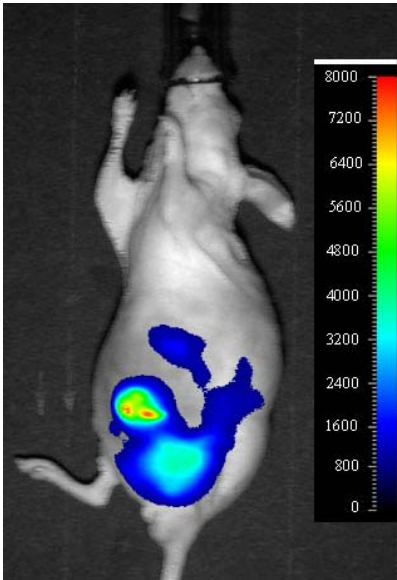
Figure 12. Detection of luciferase gene expression in the peritoneum. A mouse bearing established SKOV3.ip1 intraperitoneal tumors was injected i.p. with Ad5.pK7(GL) (10^{10} vp), a E1 CMV-driven Luc and GFP expression vector with a polylysine addition to the Ad5 fiber protein. Two days post-injection of the virus, the mouse was imaged after D-luciferin (3 mg) via the tail vein. The index scale represents the relative light units.

13. Adenovirus capsid labeling with PET-compatible HSV-TK.
Beyond the goals of our proposal to acquire proof-of-principle validation of our disease detection method, we considered the possibility of adapting our adenovirus labeling system for clinical imaging protocols such as positron emission tomography. This radiological imaging method is routinely used in the clinic for highly sensitive diagnosis of disease with no limits on signal depth. Recently, herpes simplex virus (HSV) thymidine kinase (TK) has been proposed as a molecular probe for assessing transgene expression *in vivo* and particularly for use in patients. Pursuing the application of our adenoviral imaging system for whole body imaging in clinical scenarios, we incorporated HSV TK onto pIX. Western blot analysis of the Ad-wt-IX-TK virus gradient shows that both the mature and immature virus particles are labeled with pIX-TK (Fig. 13A). A cell killing MTS assay with gancyclovir indicated that TK fused to pIX retains it enzymatic function to convert the prodrug to its toxic derivative. This conversion yielded enhanced cell killing comparable to the control Ad-wt-E3-TK while the negative control Ad-wt-E3-CD did not show additional cell killing when the drug was added (Fig. 13B). **These data establish the potential to adapt our adenovirus imaging system for PET imaging and warrant further validation of this**

A

B

Figure 13. Labeling adenovirus with PET imaging pIX-TK.
A, Western blot analysis of fractionated CsCl viral gradient of Ad-wt-IX-TK.   **B**,   Cell killing assay with Ad-wt-E3-CD (negative control), Ad-wt-E3-TK (positive control), and Ad-wt-IX-TK.   Four days post-infection and adding gancyclovir (GCV) to the culture medium (white bar = no drug, black bar = 1 mM GCV), cell viability was determined with an MTS assay. Results are presented as percent of non-infected cells. Notice cell killing due to replication alone of the virus (Ad-wt-E3-CD bars). Note enhanced killing due to GCV conversion in addition to replication induced cytoxicity observed with Ad-wt-E3-TK and Ad-wt-IX-TK

Key Research Accomplishments

- Adenovirus can be labeled at capsid protein pIX with EGFP, RFP, Luc and HSV-tk.

- Capsid incorporated label provides the basis of dynamic/real time imaging analysis via optical, light-based and PET imaging modalities.

Reportable Outcomes
Li J, Le L, Sibley DA, Mathis JM, Curiel DT. Genetic incorporation of HSV-1 thymidine kinase into the adenovirus protein IX for functional display on the virion. Virology. 2005 Jul 1; [Epub ahead of print].

Conclusion
Our preliminary data establish a number of important key points. Foremost, these results show that adenovirus can be genetically labeled with a fluorescent structural fusion protein through a complete replacement with IX-EGFP in a chimeric context. At least for our pIX-EGFP strategy, the label was incorporated into virions conferring a fluorescent property that allowed detection of individual particles. Ad-IX-EGFP binding and infection could both be detected via the fluorescent label. This capsid-labeling system is applicable to CRAds because it slightly decreased progeny yield but did not affect the cytopathic effect and spread of the virus. Notably, the level of pIX-EGFP fluorescence directly correlated with the amount of progeny production due to its dependence on E1 activity for expression. The data with pIX-EGFP fulfills all the requirements of the ideal monitoring system for CRAds except noninvasive detection which we propose to accomplish. **Both our proposed capsid-labeling approaches demonstrate great promise for detection of viral replication and spread and hence monitoring of CRAds**.

Appendix

Publications

1. Li J, Le L, Sibley DA, Mathis JM, Curiel DT. Genetic incorporation of HSV-1 thymidine kinase into the adenovirus protein IX for functional display on the virion. Virology. 2005 Jul 1; [Epub ahead of print]

2. Le LP, Rivera AA, Glasgow JN, Ternovoi VV, Wu H, Wang M, Smith BF, Siegal GP, Curiel DT. Infectivity enhancement for adenoviral transduction of canine osteosarcoma cells. Gene Ther. 2006 Mar;13(5):389-99.

3. Le LP, Le HN, N elson AM, Yamamoto M, Curiel DT. Core labeling of adenovirus with EGFP. Submitted 2005.

ELSEVIER

Genetic incorporation of HSV-1 thymidine kinase into the adenovirus protein IX for functional display on the virion

Jing Li[a], Long Le[a], Don A. Sibley[b], J. Michael Mathis[b], David T. Curiel[a],*

[a]Division of Human Gene Therapy, Departments of Medicine, Pathology, and Surgery, University of Alabama at Birmingham, 901 19th Street South, BMR2-508, Birmingham, AL 35294-2172, USA
[b]Gene Therapy Program, Department of Cellular Biology and Anatomy, LSU Health Sciences Center, Shreveport, LA 71130, USA

Abstract

Adenoviral vectors have been exploited for a wide range of gene therapy applications. Direct genetic modification of the adenovirus capsid proteins has been employed to achieve alteration of vector tropism. We have defined the carboxy-terminus of the minor capsid protein pIX as a locus capable of presenting incorporated ligands on the virus capsid surface. Thus, we sought to exploit the possibility of incorporating functional proteins at pIX. In our current study, we incorporated the herpes simplex virus type 1 (HSV-1) thymidine kinase (TK) within pIX to determine if a larger protein of this type could retain functionality in this context. Our study herein clearly demonstrates our ability to rescue viable adenoviral particles that display functional HSV-1 TK as a component of their capsid surface. DNA packaging and cytopathic effect were not affected by this genetic modification to the virus, while CAR-dependent binding was only marginally affected. Using an in vitro [^{3}H]-thymidine phosphorylation assay, we demonstrated that the kinase activity of the protein IX-TK fusion protein incorporated into adenoviral virions is functional. Analysis of cell killing after adenovirus infection showed that the protein IX-TK fusion protein could also serve as a therapeutic gene by rendering transduced cells sensitive to gancyclovir. Using 9-[4-[^{18}F]-fluoro-3-(hydroxymethyl)butyl]guanine ([^{18}F]-FHBG; a positron-emitting TK substrate), we demonstrated that we could detect specific cell binding and uptake of adenoviral virions containing the protein IX-TK fusion protein at 1 h post-infection. Our study herein clearly demonstrates our ability to rescue viable adenoviral particles that display functional HSV-1 TK as a component of their capsid surface. The alternative display of HSV-1 TK on the capsid may offer advantages with respect to direct functional applications of this gene product. In addition, the determination of an expanded upper limit of incorporable proteins on pIX highlights its unique utility as a locus for placement of functional vector constructs.
© 2005 Published by Elsevier Inc.

Keywords: HSV-1 thymidine kinase; Adenovirus protein IX; Thymidine kinase

Introduction

Adenoviral vectors have been exploited for a wide range of gene therapy applications (Glasgow et al., 2004). This utility derives from the unparalleled efficiency of gene transfer for both in vitro and in vivo delivery contexts (Mizuguchi and Hayakawa, 2004). Additional advantages derive from the plasticity of the adenoviral system, which permits directed vector modification for the achievement of selected functional gains (Rots et al., 2003). In this regard, genetic modification of the capsid proteins has been employed to achieve alteration of vector tropism for

targeting purposes (Everts and Curiel, 2004). In addition, selected capsid engineering steps have proved a useful means to circumvent the host anti-vector immune response directed against antigenic epitopes (Wu et al., 2002). More recently, the incorporation of the imaging motif enhanced green fluorescent protein (EGFP) (Le et al., 2004; Meulenbroek et al., 2004) has introduced the concept that functional motifs can be incorporated within the adenoviral capsid, thereby expanding the repertoire of utilities potentially combined within a single vector particle.

The basis of this evolving paradigm stems from the recent identification of capsid locales permissive of incorporating larger and/or more complex protein moieties (Volpers and Kochanek, 2004). In this regard, previous reports have defined clear size limits with respect to heterologous proteins incorporable at the major capsid proteins (Belousova et al., 2002; Pereboeva et al., 2004), which effectively limited the repertoire of capsid-incorporated motifs to small linear peptides. Our more recent work has defined the carboxy-terminus of the minor capsid protein pIX as a locus capable of presenting incorporated ligands on the virus capsid surface (Dmitriev et al., 2002). Of note, we have shown the pIX-incorporated EGFP is fully functional, allowing visualization of labeled viral particles for analytical purposes (Le et al., 2004).

Based on these established feasibilities, we sought to exploit the possibility of incorporating additional functional proteins at the capsid protein pIX. In this context, herpes simplex virus type 1 (HSV-1) thymidine kinase (TK) has been utilized both for molecular chemotherapy cancer gene therapy applications and as an agent in PET-based imaging schemas (Herschman, 2002). In our current study, we sought to incorporate HSV-1 TK within pIX to determine

if a larger protein of this type could retain functionality in this context. Our study herein clearly demonstrates our ability to rescue viable adenoviral particles that display functional HSV-1 TK as a component of their capsid surface. The alternative display of HSV-1 TK on the capsid may offer advantages with respect to direct functional applications of this gene product. In addition, the determination of an expanded upper limit of incorporable proteins on pIX highlights its unique utility as a locus for placement of functional vector components.

Results

Construction of Ad-wt-pIX-TK

An E3-deleted adenovirus shuttle plasmid was constructed containing a pIX-TK carboxy-terminal fusion gene in place of wild-type pIX. Between the pIX and TK coding regions, we incorporated an 18 amino acid linker, SAD-DYKDDDDKLAGSGSG, containing the octapeptide DYKDDDDK FLAG-tag sequence. This shuttle plasmid was used to construct an E3-deleted adenovirus (Ad-wt-pIX-TK; Fig. 1A), which was successfully rescued. As a control, an E3-deleted adenovirus vector was constructed, which contained the TK gene replacing the E3 region, under regulation by the adenovirus early gene promoter (Ad-wt-E3-TK; Fig. 1B). As additional controls, an E3-deleted adenovirus vector, which lacked any TK gene, was constructed (Ad-wt-dE3; Fig. 1C), as was an E3-deleted adenovirus vector, which contained the CD gene replacing the E3 region, under regulation by the adenovirus early gene promoter (Ad-wt-E3-CD; Fig. 1D).

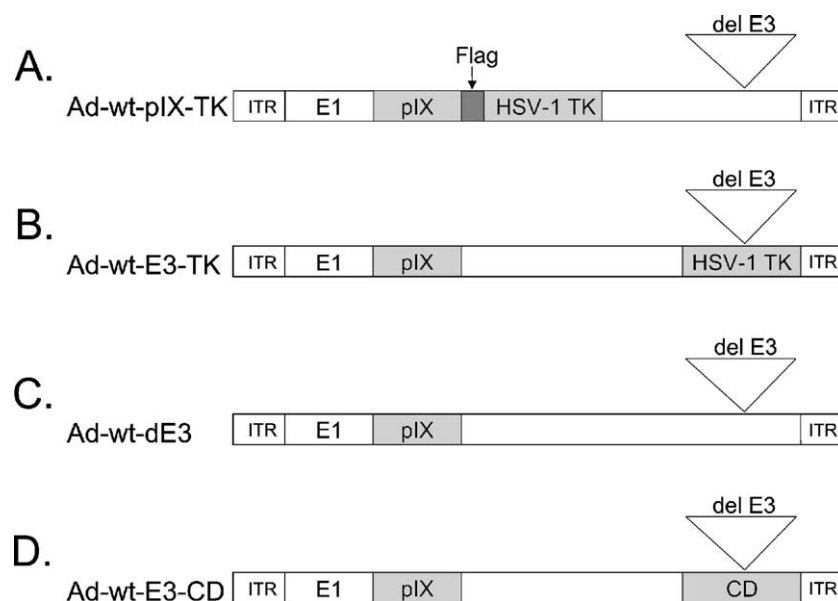Fig. 1. Recombinant adenovirus constructs. (A) Ad-wt-pIX-TK, an Ad5 construct containing a pIX-TK fusion protein, (B) control virus Ad-wt-E3-TK, an Ad5 construct containing HSV-1 TK in place of the Ad E3 gene, (C) control virus Ad-wt-dE3, a wild-type Ad5 in which the E3 gene has been deleted, (D) control virus Ad-wt-E3-CD, an Ad5 construct containing cytosine deaminase in place of the Ad E3 gene.

Incorporation of pIX-TK into Ad-wt-pIX-TK particles

Propagated Ad-wt-pIX-TK was purified by double CsCl ultracentrifugation where the top and bottom bands were preserved. The resulting gradient of virus was fractionated and analyzed for DNA content by absorbance at 260 nm. A major DNA content peak was present in the bottom band where mature, infectious virions normally migrate, as well as a minor peak where immature, empty virions normally migrate (Fig. 2A). Infectious, mature Ad-wt-pIX-TK particles were present in the bottom band as indicated by an infectivity peak in a c.p.e. assay (data not shown). The same gradient fractions of Ad-wt-pIX-TK were also analyzed with Western blots using a FLAG-tag antibody. As shown in Fig. 2B, accumulations of pIX-TK were detected in both the top and bottom band regions for Ad-wt-pIX-TK, confirming the co-localization of pIX-TK with the virions.

Cytopathic effect of Ad-wt-pIX-TK

To quantitatively evaluate viral cytotoxicity, survival of 911 cells after infection with Ad-wt-pIX-TK, and control Ad-wt-E3-TK and Ad-wt-dE3 viruses (at 0.01, 0.1, and 1.0 infectious units (i.f.u.)/cell), were monitored over 10 days (Fig. 3). On days 0, 2, 4, 6, 8, and 10, the cytopathic effect of the virus was quantitated using a non-radioactive cell proliferation MTS assay. In all concentrations of virus used, Ad-wt-pIX-TK cytopathic effect on 911 cells was the same as that of both Ad-wt-E3-TK and Ad-wt-dE$_3$. These

findings indicate that pIX-TK incorporation did not affect the cytopathic capacity and lateralization of the virus.

CAR-dependent binding of Ad-wt-pIX-TK

The coxsackie adenovirus receptor binding ability of Ad-wt-pIX-TK was determined by allowing the virus to bind to cells and quantitating the bound virus with TaqMan quantitative real-time PCR (Fig. 4). Ad-wt-pIX-TK binding to CAR (+) A549 cells was much higher than that of CAR (−) CHO cells. In addition, recombinant fiber-knob block mitigated the CAR-dependent binding of Ad-wt-pIX-TK to A549 cells. Blocking had no effect on the binding of Ad-wt-pIX-TK to CHO cells. Overall, Ad-wt-pIX-TK appeared to show similar binding compared to Ad-wt-E3-TK; in addition, the CAR-dependent binding trend was very similar between Ad-wt-pIX-TK and Ad-wt-E3-TK. These results indicate that the capsid fusion protein label did not interfere with the ability of Ad-wt-pIX-TK to recognize its primary receptor CAR.

Thermostability of Ad-wt-pIX-TK

Modification of pIX may destabilize the capsid structure; comparing the thermostability of Ad-wt-pIX-TK to that of control Ad-wt-E$_3$-TK assessed this possibility. Virus samples were incubated at 45 °C for various time periods and then quantitated in terms of infectious titer (Fig. 5). Up to 5 min of incubation, the infectious titer of Ad-wt-pIX-TK remained the same as that of control. After 5 min of
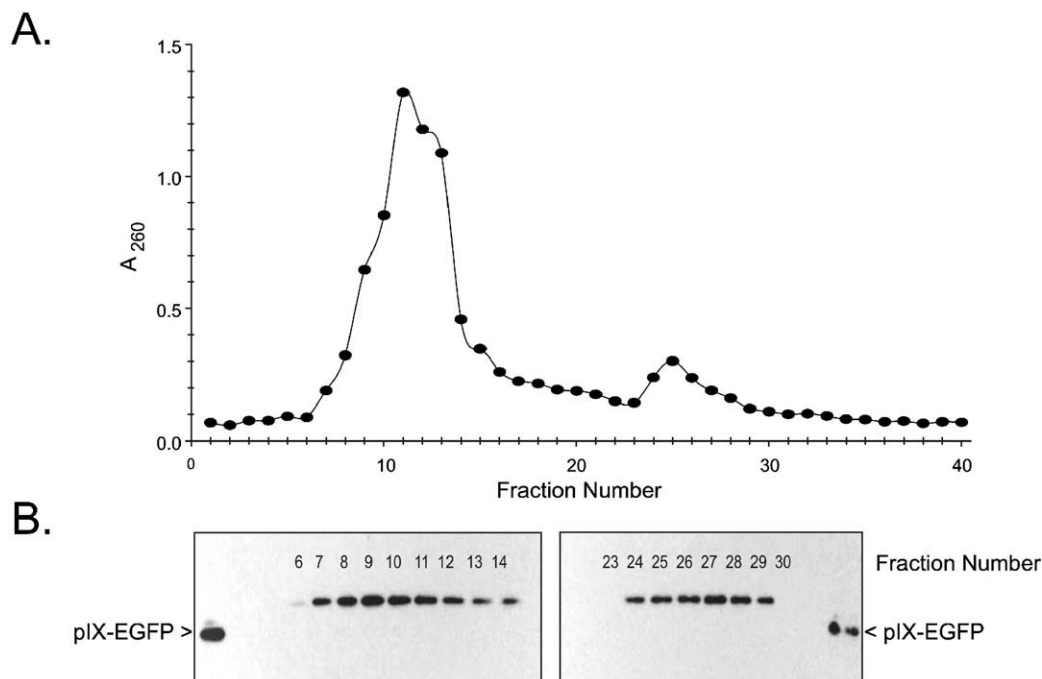
Fig. 2. CsCl gradient fraction DNA content and Western blot followed double ultracentrifugation. (A) DNA content of individual fractions (●) of Ad-wt-pIX-TK was determined by measuring absorbance at 260 nm. (B) Individual fractions were analyzed for pIX-TK fusion protein using an anti-Flag antibody following SDS–PAGE and transfer to PVDF membranes.
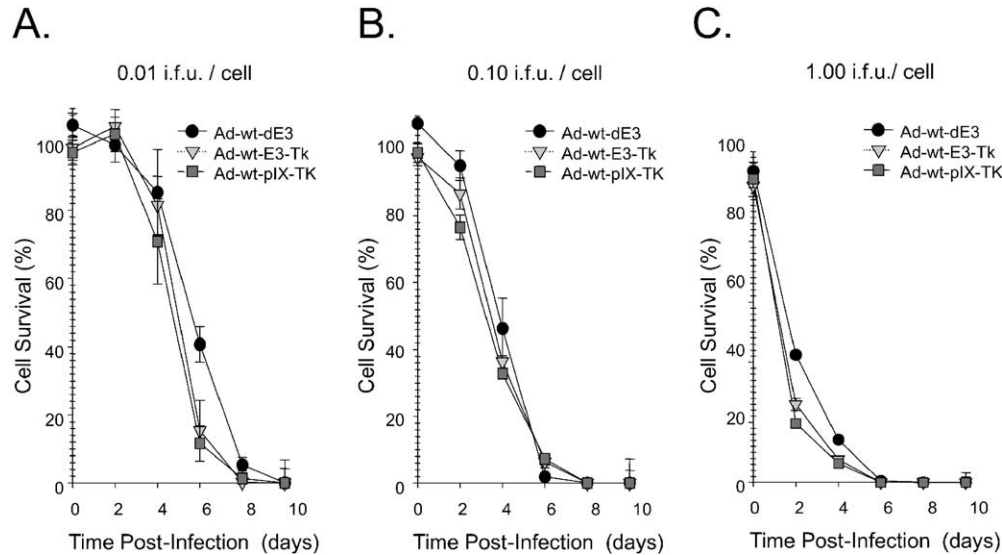
Fig. 3. Cytopathic effect. The cytopathic effect of Ad-wt-dE3 (●), Ad-wt-E3-TK (▽), and Ad-wt-pIX-TK (■) in 911 cells was determined at three different multiplicities of infection: (A) 0.01 i.f.u., (B) 0.1 i.f.u., and (C) 1.0 i.f.u. Cytotoxicity measured by non-radioactive MTS proliferation assay and expressed as percent of survival cells (mean ± standard deviation of three replicates).

incubation, the infectious titer for Ad-wt-pIX-TK and Ad-wt-E3-TK was about 60% and 80% of initial titers. Viral titers continued to decrease between 10 and 20 min of incubation, and the titers of Ad-wt-pIX-TK and Ad-wt-E3-TK were not significantly different from each other. These results indicate that the TK addition to pIX did not affect the thermostability of Ad-wt-pIX-TK following exposure of the virus to high temperature compared to a virus containing wild-type pIX.
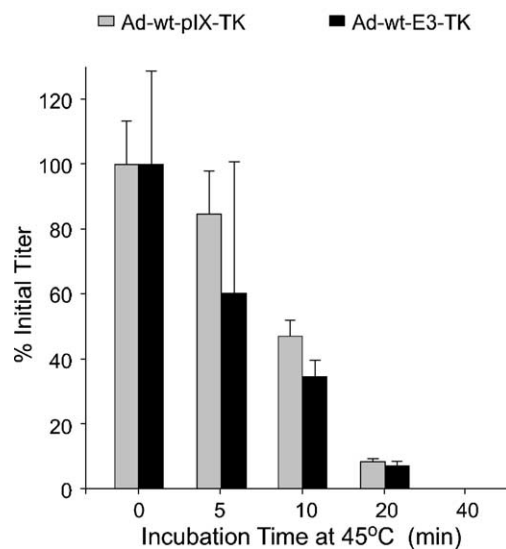
Fig. 4. Car-dependent binding of Ad-wt-pIX-TK compared to Ad-wt-E3-TK. After binding and infection of 2×10^5 CHO (CAR-negative) or 2×10^5 A549 (CAR-positive) cells with 1×10^9 i.f.u. virus, Ad-wt-E3-TK (■) and Ad-wt-pIX-TK (■) viral replications were quantitated by real-time PCR of E4 transcripts as described in Materials and methods (values are expressed as mean ± standard deviation of three replicates). Duplicate groups were initially blocked with recombinant fiber knob prior to binding and infection with Ad-wt-E3-TK (□) or Ad-wt-pIX-TK (■).

GCV cytotoxicity assays

In order to determine the growth characteristics of cells treated with a pharmacologic concentration of GCV, 911 cells were initially infected with increasing doses of Ad-wt-pIX-TK ranging from 10 to 1000 v.p./cell. As controls, 911 cells were incubated with increasing doses of either Ad-wt-E3-TK or Ad-wt-E3-CD. At 12 h post-infection, the cells were incubated in the absence or presence of 1.0 mM GCV for 4 days, and cell viability was determined using an MTS assay. As anticipated (Fig. 6), incubation of the cells with increasing doses of any of the adenoviruses resulted in a cytopathic
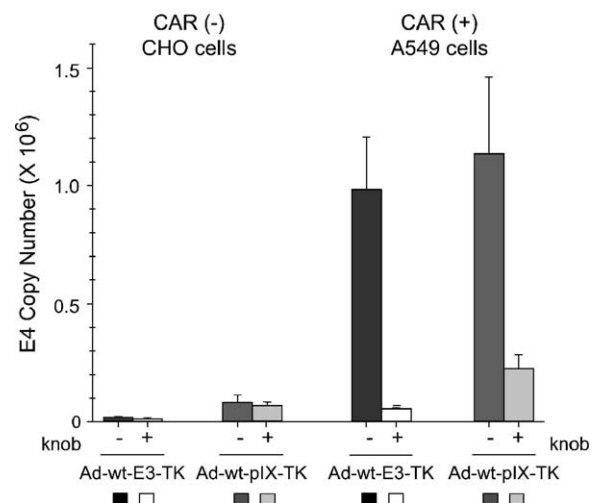
Fig. 5. Thermostability of Ad-wt-pIX-TK compared to Ad-wt-E3-TK. The thermostability of both of Ad-wt-pIX-TK (■) and Ad-wt-E3-TK (■) was determined. Both viruses were incubated at high temperature for various time periods and quantitated by infecting in terms of infectious titer as described in Materials and methods (values are expressed as mean ± standard deviation of three replicates).
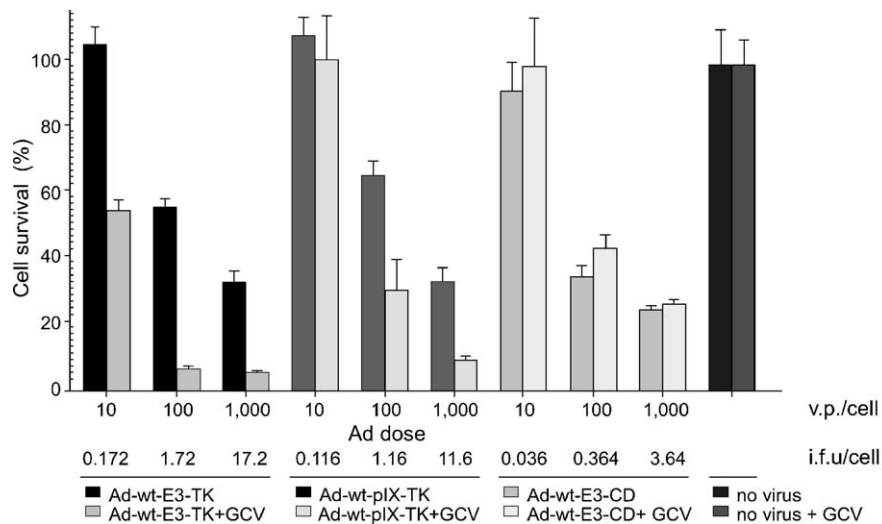
Fig. 6. Cell killing with increasing doses of virus in the absence or presence of GCV. A cell-killing assay was used to determine cell survival after infection with Ad-wt-E3-CD (at 10, 100, and 1000 v.p./cell), Ad-wt-E3-TK (at 10, 100, and 1000 v.p./cell), or Ad-wt-pIX-TK (at 10, 100, and 1000 v.p./cell). At 12 h post-infection, the cells were incubated in the absence or presence of 1.0 mM GCV for 4 days, and cell viability was determined using an MTS assay. The values are expressed as mean ± standard deviation of three replicates. Titers for the viruses were: Ad-wt-E3-TK, 58.0 v.p./i.f.u.; Ad-wt-pIX-TK, 86.0 v.p./i.f.u.; and Ad-wt-E3-CD, 274 v.p./i.f.u.

effect in the 911 cells. Importantly, however, treatment with GCV caused an increased cytopathic effect in cells infected with either Ad-wt-pIX-TK or with Ad-wt-E3-TK. In cells infected with Ad-wt-E3-CD, however, no additional cytopathic effect was observed by the addition of GCV.

Cells infected with Ad-wt-E3-TK appeared to be more sensitive to the effect of GCV than cells infected with Ad-wt-pIX-TK; doses at 10 v.p./cell and at 100 v.p./cell, a greater cytopathic effect was detected in GCV-treated cells previously infected with Ad-wt-E3-TK than with Ad-wt-pIX-TK. This observation could be due to a difference in TK gene expression in cells infected with Ad-wt-E3-TK compared to cells infected with Ad-wt-pIX-TK. Alterna-

tively, this observation could be due to differences in enzymatic activity between the wild-type TK and the pIX-TK fusion protein. To differentiate between these two possibilities, real-time RT-PCR was used to assess TK RNA levels in total RNA isolated from 911 cells infected with equivalent infectious amounts of either Ad-wt-E3-TK (0.1 i.f.u./cell) or Ad-wt-pIX-TK (0.1 i.f.u./cell). The results of this assay detected an 18-fold relative increase in TK expression in cells infected for 2 days with Ad-wt-E3-TK compared to cells infected with Ad-wt-pIX-TK (data not shown).

In the experiment shown in Fig. 7, the cells were initially infected as before for 12 h with Ad-wt-pIX-TK ranging
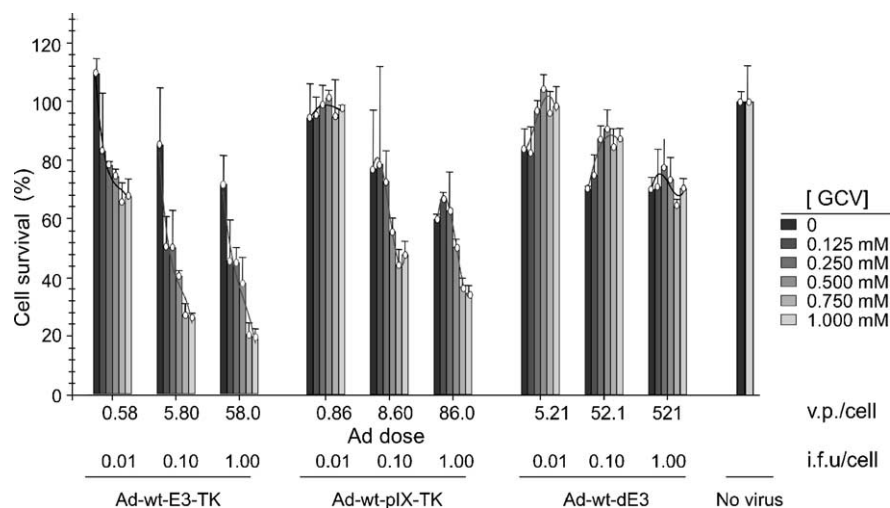
Fig. 7. Cell killing with virus and increasing doses of GCV. A cell-killing assay was used to determine cell survival after infection with Ad-wt-dE3 (at 0.01, 0.1, and 1.0 i.f.u./cell), Ad-wt-E3-TK (at 0.01, 0.1, and 1.0 i.f.u./cell), or Ad-wt-pIX-TK (at 0.01, 0.1, and 1.0 i.f.u./cell). At 12 h post-infection, the cells were incubated in the presence of GCV at 0 (■), 0.125 (■), 0.250 (■), 0.500 (■), 0.750 (■), and 1.00 mM (□) for 4 days, and cell viability was determined using an MTS assay. The values are expressed as mean ± standard deviation of three replicates. Titers for the viruses were: Ad-wt-E3-TK, 58.0 v.p./i.f.u.; Ad-wt-pIX-TK, 86.0 v.p./i.f.u.; and Ad-wt-dE3, 521 v.p./i.f.u.

from 0.01 to 1.0 i.f.u./cell. As controls, 911 cells were incubated with increasing doses of either Ad-wt-E3-TK or Ad-wt-dE3. The cells were then incubated with a variety of concentrations of GCV (ranging from 0.125 to 1.0 mM) for 4 days, and cell viability was determined by MTS assay. The viability of cells infected with either Ad-wt-pIX-TK or with Ad-wt-E3-TK was inhibited at similar concentrations (ED_{50} at approximately 0.5 mM). By contrast, the viability of cells infected with Ad-wt-dE3 showed no growth inhibition from any concentration of GCV. These results demonstrate that the wild-type TK and the pIX-TK fusion proteins had similar activities on growth inhibition in the presence of GCV.

HSV-1 TK enzymatic activity

HSV-1 TK enzymatic activity associated with the purified Ad-wt-pIX-TK virions was determined by monitoring the incorporation and conversion of [^{3}H]-thymidine substrate into the phosphorylated product (Fig. 8). In these experiments, enzymatic activity of the pIX-TK protein incorporated into virions was determined directly in vitro. As shown in Fig. 8A, incubation of [^{3}H]-thymidine with increasing amounts of purified Ad-wt-pIX-TK virus in vitro for 35 min resulted in conversion of up to 40.7% [^{3}H]-thymidine into the phosphorylated form. Importantly, Ad-wt-E3-TK showed minimal conversion of [^{3}H]-thymidine (0.23%) at the highest amount of purified virus used. To confirm these results, at time course analysis was performed from 5 to 40 min with various amounts of purified Ad-wt-pIX-TK virus. As shown in Fig. 8B, a time-dependent increase in substrate conversion was observed with hyper-

bolic kinetics. Together, these results demonstrate that the kinase activity of the pIX-TK fusion protein incorporated into adenoviral virions is functional.

MicroPET analysis of Ad-infected HEK293 cells

In order to determine the feasibility of using the pIX-TK fusion protein incorporated within the Ad virions as a reporter gene for microPET, Ad-wt-pIX-TK and a control Ad-wt-E3-TK were used to infect HEK293 cells. To preclude de novo protein pIX-TK synthesis, HEK293 cells were infected for only 1 h prior to microPET scanning. In the experiment shown in Fig. 9B, three 60-mm tissue culture dishes were plated 12 h previously with 1×10^6 of the HEK293 cell line. On the day of microPET scanning, to each of the dishes was added 50 mCi of [^{18}F]-FHBG. Immediately thereafter, to one dish was added 1×10^9 v.p. of Ad-wt-pIX-TK, to a second dish was added 1×10^9 v.p. of Ad-wt-dE3, and to a third dish was added virus buffer alone. The dishes were incubated for 1 h at 37 °C, followed by three washes with 5 ml of PBS. The three dishes were then stacked and placed in the microPET scanner (Fig. 9A), and image data were acquired for 15 min. In the dish corresponding to cells infected with Ad-wt-pIX-TK, specific labeling and incorporation were observed in the region of the tissue culture dish with cell adherence (Fig. 9B). In contrast, in the dish corresponding to cells infected with Ad-wt-E3-TK, only non-specific labeling was observed in the edges of the tissue culture dish; this pattern was also observed in the dish corresponding to uninfected cells. These results confirm the utility of the pIX-TK fusion protein for and form the foundation for further investigation
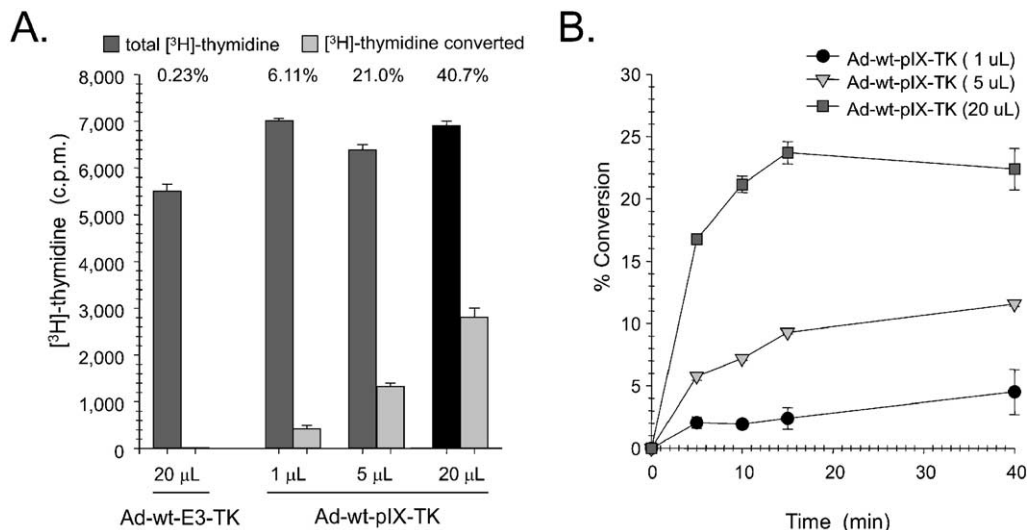
Fig. 8. Characterization of in vitro TK activity in Ad-wt-pIX-TK virions. Using purified Ad virions, TK activity was determined in vitro by the amount of phosphorylation of ^{3}H-thymidine after 35-min incubation. (A) Conversion assay using purified Ad-wt-E3-TK (as a negative control) or increasing amounts of Ad-wt-pIX-TK (1 μL, 1.6×10^9 v.p.; 5 μL, 8×10^9 v.p.; 20 μL, 3.2×10^{10} v.p.). The dark grey bars indicate the mean ± standard deviation of three replicate amounts of labeled ^{3}H-thymidine substrate added for reaction. The light grey bars indicate mean ± standard deviation of three replicate recoveries of the phosphorylated ^{3}H-thymidine product. Percent conversions are shown above. (B) Time course of phosphorylation of ^{3}H-thymidine in vitro using increasing amounts of Ad-wt-pIX-TK: (●) 1 μL- 1.6×10^9 v.p., (▽) 5 μL- 8×10^9 v.p., and (▨) 20 μL- 3.2×10^{10} v.p. The values are expressed as mean ± standard deviation of three replicates.
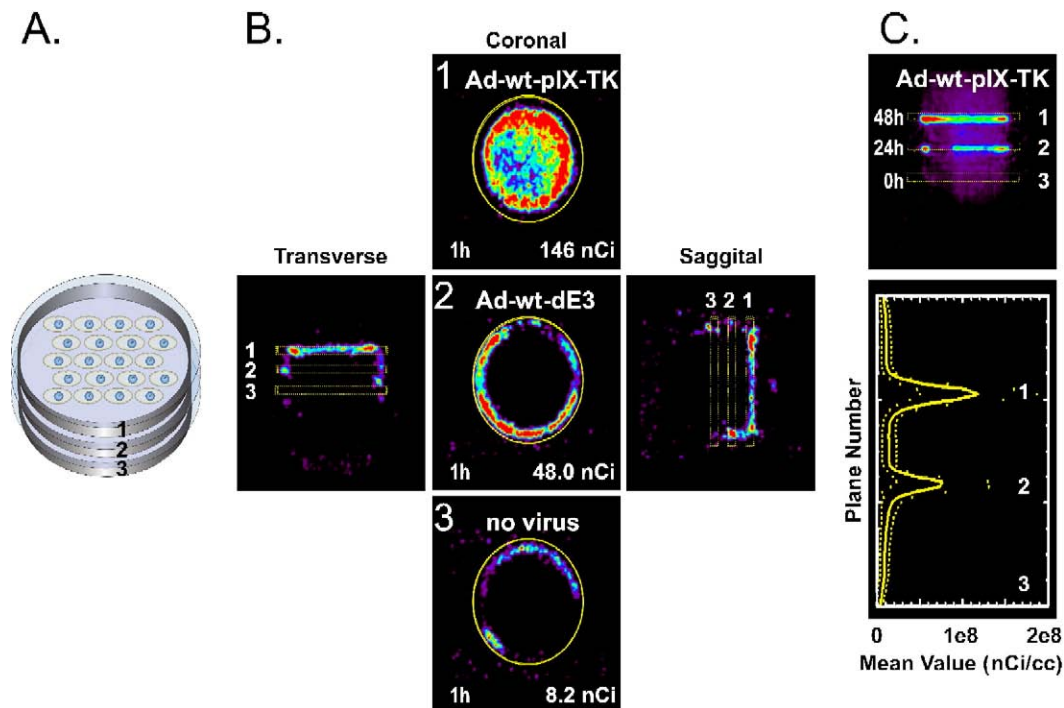
Fig. 9. MicroPET scan of tissue culture dishes plated with HEK293 cells. (A) Three dishes were stacked and placed in the microPET scanner. (B) Cells in dish 1 were simultaneously infected with Ad-wt-pIX-TK and labeled [^{18}F]-FHBG; cells in dish 2 were simultaneously infected with Ad-wt-dE3 and labeled [^{18}F]-FHBG; uninfected cells in dish 3 were labeled [^{18}F]-FHBG. The dishes were incubated for 1 h followed by 15 min of data acquisition. Shown are images of equivalent regions of interest from transverse, coronal, and sagittal planes through the dishes. (C) Cells in dish 1 were infected for 48 h with Ad-wt-pIX-TK; cells in dish 2 were infected for 24 h with Ad-wt-pIX-TK; cells in dish 3 were uninfected. The dishes were labeled with [^{18}F]-FHBG for 1 h followed by 15 min of data acquisition. Shown is an image of a transverse plane through the dishes and plot of the coronal plane number in the scan versus the mean ± standard deviation of [^{18}F] activity in each coronal plane.

of [^{18}F]-FHBG of noninvasive and repeated imaging of Ad-wt-pIX-TK in vivo with PET. However, since the [^{18}F]-FHBG and the virus were added simultaneously, this experiment does not differentiate between the possibilities that [^{18}F]-FHBG was phosphorylated extracellularly by the Ad-wt-pIX-TK virus which subsequently diffused into the cell or that [^{18}F]-FHBG was phosphorylated intracellularly.

To confirm that [^{18}F]-FHBG is phosphorylated intracellularly, three 60-mm tissue culture dishes were plated with 1×10^6 of the HEK293 cell line and infected with Ad-wt-pIX-TK for 24 or 48 h prior to labeling. At 12 h after plating, one dish was infected with 1×10^9 v.p. (1.1×10^7 i.f.u.) of Ad-wt-pIX-TK. Likewise at 36 h after plating, one dish was infected with an equivalent amount of Ad-wt-pIX-TK. A third dish remained uninfected. At 60 h after plating (i.e., 48 h, 24 h, and 0 h post-infection with Ad-wt-pIX-TK), 50 mCi of [^{18}F]-FHBG was added to each of the dishes. The dishes were incubated for 1 h at 37 °C, followed by three washes with 5 ml of PBS. The three dishes were then stacked and placed in the microPET scanner (Fig. 9A), and image data were acquired for 15 min. In the dish corresponding to cells infected for 48 h with Ad-wt-pIX-TK, specific labeling and incorporation were observed in the region of the tissue culture dish with cell adherence (Fig. 9C). Similar labeling was observed in the dish corresponding to cells infected for 24 h with Ad-wt-pIX-TK.

Importantly, in the dish corresponding to uninfected cells, no labeling was observed. These results confirm that [^{18}F]-FHBG is phosphorylated intracellularly in cells infected with Ad-wt-pIX-TK.

Discussion

We have shown herein that our novel pIX-TK labeling strategy for adenoviruses only marginally affected DNA packaging and thermostability while maintaining DNA replication, viral cytopathic effect/lateralization, and CAR-dependent binding. Most importantly, the pIX-TK label associated with the capsid demonstrated direct TK activity in vitro in progeny virions as hypothesized. In addition, infection of cells with an adenovirus containing the pIX-TK fusion protein resulted in TK activity in cells with similar activities on growth inhibition in the presence of GCV as wild-type TK. In total, these data clearly establish the functionality of the HSV-1 TK when incorporated into the adenovirus capsid at the pIX locale.

The strategy we pursued involved the fusion of HSV-1 TK with the capsid protein pIX. The reasons for selecting this locale include: (1) its function as a minor capsid protein that is not absolutely required for replication, (2) its externally exposed carboxy-terminus to which proteins

may be fused without affecting the interior of the capsid, and (3) its distant location in the hexon group of nine, which would not affect the penton base as well as the fiber-knob (Parks, 2005). The carboxy-terminus of pIX has now been defined as a locus capable of presenting incorporated ligands on the virus capsid surface (Campos et al., 2004; Pereboeva et al., 2004; Vellinga et al., 2004). More recently, the pIX-incorporated EGFP has been shown to be fully functional, allowing visualization of labeled viral particles for analytical purposes (Le et al., 2004; Meulenbroek et al., 2004). The results of our current work on the pIX-TK construct mark the largest fusion protein yet achieved in the context of adenoviral capsid proteins, with the 375 amino acid TK protein sequence and an 18 amino acid linker sequence added to the carboxy-terminus of the 140 amino acid pIX protein sequence. Thus, we have expanded the upper limit to pIX fusion proteins, a size that has not yet to be defined, and may be limited only by the size of the adenoviral genome that can be incorporated into the virion capsid.

We have shown herein that the pIX-TK labeling strategy can be used to detect specific viral uptake in cells using $[^{18}F]$-FHBG by noninvasive imaging with microPET. One of the most sensitive paradigms for gene transfer in vivo imaging is the HSV-1 TK system (Blasberg, 2002). TK catalyzes phosphorylation of the substrate, which becomes trapped intracellularly. With an ^{18}F positron emitting substitution, it is possible to determine TK substrate incorporation into cells by PET. PET is the current paradigm for sensitivity to molecular events with in vivo imaging, and animal microPET systems are now available providing greater than 1-mm resolution (Weber and Bauer, 2004). MicroPET is ideally suited to imaging molecular events in animal studies because of its sensitivity and because the animals can be repeatedly scanned to follow the course of the disease (Luker et al., 2003). The utility of the HSV-1 TK reporter gene technology has been demonstrated in vivo using cancer xenografts models, in which microPET and $[^{18}F]$-FHBG have been used to visualize and monitor tumor progression (Yaghoubi et al., 2005). In addition, microPET offers the advantage of 3D tomographic image reconstruction over that of fluorescence or bioluminescence imaging technologies.

Preclinically, microPET has been particularly useful in monitoring extracellular receptor expression and in monitoring the efficacy of gene delivery in mouse models (Chen et al., 2004a). This method of in vivo detection has been successfully used in mouse models. Injection of mice with an Ad vector expressing HSV-1 TK (or an empty control vector with no transgene) followed by PET imaging has shown specific accumulation of ^{18}F-labeled gancyclovir in the liver (the major site of infection of the recombinant adenovirus) (Chen et al., 2004b). In contrast, injection of mice with a control vector has shown no accumulation of label in the liver. PET technology offers the unique opportunity to monitor delivery and uptake of the label in

vivo and to be able to predict and modify the treatment. In oncology studies, PET provides a direct, whole body assessment of the tumor size and the pattern of distribution in normal and tumor tissues (Hustinx et al., 2002). This is particularly important in developing human clinical trials, where the use of PET imaging using $[^{18}F]$-fluorodeoxyglucose ($[^{18}F]$-FDG) is already a clinically established technique for the staging and follow-up of a wide variety of neoplasms (Alavi et al., 2004). Recently, HSV-1 TK has been proposed as a molecular probe for assessing transgene expression in vivo and particularly for use in patients (Jacobs et al., 2001).

While noninvasive imaging of adenoviral vector biodistribution poses formidable challenges, our genetic adenovirus pIX-TK labeling system may have an important impact in the field of adenoviral virotherapy. Virotherapy exploits the lytic property of virus replication to kill tumor cells (Ries and Brandts, 2004). Because this approach relies on viral replication, the virus can self-amplify and spread in the tumor from an initial infection of only a few cells (Kirn, 2000). Although early attempts were abandoned because of toxicity and inefficacy (Sinkovics and Horvath, 1993), the virotherapy approach has reemerged with great promise, in large part, due to better understanding of virus biology and the ability to genetically modify viruses (Everts and Van der Poel, 2004). In particular, conditionally replicative adenoviruses (CRAds) have been modified to be selective for tumor cells (Oosterhoff and van Beusechem, 2004). The potential of CRAds to be the next cancer therapy breakthrough has been substantiated by their rapid translation into human clinical trials (Nettelbeck, 2003). All of the initial CRAd clinical trials have validated the safety of using oncolytic adenoviruses for cancer therapy. Yet what these trials failed to ascertain and what remain to be rigorously determined are the crucial functions of CRAds: (1) selective replication and killing, (2) robustness of replication, and (3) spread of the virus.

Limited understanding of CRAd behavior is attributed to lack of a noninvasive imaging system for monitoring replicative agents. Several studies have attempted to address this problem, using reporter genes such as green fluorescent protein (GFP) (Yang et al., 2000), SSTR-2 (somatostatin receptor type 2) (Zinn et al., 2000), sodium iodide symporter (Cho et al., 2002), luciferase (Bhaumik and Gambhir, 2002), and HSV-1 TK (Liang et al., 2002) incorporated into oncolytic viruses. Detection was restricted to infected cells expressing the reporter gene, which does not truly represent the physical biodistribution of the virus itself. Conventional imaging systems for gene therapy have been designed for the detection of transgene expression of such reporters, which correlated with therapeutic outcome but could not show viral localization (Min and Gambhir, 2004).

Despite their utility for assessing gene delivery and expression, these reporters by themselves are not suitable for monitoring CRAd activity. The essence of oncolytic

virus function is to infect and kill target cells, a concept that is at odds with reporter gene expression. In addition, reporter gene expression may not truly represent the underlying level of viral replication and the physical distribution of viral progeny. No completed clinical trials so far have incorporated a monitoring component into replicative agents themselves, and therefore have had to rely on conventional histology of biopsy specimens and analysis of body fluids for the detection of virus. Such static assessments fall short of accurately depicting the dynamic mechanism of replicative agents. The ideal system for monitoring CRAds and other oncolytic viruses should provide the flexibility for dynamic detection of both viral replication and spread to yield valuable and meaningful data.

Our results confirm the utility of the pIX-TK fusion protein for and form the foundation for further investigation of [^{18}F]-FHBG for noninvasive and repeated imaging of Ad-wt-pIX-TK in vivo with PET technology. To this end, our pIX-TK genetic adenovirus capsid labeling system may offer unprecedented noninvasive dynamic imaging of CRAd replication and spread. Not only may this tool be indispensable in the preclinical development of advanced generation CRAds, but it may also be practical in the clinical setting to monitor the application of these agents for cancer therapy.

We have shown herein that our novel genetic labeling strategy of a pIX-TK fusion protein resulted in TK activity in cells with similar activities on growth inhibition in the presence of GCV as wild-type TK. One of the most promising cancer gene therapy systems involves the use of suicide gene therapy. At present, many experimental suicide gene therapy approaches using the HSV-1 TK suicide gene therapy model are in clinical trials (Fillat et al., 2003). The HSV-1 TK enzyme is the target of drugs such as acyclovir (ACV) and gancyclovir (GCV). Only cells expressing the HSV-1 TK enzyme produce the monophosphate form of these drugs. The monophosphate is subsequently converted to the highly toxic triphosphate form, which causes inhibition of cellular DNA polymerase and additional genotoxic effects through incorporation into DNA. In the absence of the drug, constitutive expression of the HSV-1 TK gene is not harmful: TK-transduced cells grow normally both in vitro and in vivo. In fact, transgenic mice expressing the HSV-1 TK gene have been produced with no toxicity in the absence of GCV (Tian et al., 2003).

In vitro, cells expressing the Ad-wt-pIX-TK construct were maximally inhibited by GCV in the 0.5 mM range, a level that is readily achieved in patients treated with the drug. These results suggest that suicide gene therapy may represent an attractive adjuvant therapeutic approach using adenoviral vectors modified with a pIX-TK fusion protein and may enhance cell killing using the adenoviral virotherapy approach. A potential advantage of combining the suicide gene therapy approach is that even when less than 100% of the tumor is genetically modified, the entire tumor

mass can be eradicated through the "bystander effect" of TK/GCV gene therapy (van Dillen et al., 2002). Thus, the combination of suicide gene therapy and virotherapy may provide an additional benefit for the pIX-TK fusion protein, together with in vivo imaging by microPET.

Materials and methods

Cell culture

Human embryonic kidney epithelial (HEK293) cells, Chinese hamster ovary (CHO), and human lung adenocarcinoma A549 cells were obtained from and cultured in the medium recommended by the American Type Culture Collection (Manassas, VA). The adenovirus helper cell line 911 (Fallaux et al., 1996) was grown in DMEM supplemented with 10% FBS, 100 IU/mL penicillin, 100 μg/mL streptomycin, and 2 mM L-glutamine. All cell lines were incubated at 37 °C and 5% CO_2 under humidified conditions.

Recombinant adenovirus construction

All viruses were constructed by homologous recombination in *Escherichia coli* using methods previously described (He et al., 1998), using The HSV-1 TK gene from PDC.SSTR.HSV-tk (Zinn et al., 2002) was cut with *Sal*I digestion (and blunt-ended by Klenow filling) followed by *Bgl*II digestion. The excised HSV-1 TK fragment was inserted into an E3-deleted shuttle plasmid pShuttleE3 after digestion with *Kpn*I (and blunt-ended by Klenow filling) and with *Bam*HI to generate pShuttle-E3-HSV1-tk. Homologous recombination was performed with plasmid PTG3602 (containing the wild-type E1, E3 Ad5 backbone) and the resultant recombinant plasmid was linearized with *Pac*I and transfected into 911 cells to generate the Ad-wt-E3-TK control virus. To construct the Ad-wt-pIX-TK virus, the HSV-1 TK gene was inserted in-frame at the carboxyl terminus of the adenovirus protein IX gene (*Nhe*I site) within pShuttle.wt.E1-IX-flag (Le et al., 2004) after an 18 amino acid linker, SADDYKDDDDKLAGSGSG, containing the octapeptide DYKDDDDK FLAG-tag sequence. Homologous recombination was performed with the resulting pShuttle.wt.E1-pIX-flag-TK and with plasmid PTG3602AmpF2dE3 (containing the E1, E3 deleted Ad5 backbone) and the resultant recombinant plasmid was linearized with *Pac*I and transfected into 911 cells to generate the Ad-wt-pIX-TK virus.

Virus propagation and purification

Viruses were propagated in 911 cells and HEK293 cells, which do not express wild-type pIX. Viruses were purified by double CsCl ultracentrifugation and dialyzed against phosphate-buffered saline with Mg^{2+}, Ca^{2+}, and 10% glycerol.

Final aliquots of virus were analyzed for viral particle titer (using absorbance at 260 nm) and infectious units (using a plaque forming assay). Viruses were stored at -80 °C until use. Final titers for the viruses were: Ad-wt-E3-TK = 58.0 v.p./i.f.u. (1.26×10^{11} v.p./mL; 2.17×10^9 i.f.u./mL), Ad-wt-pIX-TK = 86.0 v.p./i.f.u. (1.60×10^{11} v.p./mL; 1.86×10^9 i.f.u./mL), Ad-wt-dE3 = 521 v.p./i.f.u. (2.10×10^{12} v.p./mL; 4.03×10^9 i.f.u./mL), and Ad-wt-E3-CD = 274 v.p./i.f.u. (1.60×10^{11} v.p./mL; 5.85×10^8 i.f.u./mL).

Characterization of virus gradient fractions (Western blot and DNA content assay)

After double CsCl ultracentrifugation which was retained through yielding one tube from ten 150-mm tissue culture dishes, the top and bottom bands were collected from the bottom of tube by two drops each sample (~100 µl). Fractionated samples (10 µl) were ethanol precipitated, pelleted, and resuspended with 20 µl RIPA buffer. Samples (10 µl) were resolved with 10% SDS–PAGE and transferred to a PVDF membrane (BioRad, Hercules, CA). Blotting was performed with a primary monoclonal FLAG antibody (1:2000 dilution, SIGMA, F3165) followed by a secondary HRP-linked anti-mouse antibody (1:5000 dilution, Amersham Pharmacia, Piscataway, NJ). Bands were detected using a chemiluminescent ECL kit (Amersham Pharmacia). DNA content was determined by measuring the absorbance at 260 nm (MBA 2000, Perkin-Elmer, Shelton, CT).

Cytopathic effect assay

Five thousand 911 cells were infected with Ad-wt-dE3, Ad-wt-E3-TK, and Ad-wt-pIX-TK (1.0, 0.1, and 0.01 i.f.u./cell) in 100 µl of 5% DMEM medium without phenol red in 96-well plates (six replicates each plus six non-infected cells as control). Cytopathic effect was measured by MTS assay (Promega, Madison, WI) at 0, 2, 4, 6, 8, and 10 days post-infection. Results were calculated as percent of non-infected cells with blank values (medium only) subtracted.

Thermostability assay

Twenty thousand 911 cells were subcultured overnight into 48-well plates with 150 µl DMEM medium containing 5% FBS. Prior to infection, the viruses were incubated for 0-, 5-, 10-, 20-, and 40-min time periods at 45 °C, and subsequently, the heat-treated viruses were used to infect the 911 cells (at a multiplicity of infection of 0.1 i.f.u. units/cell). At 24 h post-infection, the cells were collected for total DNA preparation, and viral replication was determined using TaqMan real-time PCR of adenovirus E4 DNA. Genomic DNA from the cells was isolated and cleaned using a Qiagen Tissue Kit (Qiagen), following the instructions of the manufacturer. The concentration of isolated DNA was determined by spectrophotometry. TaqMan primers and probe design, the forward primer, the reverse primer, and

the 6-carboxyfluorescein-labeled probe to amplify the E4 gene were designed by the Primer Express 1.0 software (Perkin-Elmer, Foster City, CA) following the recommendations of the manufacturer. The sequences of the forward and the reverse E4 primers were 5′-GGAGTGCGCCGAGA-CAAC-3′ (annealing between residues 816 and 833 of the E4 orf6 open reading frame) and 5′-ACTACGTCCGGCGTTC-CAT-3′ (annealing between residues 883 and 865), respectively. The sequence of the TaqMan probe was 5′-TGGCATGACACTACGACCAACACGATCT-3′ (anneals between residues 836 and 863). The HSV-1 TK primer pairs (forward, 5′-GCACGTCTTTATCCTGGATTACG-3′ and reverse, 5′-TGGATCATCCCGGAGGTAAG-3′) and probe (5′-CCGGGACGCCCTGCTGCA-3′) were selected to be unique and non-homologous to any known human sequence. The probes were labeled with a reporter fluorescent dye FAM (6-carboxyfluorescein) at the 5′ end and a quencher-fluorescent dye TAMRA (6-carboxy-tetramethylrhodamine) at the 3′ end.

With optimized concentration of primers and probe, the components of real-time PCR mixtures were designed to result in a master mix with a final volume of 10 µl/reaction containing $1 \times$ Universal PCR Master Mix (Applied Biosystems, Foster City, CA), 100 nM forward primer, 100 nM reverse primer, 1 nM probe, and 0.025% BSA. For the assay, 1 µl of extracted DNA sample was added to 10 µl of PCR mixture in each reaction capillary. A no-template control received 10 µl of reaction mixture with 1 µl of water. All capillaries were then sealed and centrifuged using an LC Carousel Centrifuge (Roche Molecular Biochemicals, Indianapolis, IN) to facilitate mixing. All PCR reactions were carried out using a LightCycler System (Roche Molecular Biochemicals). The thermal cycling conditions were 10 min at 95 °C and 40 cycles of 15 s at 95 °C and 1 min at 60 °C.

Car binding assay

The CHO and A549 cell lines (2×10^5 cells in 100 µl of medium) were incubated at 4 °C with shaking using 100 µl of buffer alone or using 100 µl of buffer containing 2.5 µg/mL recombinant Ad5 fiber knob. After 1 h, viruses were added directly (at a multiplicity of infection of 5000 i.f.u/cell, based on TaqMan real-time PCR E4 DNA copy numbers). Following shaking for another hour at 4 °C, the cells were washed three times with 1% BSA/PBS buffer, collected for total DNA preparation, and then quantitated using TaqMan real-time PCR with E4 primers as described above.

Cell killing assay

Five thousand 911 cells were plated overnight into each well of 96-well tissue culture plates in 100 µl of DMEM medium without phenol red containing 5% FBS. The cells were infected with Ad-wt-dE3, Ad-wt-E3-TK, and Ad-wt-pIX-TK (at 1.0, 0.1, and 0.01 infectious units/cell) using

replicates of three wells and three wells of non-infected cells as a control. At 12 h post-infection, GCV was added to the cells at increasing concentrations (0.125, 0.5, and 1.0 mM). Cell killing was measured by MTS assay (Promega, Madison, WI) at 4 days post-infection. Results were calculated as percent of non-infected cells with blank values (medium only) subtracted.

pIX-TK conversion assay

Conversion of $[^3H]$-thymidine in vitro was analyzed by a modified version of a previously reported protocol (Gerber and Folkers, 1996). Triple sets of reaction mixtures containing 50 mM Tris (pH 7.2), 5 mM ATP, 5 mM $MgCl_2$, 2 mg/mL BSA, and 1 mM of $[^3H]$-thymidine (Sigma-Aldrich, St. Louis, MO), in a final volume of 330 μl, were incubated at 37 °C with increasing amount of purified Ad-wt-pIX-TK (0, 1.6×10^9, 8×10^9, and 3.2×10^{10} v.p.). Three corresponding blank reactions were performed using 1 mM unlabeled thymidine. Equivalent reactions were performed using purified Ad-wt-E3-TK (1.26×10^{10} v.p.) as negative controls. After 40 min, the reaction mixtures were inactivated by heating to 95 °C for 3 min followed by centrifugation for 1 min at $14,000 \times g$. For determination of the total amount of $[^3H]$-labeled thymidine converted to its phosphorylated form, a DEAE-cellulose binding assay was performed. Three triplicates of 10 μl from each reaction mixture were transferred onto 200 μl DEAE-cellulose (buffered with 100 mM Tris, pH 7.2) and mixed by vortexing in order to bind the negatively charged phosphorylated thymidine. After binding, the mixtures were centrifuged and washed two times with 4 mM ammonium acetate and once with methanol to remove the non-phosphorylated thymidine. The cellulose pellets were transferred directly into scintillation vials containing 8 ml of scintillation cocktail and the amount of converted $[^3H]$-thymidine was determined using a scintillation counter. Results were calculated as percent total conversion using the amount of total labeled substrate obtained from sets of 10 μl triplicates from each reaction mixture pipetted directly into scintillation vials containing 8 ml of scintillation cocktail and counted.

MicroPET scan of Ad-infected HEK293 cells

PET studies were performed using a microPET rodent four-ring system (model R4) from CTI Concorde Microsystems, LLC (Knoxville, TN). In brief, the system operates in three dimensions and is composed of 6144 lutetium oxyorthosilicate crystal (LSO) detector elements, with a 7.8 cm axial and a 10 cm transaxial field-of-view. The 9-[4-$[^{18}F]$-fluoro-3-(hydroxymethyl)butyl]guanine analog ($[^{18}F]$-FHBG) has been used as a reporter probe to image the expression of the herpes simplex virus type 1 (HSV-1) thymidine kinase (TK) reporter gene in living organisms and has been suggested to be a more effective probe for in vivo

imaging than other acycloguanosine analogs (Alauddin et al., 2004). The HSV-1 TK phosphorylates $[^{18}F]$-FHBG to its monophosphate form, leading to intracellular accumulation (Green et al., 2002). Cellular retention of radioactivity is, therefore, an indicator of HSV-1 TK gene expression. Synthesis and purification of $[^{18}F]$-FHBG have been described previously (Parks, 2005).

For in vitro experiments, three 60-mm tissue culture dishes (Costar, Corning, NY) were plated for 12 h previously with 1×10^6 of the HEK293 cell line in 3 ml of complete medium. On the day of microPET scanning, to each of the dishes was added 50 mCi of $[^{18}F]$-FHBG. Immediately thereafter, to one plate was added 1×10^9 v.p. (1.1×10^7 i.f.u.) of Ad-wt-pIX-TK, to a second dish was added 1×10^9 v.p. (1.9×10^6 i.f.u.) of the control Ad-wt-dE3 virus, and to a third dish was added PBS alone. The plates were incubated for 1 h at 37 °C, followed by three washes with 5 ml of PBS. The three dishes were stacked and placed in the microPET scanner, and image data were acquired for 15 min. MicroPET images were reconstructed by using an iterative reconstruction technique.

To confirm these results, three 60-mm tissue culture dishes (Costar, Corning, NY) were plated for 12 h previously with 1×10^6 of the HEK293 cell line in 3 ml of complete medium. At 12 h after plating, one dish was infected with 1×10^9 v.p. (1.1×10^7 i.f.u.) of Ad-wt-pIX-TK. Likewise, at 36 h after plating, one dish was infected with an equivalent amount of Ad-wt-pIX-TK. A third dish remained uninfected. At 60 h after plating (48 h, 24 h, and 0 h post-infection with Ad-wt-pIX-TK), 50 mCi of $[^{18}F]$-FHBG was added to each of the dishes. The plates were incubated for 1 h at 37 °C, followed by three washes with 5 mL of PBS. The three dishes were stacked and placed in the microPET scanner, and image data were acquired for 15 min. MicroPET images were reconstructed by using an iterative reconstruction technique.

References

Alauddin, M.M., Shahinian, A., Gordon, E.M., Conti, P.S., 2004. Direct comparison of radiolabeled probes FMAU, FHBG, and FHPG as PET imaging agents for HSV1-tk expression in a human breast cancer model. Mol. Imaging 3, 76–84.

Alavi, A., Lakhani, P., Mavi, A., Kung, J.W., Zhuang, H., 2004. PET: a revolution in medical imaging. Radiol. Clin. North Am. 42, 983–1001.

Belousova, N., Krendelchtchikova, V., Curiel, D.T., Krasnykh, V., 2002.

Modulation of adenovirus vector tropism via incorporation of polypeptide ligands into the fiber protein. J. Virol. 76, 8621–8631.

Bhaumik, S., Gambhir, S.S., 2002. Optical imaging of Renilla luciferase reporter gene expression in living mice. Proc. Natl. Acad. Sci. U.S.A. 99, 377–382.

Blasberg, R., 2002. PET imaging of gene expression. Eur. J. Cancer 38, 2137–2146.

Campos, S.K., Parrott, M.B., Barry, M.A., 2004. Avidin-based targeting and purification of a protein IX-modified, metabolically biotinylated adenoviral vector. Mol. Ther. 9, 942–954.

Chen, I.Y., Wu, J.C., Min, J.J., Sundaresan, G., Lewis, X., Liang, Q., Herschman, H.R., Gambhir, S.S., 2004. Micro-positron emission tomography imaging of cardiac gene expression in rats using bicistronic adenoviral vector-mediated gene delivery. Circulation 109 (11), 1415–1420 (Mar. 23).

Chen, X., Park, R., Tohme, M., Shahinian, A.H., Bading, J.R., Conti, P.S., 2004. MicroPET and autoradiographic imaging of breast cancer alpha v-integrin expression using 18F- and 64Cu-labeled RGD peptide. Bioconjug. Chem. 15 (1), 41–49 (Jan.–Feb.).

Cho, J.Y., Shen, D.H., Yang, W., Williams, B., Buckwalter, T.L., La Perle, K.M., Hinkle, G., Pozderac, R., Kloos, R., Nagaraja, H.N., Barth, R.F., Jhiang, S.M., 2002. In vivo imaging and radioiodine therapy following sodium iodide symporter gene transfer in animal model of intracerebral gliomas. Gene Ther. 9, 1139–1145.

Dmitriev, I.P., Kashentseva, E.A., Curiel, D.T., 2002. Engineering of adenovirus vectors containing heterologous peptide sequences in the C terminus of capsid protein IX. J. Virol. 76, 6893–6899.

Everts, M., Curiel, D.T., 2004. Transductional targeting of adenoviral cancer gene therapy. Curr. Gene Ther. 4, 337–346.

Everts, B., Van der Poel, H.G., 2005. Replication-selective oncolytic viruses in the treatment of cancer. Cancer Gene Ther. 12, 141–161.

Fallaux, F.J., Kranenburg, O., Cramer, S.J., Houweling, A., Van Ormondt, H., Hoeben, R.C., Van Der Eb, A.J., 1996. Characterization of 911: a new helper cell line for the titration and propagation of early region 1-deleted adenoviral vectors. Hum. Gene Ther. 7, 215–222.

Fillat, C., Carrio, M., Cascante, A., Sangro, B., 2003. Suicide gene therapy mediated by the herpes simplex virus thymidine kinase gene/Ganciclovir system: fifteen years of application. Curr. Gene Ther. 3, 13–26.

Gerber, S., Folkers, G., 1996. A new method for quantitative determination of tritium-labeled nucleoside kinase products adsorbed on DEAE-cellulose. Biochem. Biophys. Res. Commun. 225, 263–267.

Glasgow, J.N., Bauerschmitz, G.J., Curiel, D.T., Hemminki, A., 2004. Transductional and transcriptional targeting of adenovirus for clinical applications. Curr. Gene Ther. 4, 1–14.

Green, L.A., Yap, C.S., Nguyen, K., Barrio, J.R., Namavari, M., Satyamurthy, N., Phelps, M.E., Sandgren, E.P., Herschman, H.R., Gambhir, S.S., 2002. Indirect monitoring of endogenous gene expression by positron emission tomography (PET) imaging of reporter gene expression in transgenic mice. Mol. Imaging Biol. 4, 71–81.

He, T.C., Zhou, S., da Costa, L.T., Yu, J., Kinzler, K.W., Vogelstein, B., 1998. A simplified system for generating recombinant adenoviruses. Proc. Natl. Acad. Sci. U.S.A. 95, 2509–2514.

Herschman, H.R., 2002. Non-invasive imaging of reporter genes. J. Cell. Biochem., Suppl. 39, 36–44.

Hustinx, R., Benard, F., Alavi, A., 2002. Whole-body FDG-PET imaging in the management of patients with cancer. Semin. Nucl. Med. 32 (1), 35–46 (Jan.)

Jacobs, A., Voges, J., Reszka, R., Lercher, M., Gossmann, A., Kracht, L., Kaestle, C., Wagner, R., Wienhard, K., Heiss, W.D., 2001. Positron-emission tomography of vector-mediated gene expression in gene therapy for gliomas. Lancet 358, 727–729.

Kirn, D., 2000. Replication-selective oncolytic adenoviruses: virotherapy aimed at genetic targets in cancer. Oncogene 19, 6660–6669.

Le, L.P., Everts, M., Dmitriev, I.P., Davydova, J.G., Yamamoto, M., Curiel, D.T., 2004. Fluorescently labeled adenovirus with pIX-EGFP for vector detection. Mol. Imaging 3, 105–116.

Liang, Q., Nguyen, K., Satyamurthy, N., Barrio, J.R., Phelps, M.E., Gambhir, S.S., Herschman, H.R., 2002. Monitoring adenoviral DNA delivery, using a mutant herpes simplex virus type 1 thymidine kinase gene as a PET reporter gene. Gene Ther. 9, 1659–1666.

Luker, G.D., Sharma, V., Piwnica-Worms, D., 2003. Visualizing protein–protein interactions in living animals. Methods 29 (1), 110–122 (Jan.)

Meulenbroek, R.A., Sargent, K.L., Lunde, J., Jasmin, B.J., Parks, R.J., 2004. Use of adenovirus protein IX (pIX) to display large polypeptides on the virion-generation of fluorescent virus through the incorporation of pIX-GFP. Mol. Ther. 9, 617–624.

Min, J.J., Gambhir, S.S., 2004. Gene therapy progress and prospects: noninvasive imaging of gene therapy in living subjects. Gene Ther. 11, 115–125.

Mizuguchi, H., Hayakawa, T., 2004. Targeted adenovirus vectors. Hum. Gene Ther. 15, 1034–1044.

Nettelbeck, D.M., 2003. Virotherapeutics: conditionally replicative adenoviruses for viral oncolysis. Anticancer Drugs 14, 577–584.

Oosterhoff, D., van Beusechem, V.W., 2004. Conditionally replicating adenoviruses as anticancer agents and ways to improve their efficacy. J. Exp. Ther. Oncol. 4, 37–57.

Parks, R.J., 2005. Adenovirus protein IX: a new look at an old protein. Mol. Ther. 11, 19–25.

Pereboeva, L., Komarova, S., Mahasreshti, P.J., Curiel, D.T., 2004. Fiber-mosaic adenovirus as a novel approach to design genetically modified adenoviral vectors. Virus Res. 105, 35–46.

Ries, S.J., Brandts, C.H., 2004. Oncolytic viruses for the treatment of cancer: current strategies and clinical trials. Drug Discov. Today 9 (17), 759–768 (Sep. 1).

Rots, M.G., Curiel, D.T., Gerritsen, W.R., Haisma, H.J., 2003. Targeted cancer gene therapy: the flexibility of adenoviral gene therapy vectors. J. Controlled Release 87, 159–165.

Sinkovics, J., Horvath, J., 1993. New developments in the virus therapy of cancer: a historical review. Intervirology 36, 193–214.

Tian, B., Han, L., Kleidon, J., Henke, C., 2003. An HSV-TK transgenic mouse model to evaluate elimination of fibroblasts for fibrosis therapy. Am. J. Pathol. 163, 789–801.

van Dillen, I.J., Mulder, N.H., Vaalburg, W., de Vries, E.F., Hospers, G.A., 2002. Influence of the bystander effect on HSV-tk/GCV gene therapy. A review. Curr. Gene Ther. 2, 307–322.

Vellinga, J., Rabelink, M.J., Cramer, S.J., van den Wollenberg, D.J., Van der Meulen, H., Leppard, K.N., Fallaux, F.J., Hoeben, R.C., 2004. Spacers increase the accessibility of peptide ligands linked to the carboxyl terminus of adenovirus minor capsid protein IX. J. Virol. 78, 3470–3479.

Volpers, C., Kochanek, S., 2004. Adenoviral vectors for gene transfer and therapy. J. Gene Med. 6 (Suppl. 1), S164–S171.

Weber, S., Bauer, A., 2004. Small animal PET: aspects of performance assessment. Eur. J. Nucl. Med. Mol. Imaging 31, 1545–1555.

Wu, H., Dmitriev, I., Kashentseva, E., Seki, T., Wang, M., Curiel, D.T., 2002. Construction and characterization of adenovirus serotype 5 packaged by serotype 3 hexon. J. Virol. 76, 12775–12782.

Yaghoubi, S.S., Barrio, J.R., Namavari, M., Satyamurthy, N., Phelps, M.E., Herschman, H.R., Gambhir, S.S., 2005. Imaging progress of herpes simplex virus type 1 thymidine kinase suicide gene therapy in living subjects with positron emission tomography. Cancer Gene Ther. 12, 329–339.

Yang, M., Baranov, E., Moossa, A.R., Penman, S., Hoffman, R.M., 2000. Visualizing gene expression by whole-body fluorescence imaging. Proc. Natl. Acad. Sci. U.S.A. 97, 12278–12282.

Zinn, K.R., Buchsbaum, D.J., Chaudhuri, T.R., Mountz, J.M., Grizzle, W.E., Rogers, B.E., 2000. Noninvasive monitoring of gene transfer using a reporter receptor imaged with a high-affinity peptide radiolabeled with 99mTc or 188Re. J. Nucl. Med. 41, 887–895.

Zinn, K.R., Chaudhuri, T.R., Krasnykh, V.N., Buchsbaum, D.J., Belousova, N., Grizzle, W.E., Curiel, D.T., Rogers, B.E., 2002. Gamma Camera Dual Imaging With A Somatostatin Receptor and Thymidine Kinase After Gene Transfer With A Bicistronic Adenovirus in Mice Radiology, 223, p. 417.

npg

ORIGINAL ARTICLE

Infectivity enhancement for adenoviral transduction of canine osteosarcoma cells

LP Le[1,4], AA Rivera[1,4], JN Glasgow[1], VV Ternovoi[1], H Wu[1], M Wang[1], BF Smith[2], GP Siegal[1,3] and DT Curiel[1]

[1]Division of Human Gene Therapy, Departments of Medicine, Pathology and Surgery, and the Gene Therapy Center, University of Alabama at Birmingham, Birmingham, AL, USA; [2]Scott-Ritchey Research Center, College of Veterinary Medicine, Auburn University, Auburn, AL, USA and [3]Departments of Pathology, Cell Biology and Surgery, University of Alabama at Birmingham, Birmingham, AL, USA

The full realization of conditionally replicative adenoviruses (CRAds) for cancer therapy has been hampered by the limited knowledge of CRAd function *in vivo* and particularly in an immunocompetent host. To address this issue, we previously proposed a canine adenovirus type 2 (CAV2)-based CRAd for clinical evaluation in canine patients with osteosarcoma (OS). In this study, we evaluated infectivity-enhancement strategies to establish the foundation for designing a potent CAV2 CRAd with effective transduction capacity in dog osteosarcoma cells. The results indicate that the native CAV2 fiber–knob can mediate increased binding, and consequently gene transfer, in both canine osteosarcoma immortalized and primary cell lines relative to previously reported Ad5 infectivity-enhancement strategies. Gene delivery was further enhanced by incorporating a polylysine polypeptide onto the carboxy terminus of the CAV2 knob. This vector demonstrated improved gene delivery in osteosarcoma xenograft tumors. These data provide the rationale for generation of infectivity-enhanced syngeneic CAV2 CRAds for clinical evaluation in a dog osteosarcoma model. Gene Therapy (2006) **13**, 389–399. doi:10.1038/sj.gt.3302674; published online 17 November 2005

Introduction

Recent advances in conventional tumor therapies have yielded limited improvement in the treatment of cancer. In this regard, the oncolytic mechanism of conditionally replicative adenoviruses (CRAds) has been harnessed to selectively and effectively kill tumor cells while avoiding toxicity in normal tissues.[1,2] The promise of these agents as a broad cancer therapeutic approach has led to their rapid translation into a number of clinical trials.[3,4] Although these studies have clearly established the safety associated with the application of CRAds, they have also revealed our limited understanding of the predicates of CRAd efficacy.[5]

Human tumor xenografts in immunodeficient mice have been the model of choice to study the effectiveness of CRAd agents. Although informative about the *in vivo* oncolytic capability of designed replicative adenoviruses to some extent, several limitations exist with this system. First, it is questionable whether these xenograft tumors represent the true architecture of patient tumors.

Immortalized and transformed cell lines employed as substrates in these models can deviate significantly from the native, complex tumor environment. Second, human adenovirus in general does not productively replicate in mouse cells, precluding application of the murine xenograft system as a method to analyze toxicity in nontarget tissues. Consequently, the cotton rat model which is semipermissive for human adenovirus replication has been suggested as a preclinical model for analyzing replication toxicity of human adenovirus.[6] Third, the use of immunodeficient mice to evaluate oncolytic adenoviruses inherently disregards vector interactions with the host immune system, a key phenomenon that may constitute the basis of the rapid clearance and insufficient performance of these agents in patients.[7]

Several recent strategies have been developed to address the lack of adequate preclinical models for evaluating CRAds. One approach employs certain permissive murine tumor cell lines grown in immunocompetent animals to study human adenovirus replication.[7–9] However, the inefficient replication of human adenovirus in these cell lines, as well as the artificial establishment of these tumors as subcutaneous syngeneic grafts, raises concerns as to how well this model supports human adenovirus replication and how accurately the tumor grafts represent their natural human counterparts. An alternative approach that we have pursued is to use syngeneic Ad vectors in their natural

Correspondence: Dr DT Curiel, Division of Human Gene Therapy, Departments of Medicine, Pathology and Surgery, and the Gene Therapy Center, University of Alabama at Birmingham, 901 19th Street South, BMR2-502, Birmingham, AL 35294, USA.
E-mail: curiel@uab.edu
[4]These authors contributed equally to this work.

host system. In particular, the application of replicative canine adenovirus type 2 (CAV2) in a spontaneous osteosarcoma (OS) dog tumor model addresses the issues of tumor setting and efficient vector replication and oncolysis. In this regard, canine OS resembles human OS on several levels, including male predilection, lesion locale, high-grade histology, and metastatic potential.[10] Moreover, this spontaneous tumor system would permit the evaluation of the immune system influence on the performance of syngeneic oncolytic adenoviruses. This model is also attractive since over 8000 large breed dogs per year in the US present with this neoplasm, offering the opportunity to study a CAV2 CRAd for this disease in a rigorously controlled clinical environment.[11]

The utility of this canine model would be greatly limited unless a selective yet potent CRAd agent is applied to the target disease. The design of an effective oncolytic adenovirus relies on a number of parameters, including the use of tumor-specific control elements or mutation compensation strategies to restrict replication to tumor cells.[1] Additionally, the use of infectivity enhancement to achieve transduction via pathways that are independent from the virus's natural infection route may have to be considered should target cell transduction be insufficient through the virus's native receptor.[12,13] In humans, most cancers express very low levels of the coxsackie-adenovirus receptor (CAR), the primary attachment receptor for human adenovirus type 5, a vector on which all current human CRAds are based.[14,15] This fact has motivated the development of various genetic capsid modification strategies to augment the infectivity of oncolytic adenoviruses, including incorporation of short peptides (e.g. RGD and poly-lysine) into the hexon, penton, and fiber–knob.[16–18] Indeed, such strategies yielded profound improvements in the oncolytic capability of CRAds relative to non-modified vectors.[19,20] Recently, more radical modifications based on serotype and xenotype fiber–knob switching have been exploited to achieve enhanced transduction.[21–23] Furthermore, the ability to place large ligands onto the adenovirus fiber and protein IX by genetic means suggests the possibility of achieving truly retargeted CRAds.[24–26]

Previously, we developed an osteocalcin promoter-specific CRAd based on CAV2. This replicative virus demonstrated efficient replication and oncolytic potential in a variety of dog OS cell lines both *in vitro* and in a murine xenograft model.[27] Although we successfully applied the osteocalcin promoter to construct an OS-targeted CAV2 CRAd, development of infectivity-enhanced canine adenoviral vectors is required for efficient transduction of canine cells, and in particular, dog OS cells, which would yield improved oncolysis. In this study, we evaluated a panel of available infectivity-enhancement strategies on both immortalized and primary dog OS cells. We applied capsid modified vectors based on the RGD motif,[17] Ad5/3 chimerism,[21] and polylysine[18] to achieve enhanced transduction. Our results indicate that polylysine incorporation onto the carboxy terminus of CAV2 fiber–knob provided the best infectivity enhancement for the transduction of canine OS cells. These data establish the foundation for developing a tumor-specific infectivity-enhanced CAV2 CRAd for evaluation in a syngeneic dog OS model.

Results and discussion

Ad5 and CAV2 receptor levels on canine OS cells

The initial step of adenovirus entry into cells involves attachment of the fiber–knob region onto a primary cellular receptor.[28] For most human subgroup C adeno-viruses, including Ad2 and Ad5 on which most conventional adenoviral vectors are based, the primary receptor has been identified as the CAR.[29] Although CAV2 binds directly to soluble recombinant human CAR and can utilize human or murine CAR for cell entry *in vitro*, CAV2 also has the ability to transduce CAR-deficient cells,[23,30] suggesting the possible existence of a second receptor for CAV2. Owing to incomplete understanding of CAV2 cellular entry, and lack of antibodies against the CAV2 receptor, we analyzed CAV2 receptor levels on canine OS cells using a fluorescence-based flow cyto-metry-binding assay. We applied our recently developed genetic adenovirus-labeling system[31] to label CAV2 virions with pIX-EGFP. Specifically, CAV2-wt-IX-EGFP was constructed from the wild-type Toronto strain A 26-61 CAV2 genome (pTG5412).[32] It contains IX-EGFP (EGFP carboxy terminus fusion) in place of the native IX gene (Figure 1a). Using our green fluorescent CAV2 vector along with the pIX-EGFP-labeled Ad5 virus.[31] we could functionally analyze the respective receptor levels
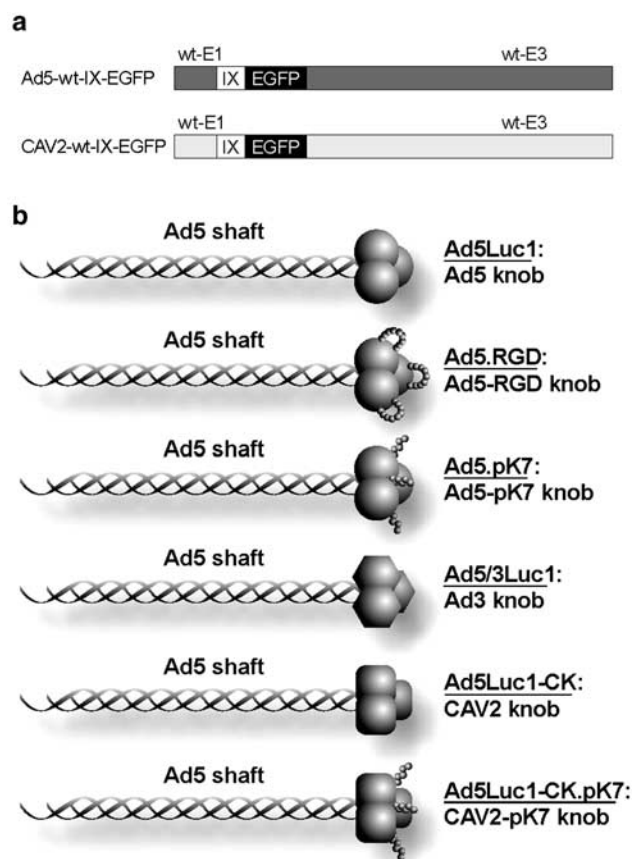

Figure 1 Adenoviral constructs. (**a**) Ad5-wt-IX-EGFP and CAV2-wt-IX-EGFP constructs. (**b**) Infectivity enhancement fiber–knob modifications used in gene transfer assays. All vectors are based on the Ad5 genome and contain the Ad5 shaft with modified knob domains as indicated.

of each virus regardless of the knowledge of their native receptors. Our panel of cells included A549 (CAR-positive control), Chinese hamster ovary (CHO) (CAR-negative control), MDCK (CAV2 receptor-positive control), three established canine OS cell lines (CF11.T, D17, and D22), and three primary canine OS cell lines (P-0, P-1, and P-2). Cell suspensions were incubated with saturating levels of virus (10 000 vp/cell) at 4°C for 1 h to allow binding but not internalization. Following three wash cycles, the cells were directly analyzed by flow cytometry using EGFP detection as an index of virus binding.

Similar to our previous data, Ad5-wt-IX-EGFP bound to A549 cells but not to CHO cells (Figure 2a).[31] Interestingly, both A549 and CHO cells were highly susceptible to CAV2-wt-IX-EGFP attachment. CAV2-wt-IX-EGFP interacted well with MDCK cells, a positive binding control for this virus, while Ad5-wt-IX-EGFP did not. In addition, CAV2-wt-IX-EGFP demonstrated cell surface attachment to all three established canine OS cell lines, ranging from modest interaction with CF11.T cells to strong binding to D17 and D22 cells. In all three primary cell lines, CAV2-wt-IX-EGFP showed a lesser degree of binding with some shift in the shape of the curve. It should be noted that these cells were highly autofluorescent as indicated by the wide and rather flat fluorescence distribution of nontreated cells. For all established and primary canine OS cells except D17, Ad5-wt-IX-EGFP demonstrated poor cell surface binding. Taken together, these results suggest that (1) all primary canine OS cells and CF11.T displayed modest levels of the CAV2 receptor, (2) D17 and D22 showed relatively strong levels of the CAV2 receptor, and (3) all canine OS cell lines except D17 were deficient in the Ad5 primary receptor, CAR (Figure 2a). The final observation corresponds with previously published data with respect to CAR deficiency in human OS cells[33] although other studies have indicated contrasting results.[34,35]

Worthy of discussion is the fact that these data strongly support the existence of a second CAV2 receptor which was implied by previous studies.[23,30] In particular, CHO cells which are known to be CAR negative[31,36] demonstrated strong CAV2-wt-IX-EGFP binding in our experiments. In situations where Ad5-wt-IX-EGFP showed no binding (all except A549 and D17) or positive binding (A549 and D17), CAV2-wt-IX-EGFP showed distinct binding or much stronger binding, respectively. In addition, blocking with nonlabeled Ad5-wt could not effectively abrogate CAV2-wt-IX-EGFP binding in D17 (Figure 2b, middle panel), MDCK (Figure 2b, right panel), and D22 (data not shown) cells; however, CAV2-wt was able to completely block Ad5-wt-IX-EGFP binding in D17 (Figure 2b, left panel) and A549 cells (data not shown). These blocking data indicate that although CAV2-wt could completely prevent Ad5-wt-IX-EGFP binding to CAR, CAV2-wt-IX-EGFP was able to circumvent Ad5 blocking by attaching to a receptor that is likely different from CAR.

The results of this binding assay are based on pIX-labeled Ad5 and CAV2 viruses. Differences in capsid proteins other than the knob region, particularly the presence of an RGD motif in the penton base of Ad5 but not CAV2,[30] may contribute to the distinct binding character of these two viruses. However, the ability of CAV2-wt (lacking penton RGD) to completely hinder Ad5-wt-IX-EGFP binding to CAR and the inability of Ad5-wt (containing penton RGD) to successfully deter CAV2-wt-IX-EGFP binding suggest that the major determinant of attachment in our experiments was mostly mediated by Ad5 and CAV2 knob interaction with their receptor(s). Another consideration that cannot be excluded with our data is the possibility that the CAV2 knob binds to CAR with higher affinity than the Ad5 knob. However, strong binding of CAV2-wt-IX-EGFP and not Ad5-wt-IX-EGFP to CAR-negative CHO cells suggest another interaction mechanism distinct from CAR. Although we demonstrated positive binding of CAV2-wt-IX-EGFP to CHO cells, a previous report noted poor transduction of CHO cells by a CAV2 vector which may be explained by poor internalization and not necessarily poor binding.[30]

Visualization of virus binding on primary canine OS cells
As noted above, the primary canine OS cells were highly autofluorescent, possibly precluding proper detection of virus binding by flow cytometry. To determine virus binding more clearly, we used our green fluorescent adenoviruses to directly visualize virus binding on these cells. Cells plated on glass coverslips were incubated with either Ad5 or CAV2 pIX-EGFP-labeled virus in excess (10 000 vp/cell) for 1 h at 4°C and then washed prior to fixation and Hoechst staining. Following a final wash, the coverslips with cells were mounted and sealed on glass slides for imaging. Fluorescence microscopy revealed the highly autofluorescent nature of these cells (white arrows, Figure 3). Despite the strong background, green fluorescent viral particles could be distinguished (orange arrows), showing apparent differences in Ad5-wt-IX-EGFP versus CAV2-wt-IX-EGFP binding on these cells. For all three primary OS samples, few cells had attached Ad5-wt-IX-EGFP particles in contrast to CAV2-wt-IX-EGFP, which bound to these cells in either appreciable or overwhelming abundance. These data confirm the availability of the CAV2 receptor(s) on primary OS cells and therefore the ability of a canine adenoviral vector to bind to these cells.

Gene transfer correlates with virus binding
Successful adenoviral entry and resulting gene delivery into cells rely not only on initial attachment to the cell surface via fiber–knob interaction with a receptor but also subsequent steps, including penton base interaction with heterodimeric integrins for endocytosis,[37,38] escape from endosomes,[39–41] intracellular trafficking,[42,43] and DNA transport into the nucleus.[41,44] The results of our cell-surface virion attachment assay confirmed that a canine adenovirus-based vector could achieve the first step of entry into canine OS cells more efficiently than a human Ad5 vector. Whether these results correspond to effective gene delivery was examined by analyzing luciferase reporter gene expression after transduction of canine OS cells. For this assay, we elected to use isogenic vectors based on the human Ad5 genome displaying either the Ad5 knob or the CAV2 knob.[23] Using a common vector structure would standardize all conditions including the reporter expression cassette and capsid structure while allowing analysis of gene transfer
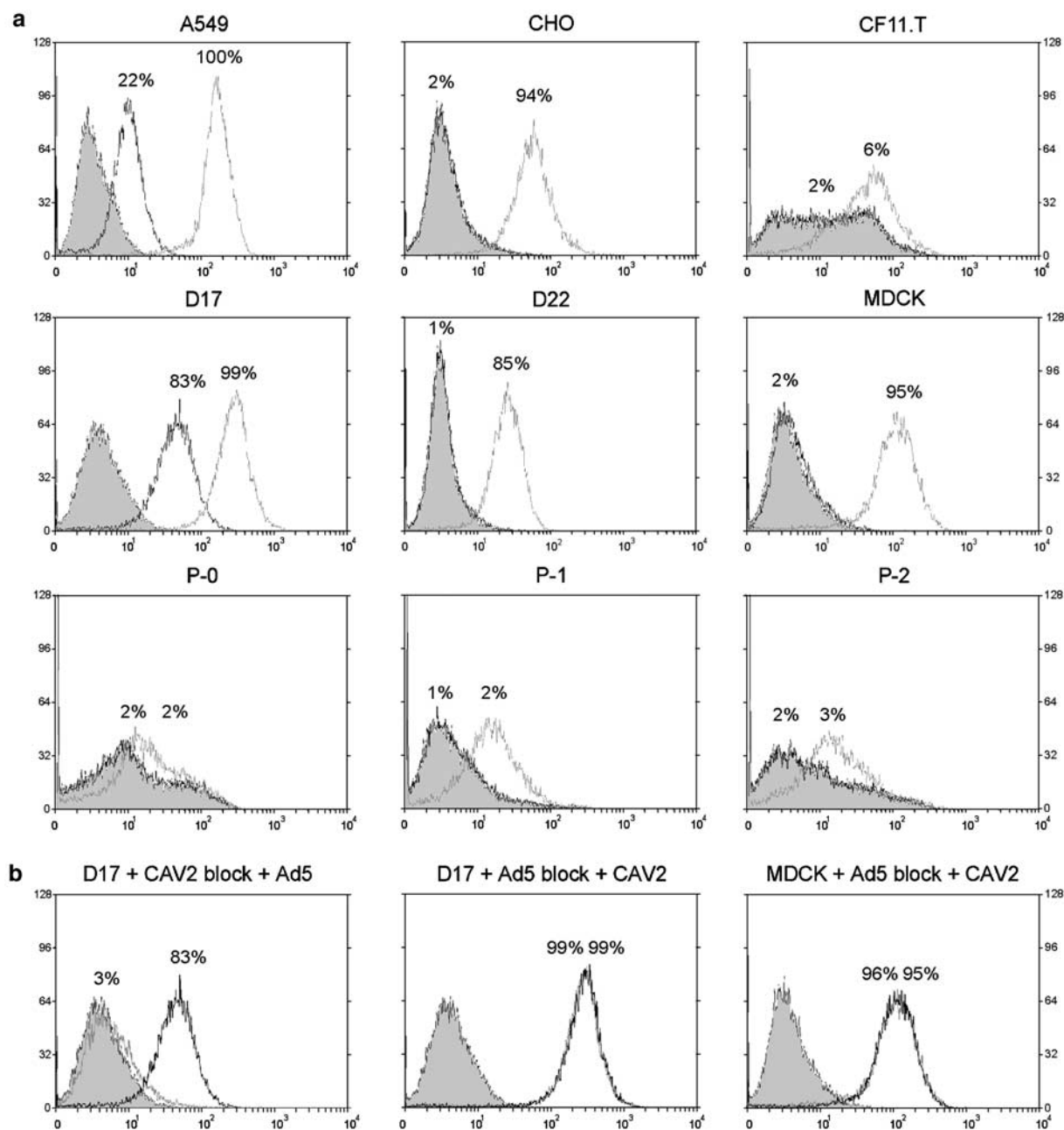
Figure 2 Flow cytometry binding assay. (**a**) Fluorescent Ad5-wt-IX-EGFP and CAV2-wt-IX-EGFP binding to cells was analyzed by flow cytometry gated for EGFP intensity. The samples include cells only (gray filled-in area), Ad5-wt-IX-EGFP (dark line), and CAV2-wt-IX-EGFP (gray line). The percentages indicate the fraction of cells gated for positive binding. In all panels, the left percentage refers to Ad5-wt-IX-EGFP, and the right percentage refers to CAV2-wt-IX-EGFP. Note that for CHO, CF11.T, D22, MDCK, P-0, P-1, and P-2 panels in a, the dark line for Ad5-wt-IX-EGFP is superimposed on top of the cells only gray filled in area. (**b**) The binding assay was also performed under competitive conditions with excess nonlabeled vector. Left panel: D17 cells blocked with nonlabeled CAV2-wt virus prior to incubation with Ad5-wt-IX-EGFP (gray filled-in area = cells only, dark line = Ad5-wt-IX-EGFP only, and gray line = CAV2-wt blocking prior to Ad5-wt-IX-EGFP incubation). Middle panel: D17 cells blocked with nonlabeled Ad5-wt virus prior to incubation with CAV2-wt-IX-EGFP (gray filled-in area = cells only, gray line = CAV-wt-IX-EGFP only, and dark line = Ad5-wt blocking prior to CAV2-wt-IX-EGFP incubation). Right panel: MDCK cells blocked with nonlabeled Ad5-wt virus prior to incubation with CAV2-wt-IX-EGFP (gray filled-in area = cells only, gray line = CAV-wt-IX-EGFP only, and dark line = Ad5-wt blocking prior to CAV2-wt-IX-EGFP incubation). The percentages indicate the fraction of cells gated for positive binding. For all three panels, the left percentage refers to blocking conditions, and the right percentage refers to nonblocking conditions.

efficacy due solely to variation of the knob. In all cells examined (CF11.T, D17, D22, P-0, P-1, and P-2), the canine knob-based vector, Ad5Luc1-CK, yielded significantly greater gene transfer versus wild-type knob-containing Ad5Luc1, ranging from roughly seven-fold

(CF11.T) to 17-fold (D17) better efficiencies (Figure 4, $P < 0.02$ for all cell lines). These results are consistent with the robust binding of the CAV2 vector relative to the Ad5 vector observed both in the flow cytometry and fluorescence microscopy-binding experiments.
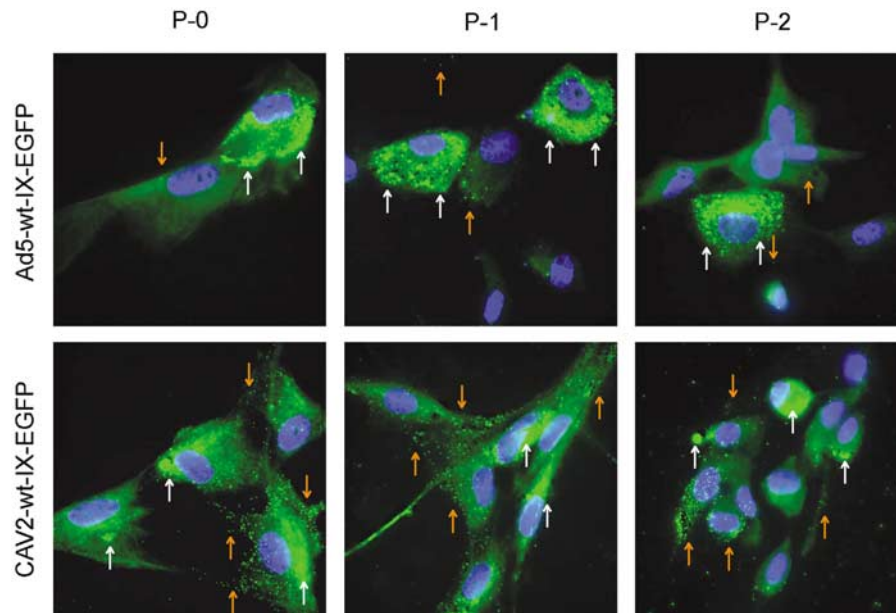
Figure 3 Visualization of virus binding. Canine primary osteosarcoma cells incubated with fluorescent Ad5-wt-IX-EGFP or CAV2-wt-IX-EGFP were visualized by epi-fluorescence microscopy to detect bound virions. Orange arrows indicate fluorescent virions while white arrows indicate cell autofluorescence.
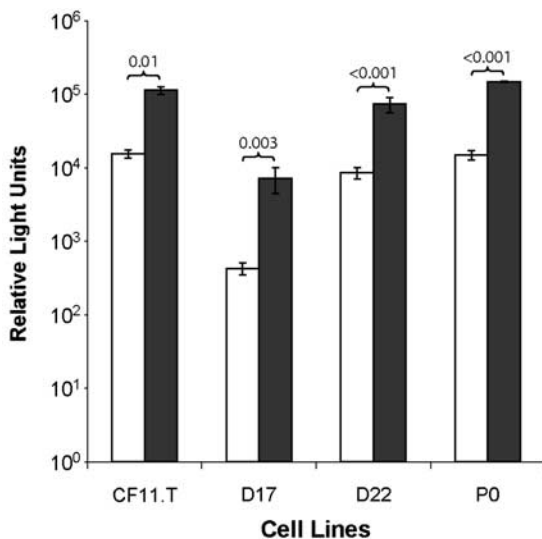
Figure 4 Gene transfer via unmodified Ad5 and CAV2 knobs. Isogenic Ad5-based luciferase expression vectors bearing the unmodified Ad5 knob or CAV2 knobs were used to assess gene transfer capacity. Ad5Luc1 with the Ad5 knob (white bar) and Ad5Luc1-CK with the CAV2 knob (black bar) ($n = 3$). P-values determined by ANOVA are shown above each set of bars.

Infectivity-enhanced vector binding/internalization into canine OS cells

Despite the ample transduction of canine OS cells obtained with an adenoviral vector containing the CAV2 knob, we explored the possibility of achieving even greater gene transfer with an array of infectivity enhancement approaches, namely RGD-4C modification of the Ad5 knob HI-loop,[17] serotype switching of the Ad5 knob with that of Ad3,[21] and polylysine incorporation onto the carboxy terminus of both the Ad5[18] and CAV2

fiber knobs. These CAR-independent transduction strategies would redirect the binding of the adenovirus to integrins (Ad.RGD), the Ad3 receptor (Ad5/3Luc1, putatively identified to be CD80 and CD86[36] and/or CD46[45]), and heparin sulfate proteoglycans (Ad5.pK7 and Ad5Luc1-CK.pK7), respectively. All of these strategies have demonstrated increased gene transfer into various human cancer cell lines that are refractory to Ad5 transduction. To determine the capacity of these viruses to transduce canine OS cells, we performed a DNA-based virus binding/internalization assay. Cells plated 1 day earlier on 24-well plates were incubated with the viruses for 1 h at 37°C. Noninteracting viruses were washed away leaving cells containing bound and internalized viruses for processing of total cellular and viral DNA. Real-time quantitative PCR was used to assess the number of bound/internalized adenoviral genome copies using E4-specific primers. The RGD-modified knob improved binding/internalization up to a half-log factor above the unmodified knob ($P < 0.001$ except in the case of D17, $P = 0.10$) while that of the Ad5/3 chimeric knob was poor relative to the other modifications ($P < 0.04$ except compared to the RGD knob in P-0 cells, $P = 0.08$) and the native Ad5 knob ($P < 0.002$ except in P-0 cells where $P = 0.50$). The Ad5Luc1-CK and Ad5Luc1-CK.pK7 vectors showed better results when compared to vectors displaying a wild-type Ad5 knob ($P < 0.02$ and $P < 0.001$, respectively, in all cells except D17 where $P = 0.17$ and 0.27, respectively) or Ad5.RGD knob ($P < 0.04$ for Ad5-Luc1-CK except in P-0 cells where $P = 0.47$, and $P < 0.004$ for Ad5Luc1-CK.pK7 except in D17 cells where $P = 0.06$). The outcome of the assay indicates that both the Ad5.pK7 and Ad5Luc1-CK.pK7 viruses achieved similar levels of cellular interaction in D17 and P-0 cells ($P = 0.53$ and 0.50, respectively) although the latter vector showed better results in CF11.T and D22 cells ($P < 0.005$). At least a six-fold

394

improvement in binding/internalization was observed in all cells ($P < 0.009$ for both vectors) except D17 relative to Ad5Luc1 ($P = 0.29$ for Ad5.pK7 and $P = 0.27$ for Ad5Luc1.CK.pK7). It should be noted that D17 cells are relatively CAR positive (Figure 2), which likely explains the minor binding/internalization enhancement observed with D17 when using the infectivity-enhanced viruses.

Enhanced gene transfer in canine OS cells

Improved gene delivery due to the various infectivity-enhancement strategies was confirmed by luciferase-based gene transfer assays. Data from the above analysis suggest the potential of the pK7 vectors to achieve better transduction of canine OS cells than the other adenoviral vectors used in this study. Indeed, the results obtained from the gene transfer assays were consistent with this prediction. In all cases, the Ad5Luc1-CK.pK7 vector consistently achieved enhanced transduction above the control Ad5 vector, ranging from a 27-fold increase in CF11.T cells to 1867-fold increase in D22 cells (Figure 6). The CAV2 knob alone also conferred appreciable augmentation in gene transfer which was close to (or more than) one-log factor higher than the Ad5 vector. Relative to the Ad5Luc1-CK vector, the Ad5Luc1-CK.pK7 vector was at least four times better in its gene transfer efficacy in CF11.T cells ($P = 0.002$) and more than 100 times better in D22 cells ($P = 0.0009$). The results with the Ad5.pK7 vector in general were not as striking as those with the Ad5Luc1-CK.pK7 vector ($P < 0.03$ except in P-0 cells in which Ad5.pK7 showed higher infectivity enhancement, $P = 0.0005$). Specifically in CF11.T, D22, and P-0 cells, respectively, 15-fold, 16-fold, and 1183-fold infectivity enhancement over the Ad5 virus was observed although no increase was seen in CAR-positive D17 cells. Relative to other fiber modifications, RGD

incorporation into the HI loop of the Ad5 knob provided only a slight improvement in gene delivery which was less than an order of magnitude above unmodified Ad5 in most cases except D22 cells (more than 11-fold higher).

Worthy of discussion are some discrepancies noted between the binding/internalization data and the gene transfer results. Although both Ad5.pK7 and Ad5Luc1-CK.pK7 showed nearly the same level of binding/internalization in D17 and P-0 cells (Figure 5), Ad5-Luc1-CK.pK7 demonstrated almost 2 orders of magnitude greater fold enhancement in gene transfer than Ad5.pK7 in D17 cells but more than 1 order of magnitude less gene transfer than Ad5.pK7 in P-0 cells (Figure 6). The difference in gene transfer between these two vectors is likely due to dissimilarity in their fiber knobs since the other capsid proteins, particularly the penton base and the fiber–shaft, of the two vectors are identical. Since the attachment/internalization between the two vectors appear to be similar, difference in intracellular trafficking as a consequence of the Ad5 and CAV2 knobs may explain the discrepancy in the gene transfer results. Likewise, previous reports have alluded to the role of the adenovirus fiber–knob in affecting intracellular viral trafficking and consequently gene transfer.[46–48] In addition, differences in cellular factors between D17 and P-0 cells may also contribute to the same phenomenon. Similar discrepancies were also noted between AdLuc1-CK and AdLuc1-CK.pK7 in CF11.T, D17, and D22 cells.

In vivo gene transfer

Applying Ad5Luc1-CK.pK7 which demonstrated the most significant gene transfer capability *in vitro*, we tested whether its enhanced gene delivery would be maintained in an *in vivo* setting. D22 dog OS xenograft tumors in nude mice were injected with the Ad5Luc1-CK.pK7 vector on the right side while the control,
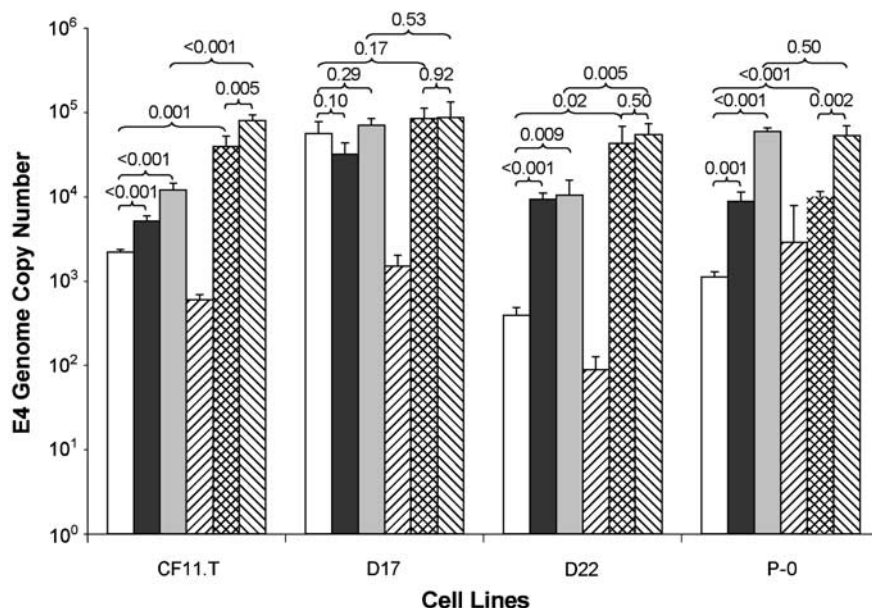
Figure 5 Real-time quantitative PCR binding/internalization assay with infectivity-enhanced vectors. Ad5 vectors with various infectivity-enhanced fiber knobs were analyzed for binding/internalization on the panel of canine OS cells. Viral genome copy numbers determined by Taqman quantitative real-time PCR represent the number of bound/internalized virions. Ad5 (white), Ad5.RGD (black), Ad5.pK7 (gray), Ad5/3Luc1 (forward stripe), Ad5Luc1-CK (cross-hatch), Ad5Luc1-CK.pK7 (reverse stripe) ($n = 4$). P-values determined by ANOVA are shown for the two bars indicated below each bracket.
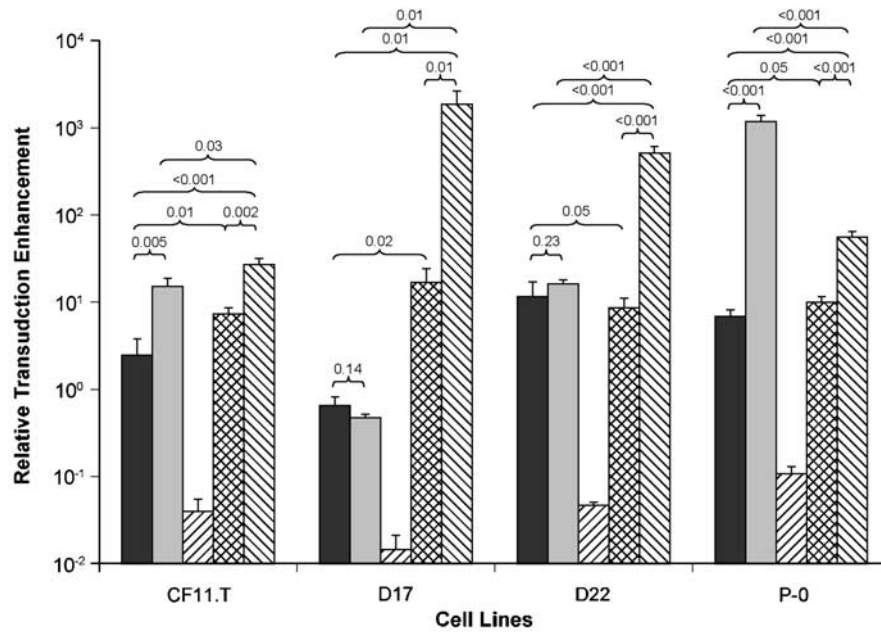
Figure 6 Gene transfer with infectivity-enhanced vectors. Improved gene delivery due to the various infectivity-enhanced vectors was analyzed on the panel of canine osteosarcoma cells using a luciferase reporter assay. Results are shown as extent of transduction enhancement fold above control Ad5Luc1. Ad5.RGD (black), Ad5.pK7 (gray), Ad5/3Luc1 (forward stripe), Ad5Luc1-CK (crosshatch), Ad5Luc1-CK.pK7 (reverse stripe) (*n* = 3). *P*-values determined by ANOVA are shown for the two bars indicated below each bracket.
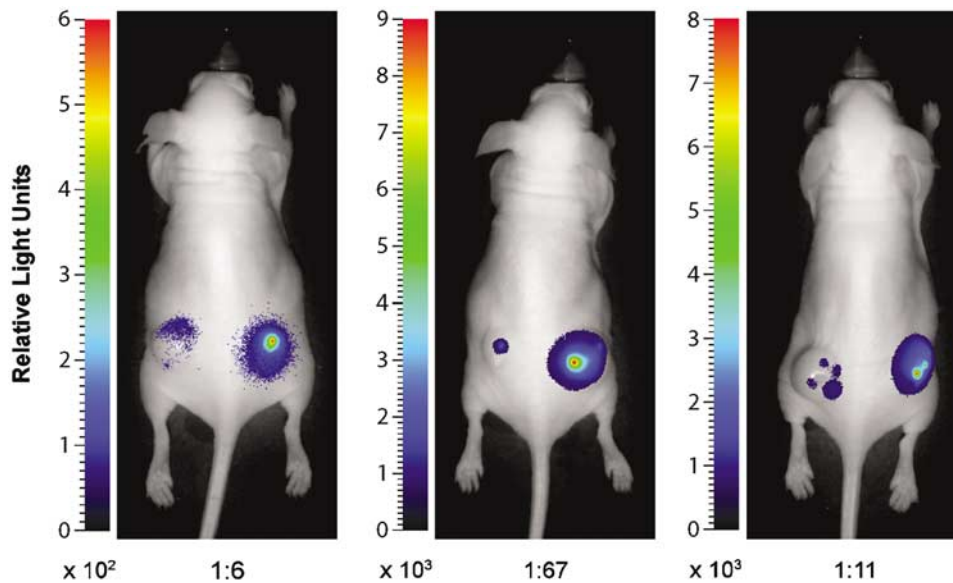
Figure 7 *In vivo* detection of gene transfer. Xenograft flank tumors established with D22 osteosarcoma cells in nude mice were injected intratumorally with Ad5-Luc1 in the left tumor and Ad5-Luc1-CK.pK7 in the right tumor. At 4 days after injection, the mice were imaged noninvasively with a bioluminescence optical imaging system. Data are presented as index color representation of the luciferase signal (in relative light units) overlayed on an image of the mouse body. Note that each image has its own index scale adjusted to best illustrate the difference in intensities between the two tumors. Scale factors are shown at the bottom left of each image. Ratios of total quantitated signal in the left tumor relative to the right tumor are included below the images.

unmodified Ad5Luc1 vector was administered in the left tumor. *In vivo* images of luciferase activities from three representative mice are shown (Figure 7). It should be noted that overall signal intensities varied from mouse to mouse, indicating how tumors and mice may respond differently to injection with the same vector. As a result, the images were scaled individually to better appreciate

the differences between the left and right tumors of each mouse. The images indicate enhanced gene expression with Ad5Luc1-CK.pK7 compared to Ad5Luc1, ranging from six- to 67-fold stronger signal in the right tumor relative to the left. Unlike the *in vitro* experiments in which vectors were washed from cells after a short incubation period, viruses remain locally concentrated

after intratumoral injections perhaps allowing more time for cellular interaction with the control vector. This consideration may reconcile the lower transduction enhancements observed *in vivo* relative to those achieved *in vitro*. Additionally, recent reports have suggested that *in vivo* adenovirus gene delivery involves complex steps not based solely on the interaction of the adenovirus knob with CAR.[49,50]

Among the vectors evaluated in this study, adenovirus displaying the Ad3 knob in place of the Ad5 knob showed the poorest binding/internalization and infectivity that was significantly lower than the unmodified Ad5 vector. Likewise an Ad vector containing both an Ad3 knob and Ad3 shaft,[51] produced similar results on the cells tested (data not shown). These findings differ from those obtained in other studies which revealed considerable gene transfer augmentation via the Ad3 knob in the context of ovarian,[51–53] renal,[54] head and neck,[55] skin,[56] and gastrointestinal[20] cancers. Important to note also is the fact that these are epithelial-derived neoplasms (carcinomas) rather than mesenchymal (sarcomas). Similar to the results in this study, certain other cancers have shown minor or no improvement in gene delivery with the Ad5/3 chimeric vector, including glioma, cervical cancer, and non-small-cell lung cancer.[57] The lack of infectivity enhancement observed with the Ad5/3 chimeric vector in our panel of canine cells could simply be due to absence of the putative Ad3 receptor or the fact that the human Ad3 knob cannot effectively interact with the canine counterpart of its human receptor. If the former argument holds true, the striking differences in transduction between the Ad5Luc1-CK vector versus the Ad5/3 chimeric vector support previous findings that CAV2 may enter cells independently of the Ad3 receptor.[23,30]

The enhanced transduction in canine OS cells seen in this study with the CAV2 knob-based vectors relative to an Ad5 knob-based vector may be a species-specific phenomenon. In other words, canine adenovirus may naturally enter canine cells better than human adenovirus. If this were the case, then the converse reasoning that human adenovirus transduces human cells better than canine adenovirus should be true. However, from our observations as well as others, adenoviral vectors with the canine knob routinely yield more efficient gene transfer than vectors with the Ad5 knob not only in canine cells but also in human cells.[23] In fact, transduction of MG63 human OS cells was close to a log factor higher with the CAV2 chimeric adenovirus than a conventional Ad5 vector (data not shown).

We have shown herein that a pIX-EGFP-labeled CAV2 vector demonstrated enhanced cell surface attachment to both established and primary canine OS cells. This improved cell binding translated into increased gene transfer capability with a chimeric Ad5 vector containing the CAV2 knob. An Ad5 recombinant adenovirus containing the CAV2 knob with a carboxy-terminal polylysine peptide consistently showed high gene expression relative to other Ad5 knob-based vectors as well as a vector displaying the unmodified CAV2 knob. The polylysine CAV2 knob-based Ad5 vector also showed enhanced gene transfer *in vivo* in dog OS xenograft tumors. These data establish the foundation for rational development of an infectivity-enhanced CAV2 CRAd with efficient transduction of canine OS

cells. Evaluation of this syngeneic vector in a controlled clinical trial with dog OS candidates would yield informative results with regard to toxicity and the interplay between the host immune system and the replicative agent. Such knowledge is required for advancing the field of oncolytic adenovirus for cancer therapy.

Materials and methods

Cell culture
Human embryonic kidney 293 (American Type Culture Collection (ATCC), Manassas, VA, USA), human embryonic retinoblast 911,[58] human lung adenocarcinoma A549 (ATCC), CHO, canine OS D17, D22, and CF11.T (ATCC), and dog kidney DK and MDCK (ATCC) cells were maintained according to the suppliers' protocols. All three canine primary OS cells (Scott-Ritchey Research Center, Auburn University, Auburn, AL, USA) were maintained in RPMI 1640 medium supplemented with 20% fetal bovine serum (FBS, Hyclone, Logan, UT, USA) and penicillin/streptomycin (1000 IU and 1000 μg/ml, respectively). Cells were incubated at 37°C and 5% CO_2 under humidified conditions.

Recombinant adenoviruses
All viruses were constructed by homologous recombination in *Escherichia coli*.[59] Both Ad5-wt-IX-EGFP[31] and CAV2-wt-IX-EGFP[60] are described in detail elsewhere. Ad5.RGD and Ad5.pK7,[18] Ad5/3luc1,[51] and Ad5Luc1-CK[23] along with their isogenic unmodified controls have been previously reported. Note that the gene transfer assay results for these vectors are expressed as fold enhancements relative to their isogenic controls since one common control vector applicable to all of the modified vectors was not available.

Construction of Ad5Luc1-CK.pK7 is described as follows. Plasmid pSHAFT, a cloning plasmid containing the Ad5 fiber gene with the knob region deleted and replaced by a small linker containing *Sma*I and *Eco*ICR1 restriction sites,[21] was linearized by *Eco*ICR1 digestion (G**AG**/CTC), leaving two blunt ends. A blunt-ended double-stranded 59-bp linker, encoding five glycine–serine repeats followed by seven lysine residues, a stop codon, and poly-adenylation sequences (underlined), was ligated into linearized pSHAFT. The linker oligonucleotides sequence was: (sense) 5′-**C GCT** TCA GGA TCA GGT TCA GGG AGT GGC TCT AAA AAG AAG AAA AAG AAG AAG <u>TAA TAAA</u>-3′ and (antisense) 5′-<u>TTTA TTA</u> CTT CTT CTT TTT CTT TTT AGA GCC ACT CCC TGA ACC TGA TCC TGA **AGC G**-3′. In the resulting plasmid, pSHAFT.pK7, the *Eco*ICR1 site was deleted by insertion of the 59-bp linker, and replaced with an *Afe*I restriction site (AGC/GCT) resulting from the last two nucleotides of pSHAFT and the first four nucleotides of the linker (bold).

The 536-bp fiber–knob domain of CAV2 was amplified from pTG5412, which contains the complete CAV2 genome (strain Toronto A 26/61)[32] using the following primers: (fwd) 5′-TGTGGACTGGGCCTGGCCCTAG CAT-3′ and (rev) 5′-TTGATTTTCGCCTACATAGGTAA-3′. This CAV2 knob PCR product lacks the endogenous stop codon (TAA). The blunt-ended CAV2 knob domain PCR product was ligated into *Sma*I–*Afe*I-digested

pSHAFT.pK7 resulting in pSHAFT-CAV2.pK7. The pSHAFT-CAV2.pK7 plasmid contains the chimeric fiber gene encoding the complete Ad5 fiber–shaft in frame with the CAV2 knob domain, five glycine–serine repeats, and seven-lysine motif followed by a stop codon and poly-adenylation sequence at the 3′ end. The chimeric fiber gene in pSHAFT-CAV2.pK7 was digested with *Nco*I and *Mfe*I to liberate a 764-bp DNA fragment containing the carboxy terminus of the shaft, the CAV2 knob domain, and lysine motif, and was ligated into the *Nco*I-*Mfe*I-digested shuttle vector pNEB.PK.3.6,[21] resulting in pNEB.PK.3.6-CAV2.pK7.

Recombinant Ad5 genomes containing the chimeric CAV2 fiber gene were derived by homologous recombination in *E. coli* BJ5183 with *Swa*I-linearized rescue plasmid pVK700[61] and the fiber-containing *Pac*I–*Pml*I-fragment of the shuttle vector pNEB.PK.3.6-CAV2.pK7 described above. pVK700 was derived from pTG3602,[62] but contains an almost complete deletion of the fiber gene and contains a firefly luciferase reporter gene driven by the cytomegalovirus immediate early promoter in place of the E1 region. Genomic clones were sequenced and analyzed by PCR prior to transfection into 293 cells.

Virus propagation and purification

All replication-defective human Ad5-based expression vectors were propagated in E1-complementing 293 cells. Replication-competent Ad5-wt-IX-EGFP was amplified in A549 cells while CAV2-wt-IX-EGFP was propagated in DK cells. Viruses were purified by double cesium chloride (CsCl) ultracentrifugation and dialyzed against phosphate-buffered saline with Mg^{2+}, Ca^{2+}, and 10% glycerol. Final aliquots of virus were analyzed for viral particle titer (absorbance at 260 nm) using a conversion factor of 1 OD $= 10^{12}$ viral particles per ml.

Flow cytometry virus-binding assay

All steps were carried out with 1% BSA/PBS buffer. Cells (2.5×10^5) in 200 μl buffer were shaken at 4°C with Ad-wt-IX-EGFP or CAV2-wt-IX-EGFP (10 000 vp/cell). After incubation with the viruses for 1 h, the cells were washed three times with buffer and then analyzed by flow cytometry with EGFP detection. Gates were set according to data obtained for cells not incubated with virus. For blocking experiments, 10-fold excess nonlabeled viruses (10^5 vp/cell Ad5-wt or CAV2-wt viruses) were incubated with the cells for 30 min prior to addition of the labeled viruses for another hour as described above.

Visualization of virus binding on primary OS cells

Primary canine OS cells (2×10^5) were plated on glass coverslips (Fisher Scientific, Pittsburg, PA, USA) in six-well plates with growth medium lacking phenol red (5% FBS/DME medium, Mediatech, Herndon, VA, USA). On the following day, the cells were incubated for 1 h at 4°C with Ad5-wt-IX-EGFP or CAV2-wt-IX-EGFP (10 000 vp/cell) in 500 μl of growth medium supplemented with 25 mM Hepes buffer. After three washes with the above medium to remove unbound virus, Hoescht 33 342 staining (2 μg/ml, Molecular Probes, Eugene, OR, USA) was performed for 5 min in 500 μl of growth medium, and the cells were washed again three times. The cells were fixed onto the glass for 5 min in 3% formaldehyde (Tousimis, Rockville, MD, USA) and then washed again

three times. The coverslips were mounted onto glass slides (Fisher Scientific, Pittsburg, PA, USA) using gel mount medium (Biomeda, Foster City, CA, USA). Images of bound viruses were acquired using epifluorescence microscopy with an inverted IX-70 microscope (Olympus, Melville, NY, USA) equipped with a Magnifire digital CCD camera (Optronics, Goleta, CA, USA). Images were acquired with a $\times 100$ objective using oil immersion and digitally deconvoluted with Iris version 4.15a (http://www.astrosurf.com/buil/) using the Richardson-Lucy algorithm with 15 iterations. EGFP and Hoechst stain images were finally merged using Adobe Photoshop 7.0 (San Jose, CA, USA).

Gene transfer assays

To determine gene transfer efficiency, cells were seeded in a 24-well plate (3×10^4 per well). The next day, the respective cells were infected with the various vectors at 10 vp/cell for 1 h at 37°C and then washed once with 10% growth medium. Luciferase activities of cell lysates were measured 48 h later using the Promega luciferase assay system (Madison, WI, USA). Experiments were performed in triplicates with error bars representing s.d. from the mean.

Taqman real-time quantitative PCR binding/internalization assay

All steps were carried out with 5% DMEM growth medium. Cells (5×10^4 per well in a 24-well plate) were incubated in 500 μl of medium containing the respective viruses (100 vp/cell). After 1 h incubation at 37°C, the cells were washed three times with Hank's buffer, collected for total DNA preparation (QIAamp DNA Blood Mini Kit, QIAGEN), and then quantitated using Taqman quantitative real-time PCR with viral E4-specific primers (LightCycler™ System, Roche Applied Science, Indianapolis, IN, USA). The experiment was performed with triplicate samples.

In vivo *imaging of gene expression*

All methods were approved by the Institutional Animal Care and Use Committee of the University of Alabama at Birmingham and performed according to their guidelines. Based on a previous protocol,[27] D22 dog OS tumors were established in the left and right flanks of athymic nude mice (National Cancer Institute-Frederick Animal Production Area, Frederick, MD, USA) with injection of 5×10^6 cells into each site. Once the tumors reached between 7 and 10 mm in diameter (in approximately 3 weeks), the left tumors were injected with Ad5Luc1 (5×10^9 vp in 25 μl total volume), and the right tumors were injected with Ad5Luc1-CK.pK7 (also 5×10^9 vp in 25 μl total volume). At 4 days after virus administration, the mice were imaged noninvasively for luciferase gene expression. *In vivo* detection of luciferase gene expression was performed with a custom-built optical imaging system. Briefly, a cryogenically cooled (-120°C, back-illuminated Princeton Instruments VersArray:1 KB digital CCD camera (Roper Scientific, Trenton, NJ, USA) with a liquid nitrogen autofill system was mounted on top of a light-tight enclosure. The camera was coupled with a 50 mm Nikkor f/1.2 lens (Nikon, Melville, NY, USA) for image acquisition. Each mouse was anesthetized with 2% isoflurane gas at a flowrate of 0.5–1 l/min (Highland

Medical Equipment, Temecula, CA, USA) and then injected with D-luciferin (3 mg in 100 µl, Nanolight Technology, Pinetop, AZ, USA). At 3 min after substrate administration, 60 s exposure images (without binning and at f/1.2) of each mouse were acquired with the WinView/32 software (Roper Scientific). An image was also taken of the mouse body at f/16 for 0.05 s under ambient lighting. Index color image overlays were generated in Photoshop CS2 (Adobe, Seattle, WA, USA) using the segmentation or thresholding parameters determined in ImageTool 3.0 (The University of Texas Health Science Center in San Antonio, TX, USA). Signal intensities are presented in relative light units (RLU). Signal over the entire tumor was quantitated in terms of integrated density (product of mean RLU and the pixel area) with ImageTool.

Statistical analysis
All *P*-values for significance between various groups were calculated with single factor analysis of variance (ANOVA). Significance was assumed if $P < 0.05$.

Acknowledgements

References

1 Alemany R, Balague C, Curiel DT. Replicative adenoviruses for cancer therapy. *Nat Biotechnol* 2000; **18**: 723–727.

2 Curiel DT. The development of conditionally replicative adenoviruses for cancer therapy. *Clin Cancer Res* 2000; **6**: 3395–3399.

3 Reid T, Warren R, Kirn D. Intravascular adenoviral agents in cancer patients: lessons from clinical trials. *Cancer Gene Ther* 2002; **9**: 979–986.

4 Hemminki A, Alvarez RD. Adenoviruses in oncology: a viable option? *BioDrugs* 2002; **16**: 77–87.

5 Kruyt FA, Curiel DT. Toward a new generation of conditionally replicating adenoviruses: pairing tumor selectivity with maximal oncolysis. *Hum Gene Ther* 2002; **13**: 485–495.

6 Wildner O, Morris JC. Subcutaneous administration of a replication-competent adenovirus expressing HSV-tk to cotton rats: dissemination, persistence, shedding, and pathogenicity. *Hum Gene Ther* 2002; **13**: 101–112.

7 Wang Y, Hallden G, Hill R, Anand A, Liu TC, Francis J et al. E3 gene manipulations affect oncolytic adenovirus activity in immunocompetent tumor models. *Nat Biotechnol* 2003; **21**: 1328–1335.

8 Ganly I, Mautner V, Balmain A. Productive replication of human adenoviruses in mouse epidermal cells. *J Virol* 2000; **74**: 2895–2899.

9 Hallden G, Hill R, Wang Y, Anand A, Liu TC, Lemoine NR et al. Novel immunocompetent murine tumor models for the assessment of replication-competent oncolytic adenovirus efficacy. *Mol Ther* 2003; **8**: 412–424.

10 Withrow SJ, Powers BE, Straw RC, Wilkins RM. Comparative aspects of osteosarcoma. Dog versus man. *Clin Orthop* 1991; **270**: 159–168.

11 Vail DM, MacEwen EG. Spontaneously occurring tumors of companion animals as models for human cancer. *Cancer Invest* 2000; **18**: 781–792.

12 Douglas JT, Kim M, Sumerel LA, Carey DE, Curiel DT. Efficient oncolysis by a replicating adenovirus (ad) *in vivo* is critically dependent on tumor expression of primary ad receptors. *Cancer Res* 2001; **61**: 813–817.

13 Wickham TJ. Ligand-directed targeting of genes to the site of disease. *Nat Med* 2003; **9**: 135–139.

14 Anders M, Hansen R, Ding RX, Rauen KA, Bissell MJ, Korn WM. Disruption of 3D tissue integrity facilitates adenovirus infection by deregulating the coxsackievirus and adenovirus receptor. *Proc Natl Acad Sci USA* 2003; **100**: 1943–1948.

15 Anders M, Christian C, McMahon M, McCormick F, Korn WM. Inhibition of the Raf/MEK/ERK pathway up-regulates expression of the coxsackievirus and adenovirus receptor in cancer cells. *Cancer Res* 2003; **63**: 2088–2095.

16 Wickham TJ, Carrion ME, Kovesdi I. Targeting of adenovirus penton base to new receptors through replacement of its RGD motif with other receptor-specific peptide motifs. *Gene Therapy* 1995; **2**: 750–756.

17 Dmitriev I, Krasnykh V, Miller CR, Wang M, Kashentseva E, Mikheeva G et al. An adenovirus vector with genetically modified fibers demonstrates expanded tropism via utilization of a coxsackievirus and adenovirus receptor-independent cell entry mechanism. *J Virol* 1998; **72**: 9706–9713.

18 Wu H, Seki T, Dmitriev I, Uil T, Kashentseva E, Han T et al. Double modification of adenovirus fiber with RGD and polylysine motifs improves coxsackievirus-adenovirus receptor-independent gene transfer efficiency. *Hum Gene Ther* 2002; **13**: 1647–1653.

19 Suzuki K, Fueyo J, Krasnykh V, Reynolds PN, Curiel DT, Alemany R. A conditionally replicative adenovirus with enhanced infectivity shows improved oncolytic potency. *Clin Cancer Res* 2001; **7**: 120–126.

20 Davydova J, Le LP, Gavrikova T, Wang M, Krasnykh V, Yamamoto M. Infectivity-enhanced cyclooxygenase-2-based conditionally replicative adenoviruses for esophageal adenocarcinoma treatment. *Cancer Res* 2004; **64**: 4319–4327.

21 Krasnykh VN, Mikheeva GV, Douglas JT, Curiel DT. Generation of recombinant adenovirus vectors with modified fibers for altering viral tropism. *J Virol* 1996; **70**: 6839–6846.

22 Shayakhmetov DM, Papayannopoulou T, Stamatoyannopoulos G, Lieber A. Efficient gene transfer into human CD34(+) cells by a retargeted adenovirus vector. *J Virol* 2000; **74**: 2567–2583.

23 Glasgow JN, Kremer EJ, Hemminki A, Siegal GP, Douglas JT, Curiel DT. An adenovirus vector with a chimeric fiber derived from canine adenovirus type 2 displays novel tropism. *Virology* 2004; **324**: 103–116.

24 Dmitriev IP, Kashentseva EA, Curiel DT. Engineering of adenovirus vectors containing heterologous peptide sequences in the C terminus of capsid protein IX. *J Virol* 2002; **76**: 6893–6899.

25 Belousova N, Korokhov N, Krendelshchikova V, Simonenko V, Mikheeva G, Triozzi PL et al. Genetically targeted adenovirus vector directed to CD40-expressing cells. *J Virol* 2003; **77**: 11367–11377.

26 Korokhov N, Mikheeva G, Krendelshchikov A, Belousova N, Simonenko V, Krendelshchikova V et al. Targeting of adenovirus via genetic modification of the viral capsid combined with a protein bridge. *J Virol* 2003; **77**: 12931–12940.

27 Hemminki A, Kanerva A, Kremer EJ, Bauerschmitz GJ, Smith BF, Liu B et al. A canine conditionally replicating adenovirus for evaluating oncolytic virotherapy in a syngeneic animal model. *Mol Ther* 2003; **7**: 163–173.

28 Henry LJ, Xia D, Wilke ME, Deisenhofer J, Gerard RD. Characterization of the knob domain of the adenovirus type 5

fiber protein expressed in *Escherichia coli*. *J Virol* 1994; **68**: 5239–5246.

29 Bergelson JM, Cunningham JA, Droguett G, Kurt-Jones EA, Krithivas A, Hong JS et al. Isolation of a common receptor for Coxsackie B viruses and adenoviruses 2 and 5. *Science* 1997; **275**: 1320–1323.

30 Soudais C, Boutin S, Hong SS, Chillon M, Danos O, Bergelson JM et al. Canine adenovirus type 2 attachment and internalization: coxsackievirus-adenovirus receptor, alternative receptors, and an RGD-independent pathway. *J Virol* 2000; **74**: 10639–10649.

31 Le LP, Everts M, Dmitriev I, Davydova J, Yamamoto M, Curiel DT. Fluorescently labeled adenovirus with pIX-EGFP for vector detection. *Mol Imaging* 2004; **3**: 105–116.

32 Kremer EJ, Boutin S, Chillon M, Danos O. Canine adenovirus vectors: an alternative for adenovirus-mediated gene transfer. *J Virol* 2000; **74**: 505–512.

33 Witlox MA, Van Beusechem VW, Grill J, Haisma HJ, Schaap G, Bras J et al. Epidermal growth factor receptor targeting enhances adenoviral vector based suicide gene therapy of osteosarcoma. *J Gene Med* 2002; **4**: 510–516.

34 Kawashima H, Ogose A, Yoshizawa T, Kuwano R, Hotta Y, Hotta T et al. Expression of the coxsackievirus and adenovirus receptor in musculoskeletal tumors and mesenchymal tissues: efficacy of adenoviral gene therapy for osteosarcoma. *Cancer Sci* 2003; **94**: 70–75.

35 Gu W, Ogose A, Kawashima H, Ito M, Ito T, Matsuba A et al. High-level expression of the coxsackievirus and adenovirus receptor messenger RNA in osteosarcoma, Ewing's sarcoma, and benign neurogenic tumors among musculoskeletal tumors. *Clin Cancer Res* 2004; **10**: 3831–3838.

36 Short JJ, Pereboev AV, Kawakami Y, Vasu C, Holterman MJ, Curiel DT. Adenovirus serotype 3 utilizes CD80 (B7.1) and CD86 (B7.2) as cellular attachment receptors. *Virology* 2004; **322**: 349–359.

37 Wickham TJ, Mathias P, Cheresh DA, Nemerow GR. Integrins alpha v beta 3 and alpha v beta 5 promote adenovirus internalization but not virus attachment. *Cell* 1993; **73**: 309–319.

38 Bai M, Harfe B, Freimuth P. Mutations that alter an Arg-Gly-Asp (RGD) sequence in the adenovirus type 2 penton base protein abolish its cell-rounding activity and delay virus reproduction in flat cells. *J Virol* 1993; **67**: 5198–5205.

39 Greber UF, Willetts M, Webster P, Helenius A. Stepwise dismantling of adenovirus 2 during entry into cells. *Cell* 1993; **75**: 477–486.

40 Seth P. Adenovirus-dependent release of choline from plasma membrane vesicles at an acidic pH is mediated by the penton base protein. *J Virol* 1994; **68**: 1204–1206.

41 Greber UF, Webster P, Weber J, Helenius A. The role of the adenovirus protease on virus entry into cells. *EMBO J* 1996; **15**: 1766–1777.

42 Leopold PL, Ferris B, Grinberg I, Worgall S, Hackett NR, Crystal RG. Fluorescent virions: dynamic tracking of the pathway of adenoviral gene transfer vectors in living cells. *Hum Gene Ther* 1998; **9**: 367–378.

43 Suomalainen M, Nakano MY, Keller S, Boucke K, Stidwill RP, Greber UF. Microtubule-dependent plus- and minus end-directed motilities are competing processes for nuclear targeting of adenovirus. *J Cell Biol* 1999; **144**: 657–672.

44 Greber UF, Suomalainen M, Stidwill RP, Boucke K, Ebersold MW, Helenius A. The role of the nuclear pore complex in adenovirus DNA entry. *EMBO J* 1997; **16**: 5998–6007.

45 Sirena D, Lilienfeld B, Eisenhut M, Kalin S, Boucke K, Beerli RR et al. The human membrane cofactor CD46 is a receptor for species B adenovirus serotype 3. *J Virol* 2004; **78**: 4454–4462.

46 Miyazawa N, Leopold PL, Hackett NR, Ferris B, Worgall S, Falck-Pedersen E et al. Fiber swap between adenovirus subgroups B and C alters intracellular trafficking of adenovirus gene transfer vectors. *J Virol* 1999; **73**: 6056–6065.

47 Miyazawa N, Crystal RG, Leopold PL. Adenovirus serotype 7 retention in a late endosomal compartment prior to cytosol escape is modulated by fiber protein. *J Virol* 2001; **75**: 1387–1400.

48 Shayakhmetov DM, Li ZY, Ternovoi V, Gaggar A, Gharwan H, Lieber A. The interaction between the fiber knob domain and the cellular attachment receptor determines the intracellular trafficking route of adenoviruses. *J Virol* 2003; **77**: 3712–3723.

49 Alemany R, Curiel DT. CAR-binding ablation does not change biodistribution and toxicity of adenoviral vectors. *Gene Therapy* 2001; **8**: 1347–1353.

50 Smith TA, Idamakanti N, Rollence ML, Marshall-Neff J, Kim J, Mulgrew K et al. Adenovirus serotype 5 fiber shaft influences *in vivo* gene transfer in mice. *Hum Gene Ther* 2003; **14**: 777–787.

51 Breidenbach M, Rein DT, Wang M, Nettelbeck DM, Hemminki A, Ulasov I et al. Genetic replacement of the adenovirus shaft fiber reduces liver tropism in ovarian cancer gene therapy. *Hum Gene Ther* 2004; **15**: 509–518.

52 Kanerva A, Mikheeva GV, Krasnykh V, Coolidge CJ, Lam JT, Mahasrethi PJ et al. Targeting adenovirus to the serotype 3 receptor increases gene transfer efficiency to ovarian cancer cells. *Clin Cancer Res* 2002; **8**: 275–280.

53 Kanerva A, Zinn KR, Chaudhuri TR, Lam JT, Suzuki K, Uil TG et al. Enhanced therapeutic efficacy for ovarian cancer with a serotype 3 receptor-targeted oncolytic adenovirus. *Mol Ther* 2003; **8**: 449–458.

54 Haviv YS, Blackwell JL, Kanerva A, Nagi P, Krasnykh V, Dmitriev I et al. Adenoviral gene therapy for renal cancer requires retargeting to alternative cellular receptors. *Cancer Res* 2002; **62**: 4273–4281.

55 Kawakami Y, Li H, Lam JT, Krasnykh V, Curiel DT, Blackwell JL. Substitution of the adenovirus serotype 5 knob with a serotype 3 knob enhances multiple steps in virus replication. *Cancer Res* 2003; **63**: 1262–1269.

56 Volk AL, Rivera AA, Kanerva A, Bauerschmitz G, Dmitriev I, Nettelbeck DM et al. Enhanced adenovirus infection of melanoma cells by fiber-modification: incorporation of RGD peptide or Ad5/3 chimerism. *Cancer Biol Ther* 2003; **2**: 511–515.

57 Takayama K, Reynolds PN, Short JJ, Kawakami Y, Adachi Y, Glasgow JN et al. A mosaic adenovirus possessing serotype Ad5 and serotype Ad3 knobs exhibits expanded tropism. *Virology* 2003; **309**: 282–293.

58 Fallaux FJ, Kranenburg O, Cramer SJ, Houweling A, Van Ormondt H, Hoeben RC et al. Characterization of 911: a new helper cell line for the titration and propagation of early region 1-deleted adenoviral vectors. *Hum Gene Ther* 1996; **7**: 215–222.

59 He TC, Zhou S, da Costa LT, Yu J, Kinzler KW, Vogelstein B. A simplified system for generating recombinant adenoviruses. *Proc Natl Acad Sci USA* 1998; **95**: 2509–2514.

60 Le LP, Li J, Ternovoi VV, Siegal GP, Curiel DT. Fluorescently tagged canine adenovirus via modification with protein IX-enhanced green fluorescent protein. *J Gen Virol* (in press).

61 Belousova N, Krendelchtchikova V, Curiel DT, Krasnykh V. Modulation of adenovirus vector tropism via incorporation of polypeptide ligands into the fiber protein. *J Virol* 2002; **76**: 8621–8631.

62 Chartier C, Degryse E, Gantzer M, Dieterle A, Pavirani A, Mehtali M. Efficient generation of recombinant adenovirus vectors by homologous recombination in *Escherichia coli*. *J Virol* 1996; **70**: 4805–4810.

1   Title: **Core Labeling of Adenovirus with EGFP**

2

3

4   Authors: Long P. Le[1], Helen N. Le[1], Amy R. Nelson[1], David A. Matthews[2],

5   Masato Yamamoto[1], David T. Curiel[1][*]

6

7

8

9

10

11

12

13

14   Authors' affiliations: [1] Division of Human Gene Therapy, Departments of Medicine,

15   Pathology and Surgery, and the Gene Therapy Center, University

16   of Alabama at Birmingham, Birmingham, Alabama 35294

17   [2] School of Biomedical Sciences, University of St. Andrews, St.

18   Andrews, UK

19

20

21

22

23

24

25   [*]Corresponding author: David T. Curiel, M. D., Ph. D.

26   901 19th Street South, BMR2- 502

27   Birmingham, AL 35294

28   Phone: 205-934-8627

29   Fax: 205-975-7476

30   E-mail: curiel@uab.edu

1 **Abstract**

2   The study of adenovirus could greatly benefit from diverse methods of virus detection.

3 Recently, it has been demonstrated that carboxy terminal EGFP fusions of adenovirus core

4 proteins Mu, V, and VII properly localize to the nucleus and display novel function in the cell.

5 Based on these observations, we hypothesized that the core proteins may serve as targets for

6 labeling the adenovirus core with fluorescent proteins. To this end, we constructed various

7 chimeric expression vectors with fusion core genes (Mu-EGFP, V-EGFP, preVII-EGFP, and

8 matVII-EGFP) while maintaining expression of the native proteins. Expression of the fusion

9 core proteins was suboptimal using E1 expression vectors with both conventional CMV and

10 modified (with adenovirus tripartite leader sequence) CMV5 promoters, resulting in non-labeled

11 viral particles. However, robust expression equivalent to the native protein was observed when

12 the fusion genes were placed in the deleted E3 region. The efficient Ad-wt-E3-V-EGFP and Ad-

13 wt-E3-preVII-EGFP expression vectors were labeled allowing viral particle detection by

14 fluorescence microscopy. These vectors maintained their viral function, including viral DNA

15 replication, viral DNA encapsidation, cytopathic effect, and thermostability. Core labeling offers

16 a means to track the adenovirus core in vector targeting studies as well as basic adenovirus

17 virology.

1 Introduction

2   There are 51 identified human adenovirus serotypes of which some manifest clinical

3   relevance while others have been applied as gene delivery vectors (Russell, 2000). The study of

4   adenoviruses with regard to virology, pathology, and gene therapy has greatly benefited from

5   various detection methods, including quantitative and localizing techniques which can probe for

6   viral DNA, RNA, and protein at the molecular level. In the context of adenoviral vector design,

7   reporter gene expression has likewise played a vital role in the evaluation of vector transduction

8   and transcriptional control both *in vitro* and *in vivo*. However, full understanding of the key

9   steps of adenovirus host-cell interaction, cell entry, genome delivery, replication, and progeny

10   dissemination require detection modalities which can follow viral components and particles at

11   the microscopic level, preferably in real-time. Indeed, methods founded on this rationale have

12   demonstrated the power of tracking individual adenoviral particles intracellularly. Studies have

13   applied *ex vivo*, non-specific chemical conjugation of the adenovirus capsid with synthetic

14   fluorophores (*e.g.*, fluorescein isothiocyanate, Texas Red, carbocyanine 3) to evaluate viral entry

15   (Leopold et al., 1998; Nakano and Greber, 2000), examine the effect of fiber modification on

16   intracellular trafficking (Bernt et al., 2003; Miyazawa et al., 1999), and show the dynein-

17   dependent nature of adenovirus interaction with microtubules (Kelkar et al., 2004).

18   Recently, we and others successfully developed *in vivo* labeling of adenovirus with the

19   enhanced green fluorescent protein (EGFP) fused to the minor capsid protein IX (Le et al., 2004;

20   Meulenbroek et al., 2004). These studies illustrated specific and homogeneous capsid labeling of

21   adenovirus by genetic means to yield fluorescent adenoviruses possessing full virus function and

22   utility in the tracking of infection as well as the detection of viral biodistribution. The ability to

23   track the adenovirus core and genome, nevertheless, represents a potential detection strategy

24   distinct from capsid labeling and would be operative in following adenovirus genome delivery,

25   an imperative step in both natural infection and gene transfer. Previously *in vivo* genome

26   labeling was demonstrated using a tetR-EGFP fusion protein which binds to tetO repeats

27   incorporated into the adenovirus genome (Glotzer et al., 2001). Although the labeling was

28   feasible, analysis by the authors showed that the tandem tetO repeat sequence was prone to

29   deletion by recombination. Furthermore, the technique was based on an exogenous, nonviral

30   fusion protein tetR-EGFP label expressed in a producer cell line. It would be ideal and perhaps

31   more efficient if *in vivo* labeling of the adenovirus genome could be accomplished with an

1 endogenous viral protein expressed from the vector itself without the need for a producer cell

2 line.

3   Adenoviruses are nonenveloped, double-stranded DNA viruses with an icosahedral

4 structure constructed from an array of twelve different proteins. Their approximate 36 kb

5 genome is covalently bound to two terminal proteins and further organized through non-covalent

6 association with the three core proteins Mu, V, and VII. All three core proteins are translated

7 from the common L2 transcript under the control of the major late promoter (Alestrom et al.,

8 1984). Protein VII (pVII) is the major core protein contributing over 800 copies per virion

9 (Lehmberg et al., 1999). Expressed as a 174 amino acid precursor from which a 24 amino acid

10 N-terminus is cleaved (Sung et al., 1983), its functional and sequence homology to histone H3

11 (Cai and Weber, 1993; Lee et al., 2003) indicates that pVII acts as a histone-like center around

12 which viral DNA is wrapped to form nucleosome structures (Chatterjee et al., 1986; Mirza and

13 Weber, 1982). Protein V (pV) is speculated to serve as a bridge between the genome core and

14 the capsid through association with proteins Mu, VI, and VII as well as the viral DNA

15 (Chatterjee et al., 1985; Matthews and Russell, 1998; Vayda and Flint, 1987). There are more

16 than 150 copies of the minor core protein V per virion which binds nonspecifically to the viral

17 DNA (Chatterjee et al., 1985, 1986; Lehmberg et al., 1999). Mu or protein X matures into a 19

18 amino acid final form (Mu) after both amino- and carboxy-terminal cleavage of the 79 amino

19 acid precursor (preMu) by the adenovirus encoded protease. The copy number per virion of Mu

20 is not known (Chatterjee et al., 1985). Because of its ability to precipitate negatively charged

21 DNA *in vitro* via its nine positively charged arginine residues, it has been postulated to play a

22 role in viral DNA condensation in the core (Anderson et al., 1989).

23   Recent intracellular localization and functional studies of Mu, pV, and pVII were

24 performed with carboxy terminal fusion of EGFP to the native proteins (Lee et al., 2003, 2004;

25 Matthews, 2001). Our attention was drawn to three established observations from these reports:

26 (i) nuclear localization of the fusion core proteins was conserved, (ii) the fusion core proteins

27 demonstrated some function in the cell, and (iii) pV and pVII are found at ample copy numbers

28 per virion. Based on these findings, we hypothesized that the core proteins may serve as targets

29 for labeling of adenoviruses with fluorescent proteins. Herein we describe the genetic labeling

30 of the adenovirus core through the use of a chimeric expression system of both the native and

31 fluorescent fusion core proteins. Adenovirus core labeling offers a unique way to follow the

1   adenovirus core with potential for studying adenovirus infection and biology as well as tracking

2   adenoviral vectors in gene therapy applications.

1   **Results**

2

3   *Fluorescent fusion core protein expression and localization.* We chose a chimeric system to

4   generate recombinant adenoviruses expressing control EGFP and the fluorescent fusion core

5   proteins: Mu-EGFP, pV-EGFP, preVII-EGFP, and matVII-EGFP (Fig. 1A). PreMu-EGFP was

6   not chosen as a candidate for labeling because it has been shown to block late adenovirus gene

7   expression when expressed concomitantly with adenovirus infection (Lee et al., 2004). In the

8   chimeric expression system, both the native, unmodified core protein and the fusion counterpart

9   were expressed from the same vector. We initially applied the AdEasy system to construct E1

10   expression vectors under the control of the constitutive cytomegalovirus (CMV) promoter (Fig.

11   1B). After transient transfection of the final genomes into 911 cells, rescue of all viruses was

12   successful. Expression and localization of the fusion core proteins from the E1 expression

13   vectors were verified 24 h postinfection in A549 cells. Fluorescence microscopy revealed

14   expression of all fusion core proteins (Fig. 2). Control EGFP localized diffusely throughout the

15   cytoplasm and nucleus while all four fusion core proteins demonstrated strong nuclear

16   localization. Mu-EGFP showed diffuse cytoplasmic signal along with nucleoplasmic and what

17   appears to be nucleolar targeting. Protein V-EGFP, like Mu-EGFP, localized to both the

18   nucleoplasm and the nucleoli; however, little protein was found in the cytoplasm. PreVII-EGFP

19   distributed exclusively to the nucleus with signals detected in the nucleoplasm, the nucleoli, and

20   areas where the DNA Hoechst stain associated with the cellular chromosomes. MatVII-EGFP

21   colocalized almost entirely with the host cell DNA while some of the protein was also visualized

22   in the nucleoplasm. The image of matVII-EGFP was nearly indistinguishable from the picture

23   captured for Hoechst stain of the same field. In 911 cells in which the viruses actively

24   replicated, we observed the same pattern of fusion core protein localization as that seen in A549

25   cells (data not shown). These results agree with published data obtained from plasmid derived

26   transient expression of the same fusion core proteins (Lee et al., 2003, 2004; Matthews, 2001).

27

28   *Fluorescence of E1-CMV expression vector viral particles.* After validating proper expression

29   and intracellular trafficking of the fusion core proteins from the E1-CMV expression vectors, we

30   analyzed the fluorescence of purified virus fractions collected from the CsCl gradient after two

31   rounds of ultracentrifugation. During purification, both the mature and immature viral bands

1   were retained. In our previous study involving fluorescent capsid-labeled adenovirus (Le et al.,

2   2004), this procedure was established as a useful assay to detect fluorescence signal colocalizing

3   with the purified viral bands. Each gradient fraction was quantitated for EGFP fluorescence and

4   viral DNA content (optical absorbance at 260 nm, data not shown). The results were

5   discouraging in that only minor fluorescent peaks were detected for the bottom mature virus

6   band of Ad-E1-CMV-preVII-EGFP and the top immature virus band of Ad-E1-CMV-V-EGFP

7   (Fig. 3), in contrast to our pIX-EGFP labeled adenovirus which showed strong peaks (Le et al.,

8   2004). We corroborated these data with fluorescence microscopy of samples from the bottom

9   and top bands for each virus and found only occasional fluorescent particles, the number of

10   which was disproportionately lower than the number of viral particles predicted by absorbance

11   measurements at 260 nm (data not shown).

12

13   *Western blot analysis of Ad-E1-CMV-V-EGFP purified virus and infected cells.* With available

14   anti-sera against the adenovirus pV, western blot analysis was performed to detect pV-EGFP

15   expression and incorporation into viral particles on a more molecular level. Purified virions

16   collected from the top and bottom bands of control Ad-E1-CMV-GFP and Ad-E1-CMV-V-

17   EGFP were examined.   Although fluorometry analysis revealed a flat response throughout the

18   gradient (Fig. 3), GFP protein was unexpectedly found in the mature band of Ad-E1-CMV-GFP

19   in contrast to our previous study (Le et al., 2004) (Fig. 4A, left panel, lane 1). Understandably,

20   more GFP was detected in the immature band where it is expected to migrate along with

21   unassociated cellular debris and proteins in the gradient (Fig. 4A, left panel, lane 2). A low level

22   of pV-EGFP was detected in the bottom band, whereas significantly more was found in the top

23   band (Fig. 4A, left panel, lanes 3 and 4, respectively), matching the results obtained in the

24   fluorometry experiment. Probing with the pV anti-sera confirmed the findings obtained with the

25   GFP antibody; however, it also showed that Ad-E1-CMV-V-EGFP virions contained

26   substantially less of the fusion core protein than the native pV (Fig. 4A, right panel, lanes 3 and

27   4), suggesting inefficient incorporation of the fusion core pV-EGFP relative to the native

28   version. We further analyzed the expression of pV-EGFP in 911 cells during Ad-E1-CMV-V-

29   EGFP infection. Western blot analysis revealed that intracellular expression of the fusion core

30   protein relative to the native protein paralleled the observations made above with the purified

31   virus. Considerably lower expression of pV-EGFP was noted relative to natural pV (Fig. 4A,

1 right panel, lane 6). These data indicate that the inefficient incorporation of pV-EGFP into

2 virions may be due to the unfavorable expression of pV-EGFP in comparison to native pV

3 although assembly defect due to EGFP fusion could also be possible.

4

5 *Enhanced expression of pV-EGFP from the E3 region.* As a result of the poor expression

6 achieved with the E1-CMV vectors, we explored the possibility of increasing the fusion core

7 protein expression relative to the native protein by using two approaches. The first strategy

8 involved the use of the CMV5 promoter (Qbiogene, Fig. 1B) to drive expression of the fusion

9 core proteins from the E1-deleted region. This modified promoter features the adenovirus

10 tripartite leader sequence downstream of the CMV promoter which has been previously shown to

11 enhance transgene expression (Sheay et al., 1993). Our attempt to generate E1-CMV5 fusion

12 core protein expression viruses unfortunately resulted in unsuccessful rescue of all candidate

13 vectors (Ad-E1-CMV5-Mu-EGFP, Ad-E1-CMV5-preVII-EGFP, and Ad-E1-CMV5-matVII-

14 EGFP) except the control Ad-E1-CMV5-EGFP and Ad-E1-CMV5-V-EGFP. The second

15 strategy to generate vectors with enhanced expression exploited the deleted E3 region of the

16 adenovirus genome to express transgenes (Fig. 1B). Previous reports have demonstrated that

17 efficient expression late in infection could be attained by using this locale for transgene insertion,

18 likely due to transcription from the major late promoter, polyadenylation, and splicing with the

19 tripartite leader sequence (Hawkins and Hermiston, 2001a, 2001b; Hawkins et al., 2001; Mittal

20 et al., 1993). Contrary to the results obtained with the E1-CMV5 expression vectors, we were

21 successful in rescuing most of the E3 expression vectors (Ad-wt-E3-EGFP, Ad-wt-E3-Mu-

22 EGFP, and Ad-wt-E3-V-EGFP) except Ad-wt-E3-mat-VII-EGFP.

23   To verify enhanced expression of the fusion core proteins was indeed achieved using the

24 E1-CMV5 and E3 chimeric expression strategies, western blot analysis was performed with cell

25 lysates from 911 cells infected with 1 CPEU/cell of the various vectors 24 h postinfection.

26 Representative analysis was performed with the V-EGFP vectors. Although we observed strong

27 expression of EGFP from the control Ad-E1-CMV-EGFP vector (Fig. 4B, left panel, lane 1), the

28 expression of V-EGFP driven by the E1-CMV and E1-CMV5 vectors was quite low when

29 probed with both the EGFP and pV antibodies (Fig. 4B, left and right panels, lanes 2 and 3,

30 respectively) . In our hands, the CMV5 did not provide improved transgene expression over the

31 unmodified CMV promoter, particularly with V-EGFP as the transgene. However, pV-EGFP

1   expression from the deleted E3 region was detected at a significant level (Fig. 4B, left and right

2   panels, lane 4) comparable to the amount of native pV (Fig. 4B, right panel, lane 4).

3

4   *Fluorescence of Ad-E1-CMV5-V-EGFP and E3 fusion core protein expression vectors.* The

5   fluorometry assay described above was repeated with CsCl gradient fractions of Ad-E1-CMV5-

6   V-EGFP (the only rescued core protein E1-CMV5 vector) and the E3 expression viruses. As

7   predicted by the western blot analysis, no fluorescent peaks in the bottom and top viral bands

8   were detected for Ad-E1-CMV5-V-EGFP like the included control vector Ad-E1-CMV5-EGFP

9   (Fig. 5, middle panel). Ad-wt-E3-Mu-EGFP revealed very small peaks for both the mature virus

10   and empty particle bands (Fig. 5, left panel). Both Ad-wt-E3-V-EGFP and Ad-wt-E3-preVII-

11   EGFP displayed strong fluorescent peaks for the bottom bands and a couple of minor peaks

12   above the mature particle band (Fig. 5, middle and right panels, respectively). All major

13   fluorescent peaks in the bottom bands of Ad-wt-E3-V-EGFP and Ad-wt-E3-preVII-EGFP

14   coincided with viral DNA peaks measured by absorbance at 260 nm (Fig. 5, middle and right

15   panels, respectively). It is interesting to note that both Ad-wt-E3-V-EGFP and Ad-wt-E3-

16   preVII-EGFP did not show major peaks in the top band (empty capsids with little or no viral

17   DNA), whereas our previous capsid-labeled Ad-IX-EGFP virus demonstrated a strong

18   fluorescent peak in the top band comparable to the bottom band (Le et al., 2004). This

19   observation may be unique to the core-labeled vectors which contain fusion core proteins with

20   the propensity to interact with viral DNA as opposed to the capsid-labeled vector.

21

22   *Visualization of Ad-wt-E3-V-EGFP and Ad-wt-E3-preVII-EGFP fluorescent particles.* After

23   confirming fluorescent labeling of the E3 fusion core protein vectors with the fractionation assay,

24   the purified viral particles were examined under fluorescence microscopy. Abundant Ad-wt-E3-

25   V-EGFP and Ad-wt-E3-preVII-EGFP fluorescent particles could be visualized (Fig. 6A and 6B,

26   respectively) while Ad-wt-E3-Mu-EGFP virions could not be detected (data not shown),

27   suggesting the poor labeling efficiency of this vector.

28

29   *DNA packaging analysis of core-labeled adenoviruses.* The core proteins play essential roles in

30   packaging of the viral genome inside the capsid. We tested whether our chimeric system of

31   expressing the fusion core proteins in competition with the endogenous proteins would affect

1   viral DNA packaging. For this analysis, we infected 911 cells with the labeled vectors Ad-wt-

2   E3-V-EGFP and Ad-wt-E3-preVII-EGFP along with the control Ad-wt-E3-EGFP (1 CPEU/cell

3   of each virus). Total intracellular viral DNA and encapsidated viral DNA inside the cell from

4   various days postinfection were quantitated by real-time Taqman PCR using E4 specific primers.

5   Even though infection with the three viruses were executed at the same multiplicity of infection

6   based on infectious titer, the control Ad-wt-E3-EGFP virus showed significantly lower total viral

7   DNA synthesis and encapsidation by about one order of magnitude compared to Ad-wt-E3-V-

8   EGFP and Ad-wt-E3-preVII-EGFP. By day 4, however, both the total intracellular viral genome

9   copy number and the amount of encapsidated viral DNA was nearly the same for all three

10   viruses, indicating that the growth kinetics of the control virus may have been delayed (Fig. 7A,

11   left and middle panels). Expressing the data as encapsidation percentage of total viral DNA

12   further illustrates the stunted dynamics and essentially lower yield of Ad-wt-E3-EGFP while

13   concomitantly showing equivalent behavior of Ad-wt-E3-V-EGFP and Ad-wt-E3-preVII-EGFP

14   (Fig. 7A, right panel).

15

16   *Cytopathic effect of core-labeled viruses.* To further evaluate the overall function of the core-

17   labeled viruses, cytopathic effect was assessed in comparison to the control virus Ad-wt-E3-

18   EGFP. 911 cells were infected with various amounts of each virus (0.5, 0.05, and 0.005

19   CPEU/cell), and their viability was assayed over the course of 10 days postinfection. The

20   cytopathic effect was not appreciably different between the three viruses even at the lowest

21   multiplicity of infection (Fig. 7B).

22

23   *Thermostability of core-labeled virions.* Finally, we tested the thermostability of the viruses by

24   exposing equal amounts (based on t.u.) of Ad-wt-E3-EGFP, Ad-wt-E3-V- EGFP, and Ad-wt-E3-

25   preVII-EGFP to 45 °C for various time periods. Following heat treatment, the samples were

26   functionally titered in terms of transduction units. The thermostabilities of the core-labeled

27   virions (especially Ad-wt-E3-V-EGFP) were actually better than that of the control Ad-wt-E3-

28   EGFP (Fig. 8).

1 **Discussion**

2   We have described herein successful labeling of the adenovirus core through the chimeric

3 expression of fluorescent fusion core proteins V-EGFP and preVII-EGFP from the deleted E3

4 region. Because of their nonutility for gene therapy objectives and perhaps their indispensible

5 role in formation of the virus core, modification of core proteins have not been exploited in

6 recombinant adenoviruses. Such basis directed us to pursue a conservative approach in labeling

7 the adenovirus core with a chimeric expression system wherein both the fluorescent fusion core

8 proteins and their native counterparts are expressed from the same vector. This cautious strategy

9 would safeguard against unpredictable compromise of the core protein function due to the EGFP

10 fusion.

11   In using a chimeric expression system, however, the relative expression levels of the

12 exogenous and endogenous core proteins must be considered in light of the fact that each is

13 competing with the other for assembly into virions. As well, any possibility of perturbing the

14 structural function of the original protein through the addition of EGFP should be taken into

15 account. In fact, the former predicament was encountered when applying our initial method of

16 CMV promoter driven expression from the deleted E1 region. The CMV promoter has been

17 widely used as a constitutive promoter to drive strong transgene expression from nonreplicative

18 adenoviral vectors. Nevertheless, adenoviral gene expression regulatory mechanisms during

19 replication pose a great challenge when using the foreign CMV promoter to match the expression

20 level of the endogenous core proteins. Late in infection, adenoviral mRNA transcripts

21 containing the spliced 5' tripartite leader sequence are preferentially translated over transcripts

22 lacking this element (Berkner and Sharp, 1985; Chow et al., 1977; Logan and Shenk, 1984).

23 Transcripts generated from the CMV promoter would not contain this tripartite leader sequence

24 and would therefore be translated at a lower level than the endogenous adenoviral L2 transcript

25 from which the core proteins are made.

26   The tripartite leader sequence has been exploited to enhance transgene expression from

27 plasmid vectors by mating the tripartite leader sequence downstream of certain nonadenoviral

28 promoters (Sheay et al., 1993). Moreover, a similar strategy was employed in stable packaging

29 cell lines to achieve strong expression of a recombinant fiber protein in the context of adenovirus

30 replication (Von Seggern et al., 2000). We pursued this approach to increase expression of the

31 fusion core proteins from the deleted E1 region. When applying the modified CMV5 promoter

1   which contains the tripartite leader sequence to improve transgene expression, we could only

2   rescue Ad-E1-CMV5-EGFP and Ad-E1-CMV5-V-EGFP. Past studies have shown that pVII can

3   interfere with adenovirus DNA synthesis (Korn and Horwitz, 1986) and mRNA transcription *in*

4   *vitro* (Nakanishi et al., 1986). Protein Mu has the ability to precipitate negatively charged DNA

5   *in vitro* and plays a role in viral DNA condensation in the core (Anderson et al., 1989). On this

6   basis, the untimely and strong expression of Mu-EGFP, preVII-EGFP, and matVII-EGFP via the

7   CMV5 promoter may explain the failure to rescue these respective vectors. However, all E1-

8   CMV vectors were rescued, and yet increased gene expression of pV-EGFP with CMV5 relative

9   to CMV was not observed under our experimental conditions. Unlike the E1-CMV5 approach,

10   the use of the deleted E3 region to express our transgenes was more fruitful in that most viruses

11   could be rescued (Ad-wt-E3-EGFP, Ad-wt-E3-Mu-EGFP, Ad-wt-E3-V-EGFP, and Ad-wt-E3-

12   preVII-EGFP) except Ad-wt-E3-matVII-EGFP. Timely expression late in infection from the

13   deleted E3 region (via the major late promoter) may explain these results.

14   Strong expression of the fusions pV-EGFP and preVII-EGFP from the deleted E3 region

15   yielded fluorescent virions under fluorescence microscopy. It should be noted that Ad-wt-E3-V-

16   EGFP and Ad-wt-E3-preVII-EGFP particles showed qualitatively less intense but more

17   heterogenous fluorescence than our capsid-labeled Ad-IX-EGFP vector (Le et al., 2004). This

18   disparity seems paradoxical in the case of Ad-wt-E3-preVII-EGFP since the copy number per

19   virion of pVII is over 800 (Lehmberg et al., 1999), whereas the copy number per virion of pIX is

20   240 (Lehmberg et al., 1999; van Oostrum and Burnett, 1985). The nature of core labeling may

21   compact the fluorescent fusion core proteins within the capsid in close proximity to each other,

22   possibly causing fluorescence resonance energy transfer which would diminish the fluorescent

23   signal. On the other hand, the labeling of the capsid with surface exposed pIX-EGFP would less

24   likely result in this phenomenon. Additionally, our capsid labeling strategy was based on

25   complete replacement of the IX gene with IX-EGFP, whereas core labeling with preVII-EGFP

26   also involved packaging of the non-labeled native pVII.

27   Various assays were performed to evaluate the viability of the core-labeled vectors Ad-

28   wt-E3-V-EGFP and Ad-wt-E3-pre-VII-EGFP. In the DNA packaging analysis, the viral DNA

29   replication and encapsidation of the control Ad-wt-E3-EGFP was poor compared to the two

30   core-labeled viruses (about one order lower) despite using the same multiplicity of infection for

31   all three vectors. Interestingly, the only difference between the control virus and the other two

1   vectors is expression of diffuse EGFP for the former versus expression of nuclear localizing

2   fusion core proteins with EGFP for the latter two. It is difficult to attribute increased DNA

3   replication to the over-expression of the core proteins (*i.e.*, native pV plus modified V-EGFP,

4   **Fig. 4b**, right panel, lane 4) in the case of Ad-wt-E3-V-EGFP and Ad-wt-E3-preVII-EGFP since

5   the high expression of these proteins occur late after DNA replication. On the other hand, it is

6   plausible that the increased presence of the core proteins may lead to increased packaging

7   efficiency late in infection. It is also likely that the high expression of EGFP by itself may

8   influence the kinetics of viral replication through its interactions with viral proteins or the host

9   cell. In this respect, EGFP has been reported to cause toxicity both in living cells and in mice

10   (Huang et al., 2000; Liu et al., 1999).

11   Another anomaly between control Ad-wt-E3-EGFP and the core-labeled vectors was

12   discovered in the thermostability assay. Both modified viruses appeared more thermostable than

13   the control. Following exposure of the viruses to 45 °C, transduction unit titer was used as an

14   infectious index of viral function. Because the control virus was practically wild-type with

15   respect to its capsid and core structure, the incorporation of the fusion core proteins into the

16   modified viruses may have imparted additional stablility. Whether the increased thermostability

17   pertains to the entire adenovirus structure or just the core is uncertain. It is possible that a more

18   thermostable core alone would produce the results we obtained since a DNA-pVII complex by

19   itself has transfection capability (Wienhues et al., 1987). Such "nonviral" transduction would

20   likely contribute to the increased t.u. titers we measured for the core labeled vectors.

21   In summary, we have demonstrated the fluorescent labeling of the adenovirus core by

22   competitive expression of fusions pV-EGFP and preVII-EGFP from the deleted E3 region.

23   Strong expression of these fusion core proteins from the E3 region did not negatively impact

24   DNA replication, DNA encapsidation, thermostability, and cytopathic effect of the viruses. The

25   purified particles were labeled and fluorescent, allowing their detection under fluorescence

26   microscopy. A future extension of the techniques described here is to generate recombinant

27   adenoviruses with complete replacement of the native V or preVII gene with the fusion V-EGFP

28   or preVII-EGFP. Core-labeling of adenoviruses would allow the tracking of the adenovirus core

29   and complements our capsid-labeling technique in the study of adenovirus biology, pathogenesis,

30   and vector design.

1   **Methods**

2

3   *Cell culture.* Human embryonic retinoblast 911 (Fallaux et al., 1996), human lung

4   adenocarcinoma A549 (American Type Culture Collection, Manassas, VA), and Chinese

5   hamster ovary cells were maintained according to the suppliers' protocols. Cells were incubated

6   at 37 °C and 5% CO_2 under humidified conditions.

7

8   *Recombinant adenovirus construction.* All viruses were constructed by homologous

9   recombination in *Escheria coli* (He et al., 1998). The base plasmids were acquired from the

10   following sources: pShuttle-CMV, pAdenoVator-CMV5, and pAdEasy (Qbiogene, Irvine, CA);

11   pcDNA3-CMV-V-EGFP (Matthews, 2001), pcDNA3-CMV-Mu-EGFP (Lee et al., 2004),

12   pcDNA3-CMV-preVII-EGFP (Lee et al., 2003), pcDNA3-CMV-matVII-EGFP (Lee et al.,

13   2003); Shuttle plasmids for the E1-CMV/E3-deleted chimeric expression vectors were

14   constructed as follows using restriction cloning: *pShuttle-E1-CMV-V-EGFP* → pShuttle-

15   CMV/SalI/blunt/KpnI + pcDNA3-CMV-V-EGFP/

16   ApaI/blunt/KpnI; *pShuttle-E1-CMV-Mu-EGFP* → pShuttle-CMV/EcoRV/KpnI + pcDNA3-

17   CMV-Mu-EGFP/ApaI/blunt/KpnI; *pShuttle-E1-CMV-preVII-EGFP* → pShuttle-

18   CMV/EcoRV/KpnI + pcDNA3-CMV-preVII-EGFP/ApaI/blunt/KpnI; *pShuttle-E1-CMV-matVII-*

19   *EGFP* → pShuttle-CMV/EcoRV/KpnI + pcDNA3-CMV-matVII-EGFP/

20   ApaI/blunt/KpnI. pShuttle-E1-CMV-EGFP was cloned in two steps. pcDNA3-CMV-V-EGFP

21   was cut with BamHI and self-ligated to remove the V fusion. Then the resulting plasmid was cut

22   with ApaI/blunt/KpnI to liberate the EGFP gene for ligation into pShuttle-CMV cut with

23   EcoRV/KpnI.

24   Shuttle plasmids for vectors expressing the fusion core proteins under the modified

25   CMV5 promoter (containing the adenovirus tripartite leader sequence) were constructed with

26   pAdenoVator-CMV5. For EGFP, Mu-EGFP, preVII-EGFP, and matVII-EGFP, the respective

27   pShuttle-E1-CMV plasmids containing these genes as described above were cut with

28   BglII/BstXI to release the transgene and a portion of the right homologous arm. These fragments

29   were ligated into pAdenoVator-CMV5 cut with BamHI/BstXI (fragment which contains the

30   CMV5 promoter). To generate pAdenoVator-CMV5-V-EGFP, pShuttle-E1-CMV-V-EGFP was

1   cut with SalI/blunt/BstXI to give a fragment with the fusion gene and then ligated into

2   pAdenoVator cut with PmeI/BstXI.

3   Finally, a parent E3 shuttle plasmid was made to insert the same fusion genes into the

4   adenovirus E3 region by double selection homologous recombination. Briefly, pShuttlE3

5   contains the left and right homologous arms from pBHG10 (Microbix, Toronto, CA) flanking the

6   E3-deleted region which has been replaced by a unique PacI site. The kanamycin gene along

7   with the multiple cloning site from pABS.4 (Microbix) was cloned into the unique PacI site,

8   elminating it in the process, to make the final pShuttlE3. Detailed steps will be provided upon

9   request. pShuttlE3-V-EGFP was constructed by first subcloning the KpnI/SphI V-EGFP cut

10   from pcDNA3-CMV-V-EGFP into pABS.4 also cut with the same enzymes. An SphI/XhoI

11   partial digest was performed on the resulting plasmid to move the V-EGFP gene into the

12   corresponding restriction sites in pShuttlE3. All of the other pShuttlE3 plasmids were made by

13   cutting the respective fusion core genes out of the pShuttle-E1-CMV vectors described above

14   with BglII/HpaI and then inserting it into pShuttlE3 cut with SalI/blunt/BglII. All blunted

15   fragments were generated with the large Klenow fragment (New England Biolabs, Beverly,

16   MA). The plasmids were verified by restriction cutting. All E1 shuttle plasmids were

17   recombined with the pAdEasy rescue plasmid in BJ5183 cells, whereas the E3 shuttle plasmids

18   were recombined with the pTG3602 rescue backbone. Since the pShuttlE3 plasmids contain the

19   kanamycin gene and the fusion core gene flanked by the homologous arms, recombination was

20   performed using double selection for ampicillin from the rescue plasmid pTG3602 and

21   kanamycin from pShuttlE3. Subsequently kanamycin was cut out of the genomes with the two

22   surrounding SwaI sites. After self-ligation, the final adenoviral genomes were linearized with

23   PacI and then transiently transfected into 911 cells.

24

25   *Virus propagation and purification.* Viruses were propagated in 911 cells and purified by double

26   cesium chloride (CsCl) ultracentrifugation followed by dialysis against phosphate-buffered

27   saline with Mg^{2+}, Ca^{2+}, and 10% glycerol. Final aliquots of virus were analyzed for viral particle

28   titer (absorbance at 260 nm) and transduction unit (t.u.) titer. Based on a previously described

29   protocol (Alemany et al., 2000), t.u. was determined by infecting 15,000 911 cells in 96-well

30   plates with 1/10 serial dilutions of the virus and counting the number of green cells 2 d

31   postinfection ($n = 6$). In addition, all viruses were quantitated for cytopathic effect unit (CPEU)

1   titer. 911 cells 96-well plates (15,000 per well) were infected with 1/10 serial dilutions of the

2   virus. Two days postinfection, cell viability was determined with an MTS assay (3-(4,5-

3   dimethylthiazol-2-yl)-5-(3-carboxymethoxyphenyl)-2-(4-sulfophenyl)-2H-tetrazolium, Promega,

4   Madison, WI). The TCID50 dose was determined and back-calculated to obtain the CPEU titer

5   where theoretically 1 CPEU kills one cell in 2 d. All viruses were stored at -80 ºC until use.

6

7   *Fluorescence microscopy.* A549 cells seeded on glass coverslips were transduced with 100 viral

8   particles per cell of Ad-E1-CMV-EGFP, Ad-E1-CMV-Mu-EGFP, Ad-E1-CMV-V-EGFP, Ad-

9   E1-CMV-preVII-EGFP and Ad-E1-CMV-matVII-EGFP. Twenty-four hours postinfection, the

10   cells were washed with PBS, fixed, stained with Hoechst 33342 (Molecular Probes, Eugene,

11   OR), and mounted on glass slides (Fisher Scientific, Pittsburg, PA). Epifluorescence microscopy

12   was performed with an inverted IX-70 microscope (Olympus, Melville, NY) equipped with a

13   Magnifire digital CCD camera (Optronics, Goleta, CA). Images were acquired with a 100X

14   objective using oil immersion and digitally deconvoluted with Iris, version 4.15a

15   (http://www.astrosurf.com/buil/), by applying the Richardson-Lucy algorithm with 15 iterations.

16   An image of a single fluorescent Ad-IX-EGFP (Le et al., 2004) virus particle with strong signal-

17   to-noise ratio was used to determine the point spread function as suggested by the software

18   documentation. EGFP and Hoechst stain images were merged using Adobe Photoshop 7.0 (San

19   Jose, CA).

20

21   *Characterization of virus gradient fractions.* For the fractionation studies, viruses were

22   propagated each in ten 150 mm dishes of 911 cells. Collected crude viral lysates were purified

23   by CsCl ultracentrifugation where the top and bottom bands were retained through two

24   centrifugation steps yielding one gradient from the 10 dishes. After the second spin, fractions

25   (~100 μL) were collected dropwise through a perforation at the bottom of the tube into 96-well

26   white opaque plates. Plates with the viral fractions were measured with a microplate fluorometer

27   (Fluostar Optima, BMG Labtechnologies, Durham, NC) using 490/10 nm excitation and 510/10

28   nm emission filters. To determine viral DNA content, a sample of each fraction (10 μL) was

29   diluted in 90 μL 0.5% SDS/PBS and incubated at room temperature for 10 min to release the

30   viral genomes. Absorbance at 260 nm was then measured for each sample (MBA 2000, Perkin

31   Elmer, Shelton, CT).

1

2 *Western blot.* Top and bottom band samples of purified control Ad-E1-CMV-EGFP and Ad-E1-

3 CMV-V-EGFP (8 µg) were subjected were resolved with SDS-PAGE and then transferred to a

4 polyvinylidene difluoride membrane (BioRad, Hercules, CA). Blotting was performed with a

5 primary monoclonal GFP antibody (1:1000 dilution, BD Biosciences Clontech) followed by a

6 secondary HRP-linked anti-mouse antibody (1:5000 dilution, Amersham Pharmacia, Piscataway,

7 NJ) or a primary polyclonal pV antibody (1:1000 dilution, Chemicon International, Inc.,

8 Temecula, CA) followed by a secondary HRP-linked anti-rabbit antibody (1:5000 dilution,

9 Dako, Carpinteria, CA). Bands were detected with a chemiluminescent ECL kit (Amersham

10 Pharmacia, Piscataway, NJ). For analysis of protein expression from the V-EGFP vectors, 2 x

11 10^5 911 cells were infected with 1 CPEU/cell of Ad-E1-CMV-EGFP, Ad-E1-CMV-V-EGFP,

12 Ad-E1-CMV5-V-EGFP, and Ad-wt-E3-V-EGFP in 12-well plates. Twenty-four hours

13 postinfection, the cells were collected and lysed with RIPA buffer (100 µL). Samples (10 µg)

14 were subjected to SDS-PAGE and blotting with GFP and pV antibodies as described above.

15

16 *DNA packaging analysis. DNA* packaging was analyzed by using a previously reported protocol

17 (Yamamoto et al., 2003). Briefly, 911 cells (5 x 10^4) were infected with Ad-wt-E3-EGFP, Ad-

18 wt-E3-V-EGFP, and Ad-wt-E3-preVII-EGFP with 1 CPEU/cell in 12-well plates. On days 1, 2,

19 3, and 4 postinfection, the cells were collected. One half of the cell pellet was processed for total

20 viral genome copy number, and the other half was processed for encapsidated viral genome copy

21 number (QIAamp DNA Blood Mini Kit, QIAGEN, Valencia, CA). The viral DNA pools were

22 quantitated with Taqman quantitative real-time PCR using E4 specific primers (LightCycler

23 System, Roche Applied Science, Indianapolis, IN).

24

25 *Cytopathic effect assay.* Five thousand 911 cells were infected with Ad-wt-E3-EGFP, Ad-wt-

26 E3-V-EGFP, and Ad-wt-E3-preVII-EGFP (0.5 CPEU/cell, 0.05 CPEU/cell, and 0.005

27 CPEU/cell of each vector) in 100 µL of 5% DME medium without phenol red (five replicates for

28 each condition plus five noninfected wells as controls). Cytopathic effect was measured by an

29 MTS assay (3-(4,5-dimethylthiazol-2-yl)-5-(3-carboxymethoxy-phenyl)-2-(4-sulfophenyl)-2H-

30 tetrazolium, Promega, Madison, WI) on days 0, 2, 4, 6, 8, and 10 post-infection. Results were

1   calculated as viability percent of noninfected cells with blank values (medium only) subtracted

2   beforehand.

3

4   *Thermostability assay.* Thermostability was analyzed using a modified version of a previously

5   reported protocol (Dmitriev et al., 2002). Samples of Ad-CMV-EGFP and Ad-IX-EGFP (10^6 t.u.

6   in 100 μL PBS) were incubated for various time periods at 45 °C (0, 5, 10, 20, and 40 min).

7   Transduction unit infectious titers were then determined for the samples using the above

8   mentioned protocol.

9

10

11   **Acknowledgements**

References

Alemany, R., Suzuki, K., and Curiel, D. T. (2000). Blood clearance rates of adenovirus type 5 in mice. *J Gen Virol* **81**(Pt 11)**,** 2605-2609.

Alestrom, P., Akusjarvi, G., Lager, M., Yeh-kai, L., and Pettersson, U. (1984). Genes encoding the core proteins of adenovirus type 2. *J Biol Chem* **259**(22)**,** 13980-13985.

Anderson, C. W., Young, M. E., and Flint, S. J. (1989). Characterization of the adenovirus 2 virion protein, mu. *Virology* **172**(2)**,** 506-512.

Berkner, K. L., and Sharp, P. A. (1985). Effect of the tripartite leader on synthesis of a non-viral protein in an adenovirus 5 recombinant. *Nucleic Acids Res* **13**(3)**,** 841-857.

Bernt, K. M., Ni, S., Li, Z. Y., Shayakhmetov, D. M., and Lieber, A. (2003). The effect of sequestration by nontarget tissues on anti-tumor efficacy of systemically applied, conditionally replicating adenovirus vectors. *Mol Ther* **8**(5)**,** 746-755.

Cai, F., and Weber, J. M. (1993). Primary structure of the canine adenovirus PVII protein: functional implications. *Virology* **193**(2)**,** 986-988.

Chatterjee, P. K., Vayda, M. E., and Flint, S. J. (1985). Interactions among the three adenovirus core proteins. *J Virol* **55**(2)**,** 379-386.

Chatterjee, P. K., Vayda, M. E., and Flint, S. J. (1986). Identification of proteins and protein domains that contact DNA within adenovirus nucleoprotein cores by ultraviolet light crosslinking of oligonucleotides 32P-labelled in vivo. *J Mol Biol* **188**(1)**,** 23-37.

Chow, L. T., Gelinas, R. E., Broker, T. R., and Roberts, R. J. (1977). An amazing sequence arrangement at the 5' ends of adenovirus 2 messenger RNA. *Cell* **12**(1)**,** 1-8.

Dmitriev, I. P., Kashentseva, E. A., and Curiel, D. T. (2002). Engineering of adenovirus vectors containing heterologous peptide sequences in the C terminus of capsid protein IX. *J Virol* **76**(14)**,** 6893-6899.

Fallaux, F. J., Kranenburg, O., Cramer, S. J., Houweling, A., Van Ormondt, H., Hoeben, R. C., and Van Der Eb, A. J. (1996). Characterization of 911: a new helper cell line for the titration and propagation of early region 1-deleted adenoviral vectors. *Hum Gene Ther* **7**(2)**,** 215-222.

Glotzer, J. B., Michou, A. I., Baker, A., Saltik, M., and Cotten, M. (2001). Microtubule-independent motility and nuclear targeting of adenoviruses with fluorescently labeled genomes. *J Virol* **75**(5)**,** 2421-2434.

Hawkins, L. K., and Hermiston, T. (2001a). Gene delivery from the E3 region of replicating human adenovirus: evaluation of the E3B region. *Gene Ther* **8**(15)**,** 1142-1148.

Hawkins, L. K., and Hermiston, T. W. (2001b). Gene delivery from the E3 region of replicating human adenovirus: evaluation of the ADP region. *Gene Ther* **8**(15)**,** 1132-1141.

Hawkins, L. K., Johnson, L., Bauzon, M., Nye, J. A., Castro, D., Kitzes, G. A., Young, M. D., Holt, J. K., Trown, P., and Hermiston, T. W. (2001). Gene delivery from the E3 region of replicating human adenovirus: evaluation of the 6.7 K/gp19 K region. *Gene Ther* **8**(15)**,** 1123-1131.

He, T. C., Zhou, S., da Costa, L. T., Yu, J., Kinzler, K. W., and Vogelstein, B. (1998). A simplified system for generating recombinant adenoviruses. *Proc Natl Acad Sci U S A* **95**(5)**,** 2509-2514.

Huang, W. Y., Aramburu, J., Douglas, P. S., and Izumo, S. (2000). Transgenic expression of green fluorescence protein can cause dilated cardiomyopathy. *Nat Med* **6**(5)**,** 482-483.

Kelkar, S. A., Pfister, K. K., Crystal, R. G., and Leopold, P. L. (2004). Cytoplasmic dynein mediates adenovirus binding to microtubules. *J Virol* **78**(18)**,** 10122-10132.

Korn, R., and Horwitz, M. S. (1986). Adenovirus DNA synthesis in vitro is inhibited by the virus-coded major core protein. *Virology* **150**(2)**,** 342-351.

Le, L. P., Everts, M., Dmitriev, I. P., Davydova, J. G., Yamamoto, M., and Curiel, D. T. (2004). Fluorescently labeled adenovirus with pIX-EGFP for vector detection. *Mol Imaging* **3**(2)**,** 105-116.

Lee, T. W., Blair, G. E., and Matthews, D. A. (2003). Adenovirus core protein VII contains distinct sequences that mediate targeting to the nucleus and nucleolus, and colocalization with human chromosomes. *J Gen Virol* **84**(Pt 12)**,** 3423-3428.

Lee, T. W., Lawrence, F. J., Dauksaite, V., Akusjarvi, G., Blair, G. E., and Matthews, D. A. (2004). Precursor of human adenovirus core polypeptide Mu targets the nucleolus and modulates the expression of E2 proteins. *J Gen Virol* **85**(Pt 1)**,** 185-196.

Lehmberg, E., Traina, J. A., Chakel, J. A., Chang, R. J., Parkman, M., McCaman, M. T., Murakami, P. K., Lahidji, V., Nelson, J. W., Hancock, W. S., Nestaas, E., and Pungor, E., Jr. (1999). Reversed-phase high-performance liquid chromatographic assay for the adenovirus type 5 proteome. *J Chromatogr B Biomed Sci Appl* **732**(2)**,** 411-423.

Leopold, P. L., Ferris, B., Grinberg, I., Worgall, S., Hackett, N. R., and Crystal, R. G. (1998). Fluorescent virions: dynamic tracking of the pathway of adenoviral gene transfer vectors in living cells. *Hum Gene Ther* **9**(3)**,** 367-378.

Liu, H. S., Jan, M. S., Chou, C. K., Chen, P. H., and Ke, N. J. (1999). Is green fluorescent protein toxic to the living cells? *Biochem Biophys Res Commun* **260**(3)**,** 712-717.

Logan, J., and Shenk, T. (1984). Adenovirus tripartite leader sequence enhances translation of mRNAs late after infection. *Proc Natl Acad Sci U S A* **81**(12)**,** 3655-3659.

Matthews, D. A. (2001). Adenovirus protein V induces redistribution of nucleolin and B23 from nucleolus to cytoplasm. *J Virol* **75**(2)**,** 1031-1038.

Matthews, D. A., and Russell, W. C. (1998). Adenovirus core protein V is delivered by the invading virus to the nucleus of the infected cell and later in infection is associated with nucleoli. *J Gen Virol* **79** (**Pt 7**)**,** 1671-1675.

Meulenbroek, R. A., Sargent, K. L., Lunde, J., Jasmin, B. J., and Parks, R. J. (2004). Use of adenovirus protein IX (pIX) to display large polypeptides on the virion--generation of fluorescent virus through the incorporation of pIX-GFP. *Mol Ther* **9**(4)**,** 617-624.

Mirza, M. A., and Weber, J. (1982). Structure of adenovirus chromatin. *Biochim Biophys Acta* **696**(1)**,** 76-86.

Mittal, S. K., McDermott, M. R., Johnson, D. C., Prevec, L., and Graham, F. L. (1993). Monitoring foreign gene expression by a human adenovirus-based vector using the firefly luciferase gene as a reporter. *Virus Res* **28**(1)**,** 67-90.

Miyazawa, N., Leopold, P. L., Hackett, N. R., Ferris, B., Worgall, S., Falck-Pedersen, E., and Crystal, R. G. (1999). Fiber swap between adenovirus subgroups B and C alters intracellular trafficking of adenovirus gene transfer vectors. *J Virol* **73**(7)**,** 6056-6065.

Nakanishi, Y., Maeda, K., Ohtsuki, M., Hosokawa, K., and Natori, S. (1986). In vitro transcription of a chromatin-like complex of major core protein VII and DNA of adenovirus serotype 2. *Biochem Biophys Res Commun* **136**(1)**,** 86-93.

Nakano, M. Y., and Greber, U. F. (2000). Quantitative microscopy of fluorescent adenovirus entry. *J Struct Biol* **129**(1)**,** 57-68.

Russell, W. C. (2000). Update on adenovirus and its vectors. *J Gen Virol* **81**(Pt 11)**,** 2573-2604.

Sheay, W., Nelson, S., Martinez, I., Chu, T. H., Bhatia, S., and Dornburg, R. (1993). Downstream insertion of the adenovirus tripartite leader sequence enhances expression in universal eukaryotic vectors. *Biotechniques* **15**(5)**,** 856-862.

Sung, M. T., Cao, T. M., Lischwe, M. A., and Coleman, R. T. (1983). Molecular processing of adenovirus proteins. *J Biol Chem* **258**(13)**,** 8266-8272.

van Oostrum, J., and Burnett, R. M. (1985). Molecular composition of the adenovirus type 2 virion. *J Virol* **56**(2)**,** 439-448.

Vayda, M. E., and Flint, S. J. (1987). Isolation and characterization of adenovirus core nucleoprotein subunits. *J Virol* **61**(10)**,** 3335-3339.

Von Seggern, D. J., Huang, S., Fleck, S. K., Stevenson, S. C., and Nemerow, G. R. (2000). Adenovirus vector pseudotyping in fiber-expressing cell lines: improved transduction of Epstein-Barr virus-transformed B cells. *J Virol* **74**(1)**,** 354-362.

Wienhues, U., Hosokawa, K., Hoveler, A., Siegmann, B., and Doerfler, W. (1987). A novel method for transfection and expression of reconstituted DNA-protein complexes in eukaryotic cells. *DNA* **6**(1)**,** 81-89.

Yamamoto, M., Davydova, J., Wang, M., Siegal, G. P., Krasnykh, V., Vickers, S. M., and Curiel, D. T. (2003). Infectivity enhanced, cyclooxygenase-2 promoter-based conditionally replicative adenovirus for pancreatic cancer. *Gastroenterology* **125**(4)**,** 1203-1218.

1   Fig. 1. Schematic of vectors. (A) Control EGFP gene and candidate fusion core genes. (B)

2   Nomenclature and configuration of expression vectors where X represents any of the genes

3   depicted in A. The employed expression strategies include transcription via the typical CMV

4   promoter, a modified CMV promoter containing the adenovirus tripartite leader sequence

5   (CMV5), and the adenovirus major late promoter (by virtue of transgene cassette insertion into

6   the deleted E3 region).

7

8   Fig. 2. Fluorescent core fusion protein expression and localization. A549 cells were infected

9   with nonreplicative E1-CMV adenovirus vectors expressing the indicated genes. The cells were

10   fixed and stained for nuclear DNA 24 h postinfection followed by visualization of the fluorescent

11   proteins by epifluorescence microscopy.

12

13   Fig. 3. Analysis of E1-CMV fusion core protein viral gradients. Fluorescence quantitation of

14   fractions from viral CsCl gradients of Ad-E1-CMV-EGFP, Ad-E1-CMV-Mu-EGFP, Ad-E1-

15   CMV-V-EGFP, Ad-E1-CMV-preVII-EGFP, and Ad-E1-CMV-matVII-EGFP after double

16   ultracentrifugation.

17

18   Fig. 4. Western blot analysis of Ad-E1-CMV-V-EGFP purified virus and cells infected with

19   various expression vectors. (A) Purified viruses (8 µg protein each sample) and infected cell

20   lysates (4 µg protein each sample) were subjected to SDS-PAGE and blotted with GFP and pV

21   antibodies. Lanes (1) Ad-E1-CMV-EGFP bottom band, (2) Ad-E1-CMV-EGFP top band, (3)

22   Ad-E1-CMV-V-EGFP bottom band, (4) Ad-E1-CMV-V-EGFP top band, (5) Ad-E1-CMV-GFP

23   infected 911 cells, and (6) Ad-E1-CMV-V-EGFP infected 911 cells. (B) Protein lysates (10 µg)

24   from 911 cells infected with the various V-EGFP expression vectors were subjected to SDS-

25   PAGE and blotted with GFP and pV antibodies. Lanes (1) Ad-E1-CMV-EGFP, (2) Ad-E1-

26   CMV-V-EGFP, (3) Ad-E1-CMV5-V-EGFP, and (4) Ad-wt-E3-V-EGFP.

27

28   Fig. 5. Analysis of fusion core protein viral gradients with improved expression. Fusion core

29   protein vectors with enhanced expression were purified and fractionated to determine

30   fluorescence of CsCl gradient fractions. For all panels, unlabeled Ad-E1-CMV5-EGFP was

31   included as a control (—□—). Ad-E1-CMV5-X (—△—) and Ad-wt-E3-X (—○—) are shown

1 where X is the indicated fusion protein at the top of the panel. Note that Ad-E1-CMV5-Mu-

2 EGFP, Ad-E1-CMV5-pre-VII-EGFP, Ad-E1-CMV5-mat-VII-EGFP, and Ad-wt-E3-matVII-

3 EGFP could not be rescued for analysis. For Ad-wt-E3-V-EGFP and Ad-wt-E3-preVII-EGFP,

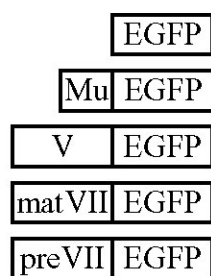4 viral DNA content was also analyzed for the respective fractions (─○─).

5

6 Fig. 6. Visualization of Ad-wt-E3-V-EGFP and Ad-wt-E3-preVII-EGFP particles. Purified Ad-

7 wt-E3-V-EGFP (A) and Ad-wt-E3-preVII-EGFP (B) were prepared on slides with coverslips and

8 imaged with epifluorescence microscopy.

9

10 Fig. 7. DNA packaging efficiency and cytopathic effect of core-labeled viruses. (A) 911 cells

11 were infected over the course of 4 d with control Ad-wt-E3-EGFP (- -○- -), Ad-wt-E3-V-EGFP

12 (─△─), and Ad-wt-E3-preVII-EGFP (─□─). Each day, half of the cells collected were

13 processed for total viral DNA while the other half was processed for encapsidated viral DNA.

14 Both viral DNA pools were quantitated by Taqman real-time quantitative PCR using E4 specific

15 primers ($n = 3$). The third panel shows the percent of encapsidated viral DNA for each

16 respective virus (encapsidated divided by total and then multiplied by 100%). (B) The

17 cytopathic effect of the same three viruses were analyzed on 911 cells over the course of 10 d

18 using the indicated multiplicities of infection. Every 2 d, the cell viability was quantitated by

19 MTS assay. Cell viability is expressed as percentage relative to noninfected cells ($n = 5$). Ad-

20 wt-E3-EGFP (- -○- -), Ad-wt-E3-V-EGFP (─△─), and Ad-wt-E3-preVII-EGFP (─□─).
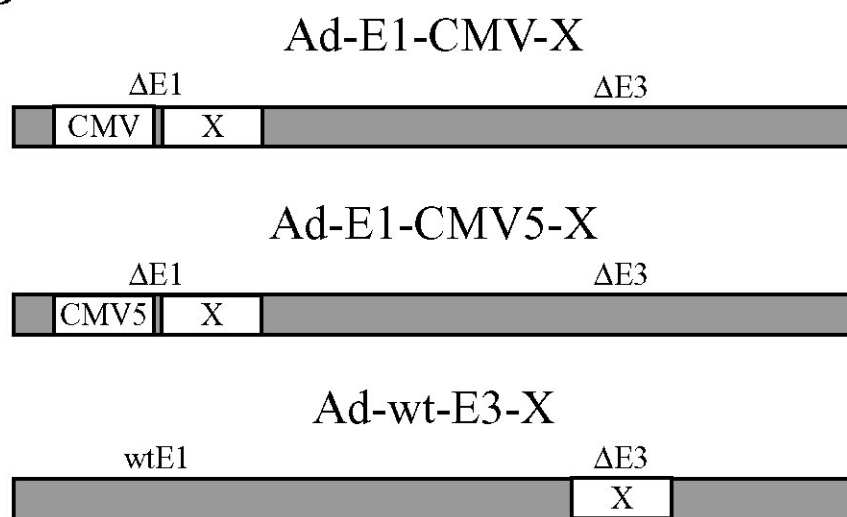
21

22 Fig. 8. Thermostability of core-labeled vectors. Ad-wt-E3-EGFP (white), Ad-wt-V-EGFP

23 (black), and Ad-wt-E3-pre-VII-EGFP (striped) were incubated at 45 °C for various times and

24 then quantitated by transduction unit titer. Bars represent percent of remaining infectivity

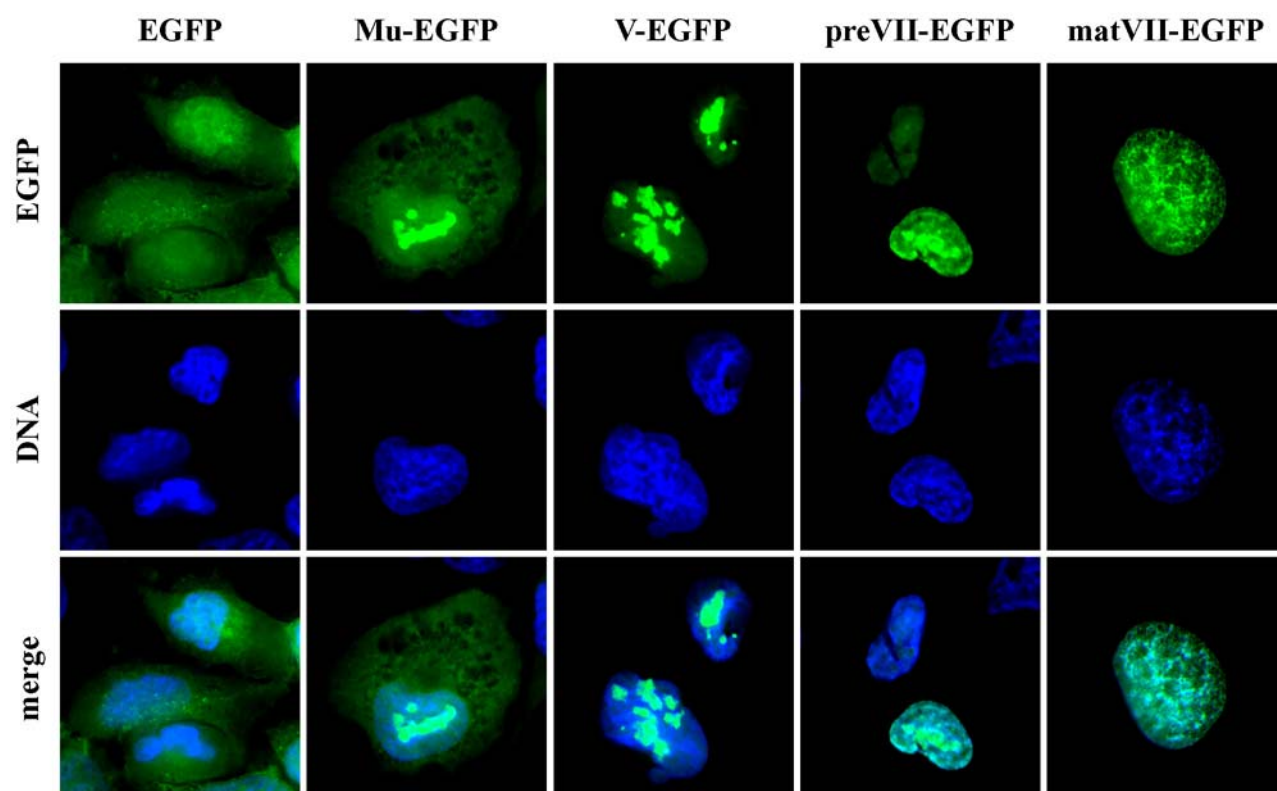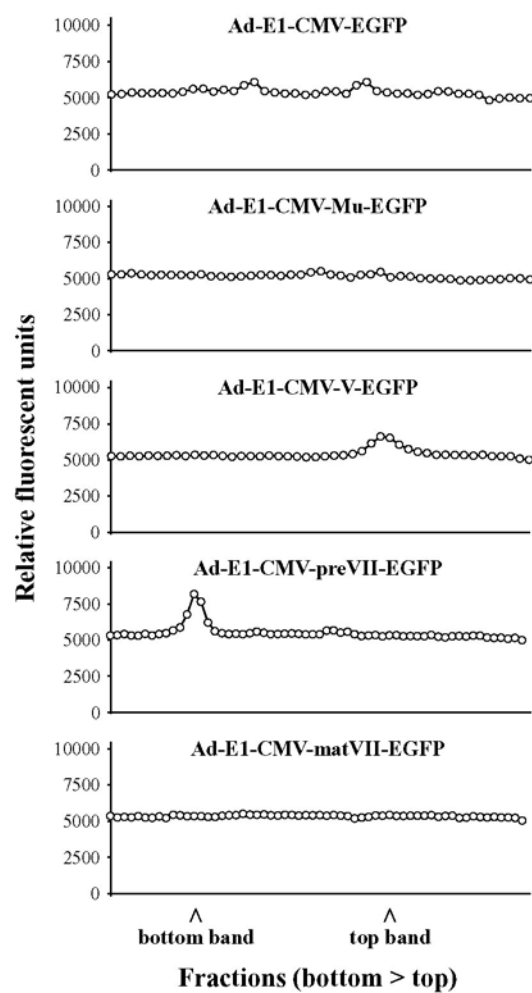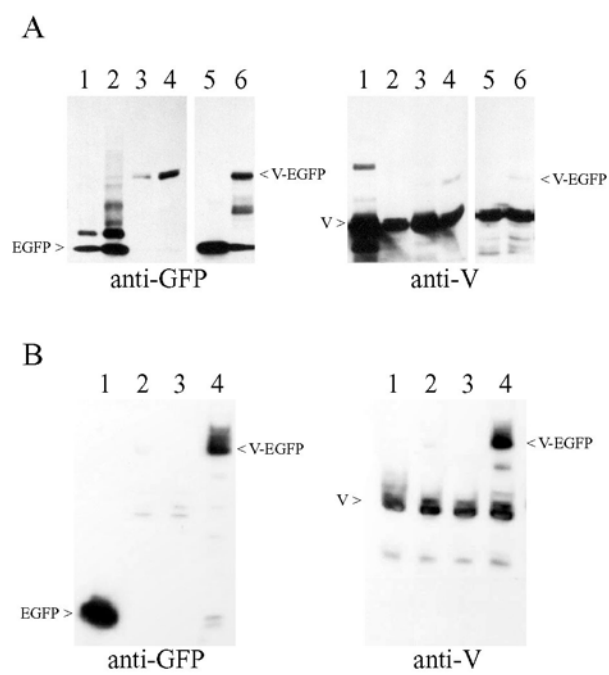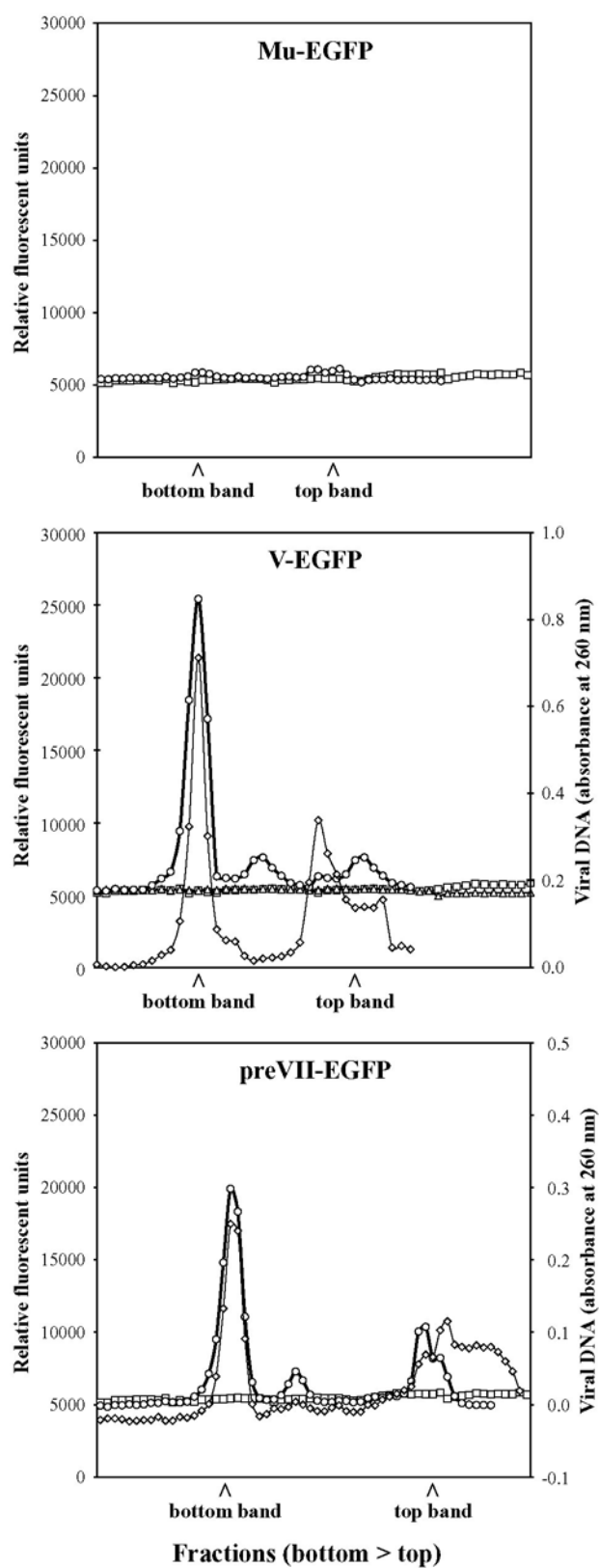25 relative to untreated samples ($n = 3$).

1   **Figure 1**

A

B

Ad-E1-CMV-X

Ad-E1-CMV5-X

Ad-wt-E3-X
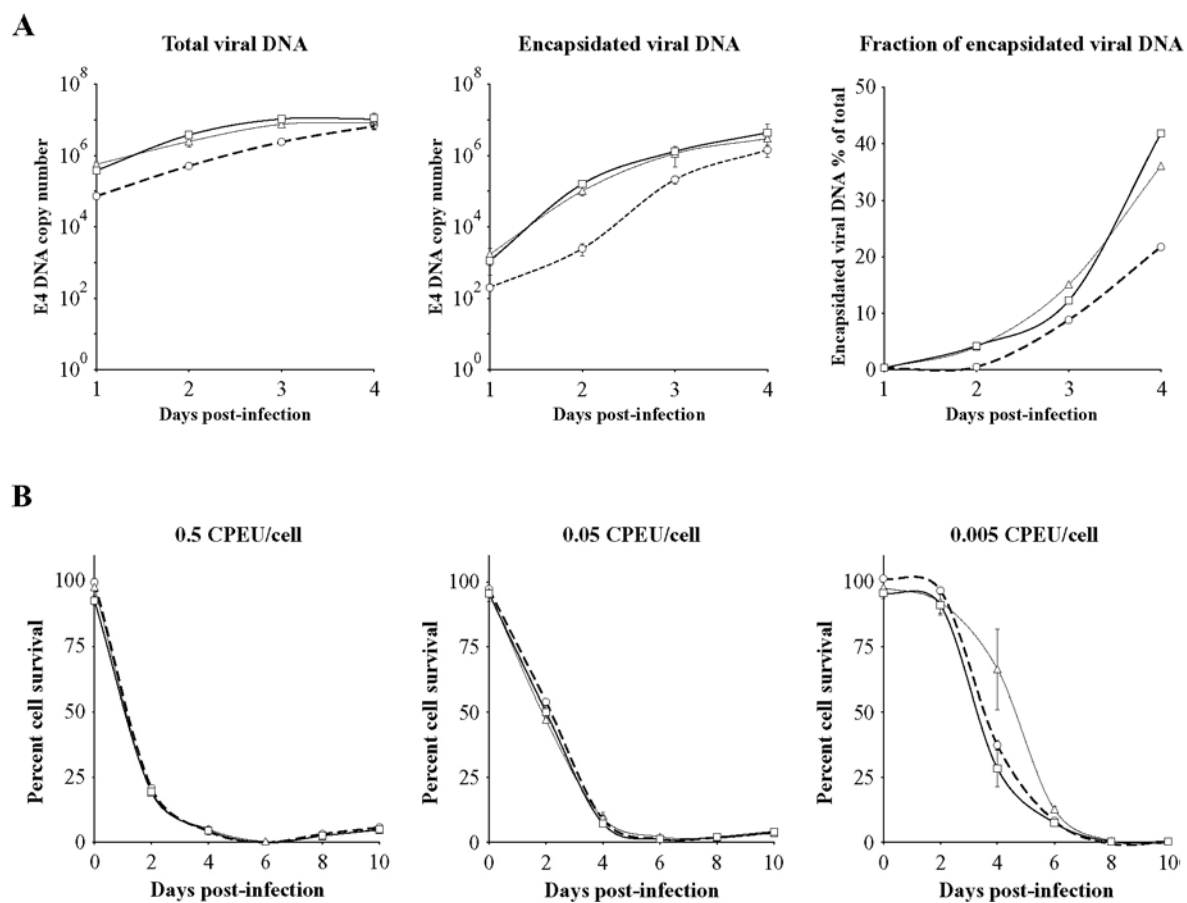
1 **Figure 2**

1   **Figure 3**

1   **Figure 4**

A

anti-GFP   anti-V

B

anti-GFP   anti-V

1   **Figure 5**

Fractions (bottom > top)

1   **Figure 6**

1   **Figure 7**

A

Total viral DNA

Encapsidated viral DNA

Fraction of encapsidated viral DNA

B

0.5 CPEU/cell

0.05 CPEU/cell

0.005 CPEU/cell

1   **Figure 8**